uOttawa

L'Université canadienne
Canada's university

FACULTÉ DES ÉTUDES SUPÉRIEURES ET POSTOCTORALES

uOttawa

L'Université canadienne
Canada's university

FACULTY OF GRADUATE AND POSDOCTORAL STUDIES

Farzaneh Shemshaki

AUTEUR DE LA THÈSE / AUTHOR OF THESIS

M.A.Sc. (Chemical Engineering)

GRADE / DEGREE

Department of Chemical Engineering

FACULTÉ, ÉCOLE, DÉPARTEMENT / FACULTY, SCHOOL, DEPARTMENT

Prediction of Time Lag in Vacuum Tubes and its Implications for Characterization of Membranes in Constant Volume Systems. Effect of Resistance-free Accumulation Tank

TITRE DE LA THÈSE / TITLE OF THESIS

Boguslaw Kruczek

DIRECTEUR (DIRECTRICE) DE LA THÈSE / THESIS SUPERVISOR

CO-DIRECTEUR (CO-DIRECTRICE) DE LA THÈSE / THESIS CO-SUPERVISOR

EXAMINATEURS (EXAMINATRICES) DE LA THÈSE / THESIS EXAMINERS

David Taylor

André Tremblay

Gary W. Slater

LE DOYEN DE LA FACULTÉ DES ÉTUDES SUPÉRIEURES ET POSTDOCTORALES /
DEAN OF THE FACULTY OF GRADUATE AND POSTDOCORAL STUDIES

PREDICTION OF TIME LAG IN VACUUM TUBES AND ITS IMPLICATIONS FOR CHARACTERIZATION OF MEMBRANES IN CONSTANT VOLUME SYSTEMS. EFFECT OF RESISTANCE- FREE ACCUMULATION TANK

BY

Farzaneh Shemshaki

A thesis submitted to the faculty of graduate and Postdoctoral Studies in partial fulfillment of the requirement for the Degree of

Master of Applied Science

In Chemical Engineering

Department of Chemical Engineering

UNIVERSITY OF OTTAWA

September 2005

Your file Votre référence
ISBN: 0-494-11408-8
Our file Notre référence
ISBN: 0-494-11408-8

ABSTRACT

The constant volume method is a well-known technique for measuring and monitoring low gas flows, as well as for characterizing porous and nonporous membranes. The major assumption of no resistance to gas transport downstream from the tested medium, on which this technique relies, was shown previously to fail in situations in which the gas accumulates in a long cylindrical tube of small cross sectional area. The previous analysis, because of the assumption of constant diffusion coefficient downstream from the tested medium, was limited to only short times after initiation of the flow in the testing system, and thus could not predict the full extend of the effects of resistance to gas accumulation.

In this project a "time limitation" of the previous analysis has been overcome by allowing the diffusion coefficient downstream from the tested medium to vary with pressure, describing this relationship using the empirical model of Knudsen. This required a numerical solution of the governing partial differential equation, which has been done by applying a finite difference scheme. The theoretically obtained pressure responses have been compared with the experimental pressure responses in two different flow cases, a constant flow and a time-dependent flow at a tube entrance. The former case was realized by using a low-flow mass flow controller as a flow source. The latter case was realized by using a homogeneous polymeric film, whose one side was instantaneously pressurized in a step-wise manner (time lag technique). The theoretical model slightly underestimates the resistance effects. This has been attributed to an unavoidable presence of a dead volume in the experimental system, i.e. the volume associated with valves, pressure sensors, bypass tubes, etc. A procedure for correcting the experimentally determined transport coefficients of gas in a membrane for the resistance effects has been developed and demonstrated.

An extreme example of dead volume is an accumulation tank attached to a collector tube. Practical constant volume systems may have several such tanks, which can be incorporated into the outflow volume depending on the anticipated gas flow. Because of their large cross-sectional area for flow, the accumulation tanks have practically negligible resistance to accumulation of gases, even at ultrahigh vacuum. The second part

of this project deals with the effect of a resistance-free accumulation tank on the resistance to gas transport in a cylindrical tube. To simplify the modeling, the accumulation tank was placed at the end of the tube, and the diffusion coefficient of the gas in tube was assumed to be constant. This allowed an analytical equation to be derived for the time lag of the tube in terms of the position of pressure sensor, the length and cross-sectional area of the tube, and the volume of the tank. In the derivation of this equation the governing partial differential equation along with the boundary conditions has been transferred into the Laplace domain and then after solving the resulting ordinary differential equation, a concept of asymptotic solution has been used.

The derived equation indicates a great effect of the accumulation tank on the resistance in the tube. More specifically, the tank introduces a large negative error in the time lag of the tube, whose magnitude increases with the distance from the tank. The theoretical results were compared with the experimental data obtained in a typical time lag experiment, and the actual error in the experimental time lag of the membrane due to the resistance to gas transport in the tube was even greater than the theoretically predicted error. The discrepancy between the experimental and theoretically predicted errors is due to the assumption of a constant diffusion coefficient in the tube, without which the derivation of the theoretical equation would not be possible.

The second part of this project indicates that the resistance to gas transport in the vacuum tube might significantly affect the experimentally determined transport coefficients of gas in a membrane, even when the length of tube in the outflow volume is minimized. Consequently, all the membrane data obtained using the time lag method in constant volume systems from the last half of the century should be re-examined.

Sommaire

Une méthode à volume constant est une technique bien connue pour mesurer et suivre les écoulements de gaz à faibles débits, ainsi que pour la caractérisation des membranes poreuses et non-poreuses. Cette technique, fondée sur l'hypothèse principale d'aucune résistance au transport de gaz en aval du milieu examiné, a été montrée à échouer lorsque le gaz s'accumule dans un long tube cylindrique de petite section transversale. L'analyse précédente, en raison de l'hypothèse d'un coefficient de diffusion constant en aval du milieu examiné, a été limitée seulement aux périodes courtes après le déclenchement de l'écoulement dans le système d'essai, et ne pouvait donc pas prévoir la totalité des effets de la résistance à l'accumulation de gaz.

Dans ce projet la "limitation temporelle" de l'analyse précédente a été surmontée en permettant au coefficient de diffusion en aval du milieu examiné de varier avec la pression à l'aide du modèle empirique de Knudsen. La solution des équations différentielles partielles régissantes a été obtenue par la méthode numérique des différences finies. Les profils de pression théoriques ont été comparés aux mesures expérimentales pour des écoulements constant et transitoire à l'entrée d'un tube. L'écoulement constant a été réalisé en employant un contrôleur massique à faible débit comme source d'écoulement. Alors que l'écoulement transitoire a été accompli en utilisant un film polymérique homogène, dont l'un côté a été instantanément pressurisé (technique du délai temporel). Le modèle théorique sous-estime légèrement les effets de résistance. Ceci a été attribué à une présence inévitable d'un volume mort dans le système expérimental, c.-à-d. le volume lié aux sondes de pression, aux valves, aux tubes de déviation (by-pass), etc... Une procédure a été développée et démontrée pour corriger les coefficients expérimentaux de transport de gaz dans la membrane et tenir compte des effets de résistance.

Un exemple extrême d'un volume mort est un réservoir d'accumulation fixé à un tube collecteur. Les systèmes pratiques à volume constant peuvent avoir plusieurs de tels

réservoirs, qui peuvent être incorporés au volume de sortie selon l'écoulement de gaz prévu. En raison d'une grande section transversale pour l'écoulement, les réservoirs d'accumulation ont une résistance pratiquement négligeable à l'accumulation de gaz même sous un vide ultra-haut. La deuxième partie de ce projet traite l'effet d'un réservoir d'accumulation sans résistance sur la résistance au transport de gaz dans un tube cylindrique. Afin de simplifier la modélisation, le réservoir d'accumulation a été placé à l'extrémité du tube, et on a assumé que le coefficient de diffusion du gaz dans le tube est constant. Ceci a permis d'obtenir une solution analytique du délai temporel du tube en termes de position de la sonde de pression, de longueur et section du tube, et du volume du réservoir. L'équation différentielle partielle régissante avec ses conditions frontières a été transférée dans le domaine de Laplace et puis après la solution de l'équation différentielle ordinaire résultante, un concept de solution asymptotique a été employé.

L'équation dérivée indique un effet important du réservoir d'accumulation sur la résistance dans le tube. Plus spécifiquement, le réservoir présente une grande erreur négative dans le délai temporel du tube, dont la grandeur augmente avec la distance du réservoir. Les résultats théoriques ont été comparés aux données expérimentales obtenues lors d'une expérience typique de délai temporel, et l'erreur réelle dans le délai temporel de la membrane dû à la résistance au transport de gaz dans le tube était même plus grande que l'erreur théorique prédite. La différence entre les erreurs expérimentale et théorique est due à l'hypothèse d'un coefficient de diffusion constant dans le tube, sans laquelle la dérivation de l'équation théorique ne serait pas possible.

La deuxième partie de ce projet indique que la résistance au transport de gaz dans le tube à vide pourrait significativement affecter les coefficients expérimentaux de transport de gaz dans la membrane même lorsque la longueur du tube dans le volume de sortie est minimisée. En conséquence, toutes les données de membrane obtenues en utilisant la méthode du délai temporel dans les systèmes de volume constant au cours de la dernière moitié du siècle devraient être examinées de nouveau.

ACKNOWLEDGEMENTS

I wish to express my gratitude to Professor B. Kruczek for his advises, guidance, and supporting me financially. His unforgettable support, bring it a deep respect to him in my heart forever.

I am also thankful to my family members and friends for supporting me unconditionally.

The technical support from machine shop of department of Chemical engineering cannot be ignored. Without their work, it would have been impossible to get to end of the experiments. Their friendly assistance with a wide range of practical knowledge is really appreciated, so I am deeply thankful to Louis Tremblay, Franco Ziroldo, and Gerard Nina.

TABLE OF CONTENTS

LIST OF TABLES

CHAPTER 2: PART II

CHAPTER 3

LIST OF FIGURES

CHAPTER 2: PART I

response was generated by solving numerically Eq. (4) in which D varies with pressure according to the empirical model of Knudsen. Parameters for the model: $Q(x=0,t)$ = 0.028 cm^3/min, L = 3.60 m, V = 80.4 x 10^{-6} m^3, T = 296 K, p_o = 0.13 Pa, f = 1.

Figure 8 Effect of time on a theoretical error in flow rate determined from the rate of pressure rise at two different distances from the MFC and for two different flow rates entering the tube. Parameters for the model: L = 3.60 m, V = 80.4 x 10^{-6} m^3, T = 296 K, p_o = 0.13 Pa, f = 1. Figure 8a shows the period between 0 and 20 s from the flow initiation; Figure 8b shows the period between 20 and 100 s from the flow initiation.

CHAPTER 2: PART II

Figure 1 Schematic diagram of the experimental CV system. P_1 and P_2 are the MKS pressure transducers (model 627B11TBC1B); P_f is the absolute pressure transducer; PR is the pressure regulator, and RV is the relief valve.

Figure 2 Progress of N_2 permeation experiment through PPO membrane monitored at two different distances from the membrane in a standard ¼" stainless steel tube of length L = 3.65 m. Initial pressure, p_o = 0.13 Pa; feed pressure p_f = 206.8 kPa; temperature T = 23°C.

Figure 3 Determination of the experimental time lag at different distances from the membrane. Gas: N_2; polymer: PPO; tube of length L = 3.65 m; initial pressure p_o = 0.13 Pa; feed pressure p_f = 206.8 kPa; temperature T = 23°C.

Figure 4 Modeling of the of N_2 permeation experiment through the PPO film at two different positions in the standard ¼" stainless steel tube using D_m = 6.05 x 10^{-12} [m^2/s] and P_m = 7.18 x 10^{-17} [m^3(STP)/s m Pa] determined by the least square method. Other parameters: tube length L = 3.65 m; initial pressure p_o = 0.13 Pa; feed pressure p_f = 206.8 kPa; temperature T = 23°C; membrane thickness l_m = 39.5 x 10^{-6} m.

CHAPTER 3

CHAPTER 5

APPENDIX A

Figure AA-1-a Pressure responses to the set flow of N_2 of 0.005 cm^3 (STP)/min at two positions x = 0.44 m and x = 2.22 m in a 3.60 m long tube with internal diameter of 0.00386 m. The initial pressure is equal to 0.4 Pa; comparing with pressure responses from non-constant D model at the same positions.

Figure AA-1-b Dimensionless Pressure response which indicates the error to the constant set flow of N_2 of 0.005 cm^3 (STP)/min at two positions x = 0.44 m and x = 2.22 m in a 3.60 m long tube with internal diameter of 0.00386 m. The initial pressure is equal to 0.4 Pa comparing with dimensionless pressure responses from non-constant D model at the same positions.

Figure AA-2-a Pressure responses to the constant set flow of N_2 of 0.01 cm^3 (STP)/min at two positions x = 0.44 m and x = 2.22 m in a 3.60 m long tube with internal diameter of 0.00386 m. The initial pressure is equal to 0.533 Pa comparing with pressure responses from non-constant D model at the same positions.

Figure AA-2-b Dimensionless Pressure response which indicates the error to the constant set flow of N_2 of 0.01 cm^3 (STP)/min at two positions x=0.44 m and x = 2.22 m in a 3.60 m long tube with internal diameter of 0.00386 m. The initial pressure is equal to 0.533 Pa comparing with dimensionless pressure responses from non-constant D model at the same positions.

Figure AA-3-a Pressure responses to the constant set flow of N_2 of 0.05 cm^3 (STP)/min at two positions x = 0.44 m and x = 2.22 m in a 3.60 m long tube with internal diameter of 0.00386 m. The initial pressure is equal to 1.4 Pa comparing with pressure responses from non-constant D model at the same positions.

Figure AA-3-b Dimensionless Pressure response which indicates the error to the constant set flow of N_2 of 0.05 cm^3 (STP)/min at two positions x = 0.44

m and x = 2.22 m in a 3.60 m long tube with internal diameter of 0.00386 m. The initial pressure is equal to 1.4Pa comparing with dimensionless pressure responses from non-constant D model at the same positions.

Figure AA-4-a Pressure responses to the constant set flow of N_2 of 0.1 cm^3 (STP)/min at two positions x = 0.44 m and x = 2.22 m in a 3.60 m long tube with internal diameter of 0.00386 m. The initial pressure is equal to 0.87 Pa comparing with pressure responses from non-constant D model at the same positions.

Figure AA-4-b Dimensionless Pressure response which indicates the error to the constant set flow of N_2 of 0.05 cm^3 (STP)/min at two positions x = 0.44 m and x = 2.22 m in a 3.60 m long tube with internal diameter of 0.00386 m. The initial pressure is equal to 1.4Pa comparing with dimensionless pressure responses from non-constant D model at the same positions.

Figure AA-5-a Pressure responses to the constant set flow of N_2 of 0.2 cm^3 (STP)/min at two positions x = 0.44 m and x = 2.22 m in a 3.60 m long tube with internal diameter of 0.00386 m. The initial pressure is equal to 0.667 Pa comparing with pressure responses from non-constant D model at the same positions.

Figure AA-5-b Dimensionless Pressure response which indicates the error to the constant set flow of N_2 of 0.2 cm^3 (STP)/min at two positions x = 0.44 m and x = 2.22 m in a 3.60 m long tube with internal diameter of 0.00386 m. The initial pressure is equal to 0.667 Pa comparing with dimensionless pressure responses from non-constant D model at the same positions.

Figure AB-1-a Effect of initial pressure, pressure responses to actual flow of 0.024 cm3 (STP)/min in 1/4" tube with length of 3.6 m at two different location x_1 = 0.44 m and x_2 = 0.222 m and initial pressure of 0.12 Pa. Comparison

APPENDIX B

Figure BA-1-a Pressure responses to the constant set flow of N_2 of 0.005 cm^3 (STP)/min at two positions x_1 = 0.44 m and x_2 = 2.22 m in a 2.34 m short tube with internal diameter of 0.00386 m. The initial pressure is equal to 0.76 Pa comparing with pressure responses from non-constant D model at the same positions.

Figure BA-1-b Dimensionless Pressure response which indicates the error to the constant set flow of N_2 of 0.005 cm^3 (STP)/min at two positions x_1 = 0.44 m and x_2 = 2.22 m in a 2.34 m short tube with internal diameter of 0.00386 m. The initial pressure is equal to 0.76 Pa comparing with dimensionless pressure responses from non-constant D model at the same positions.

Figure BA-2-a Pressure responses to the constant actual flow of N_2 of 0.032 cm^3 (STP)/min at two positions x_1 = 0.44 m and x_2 = 2.22 m in a 2.34 m short tube with internal diameter of 0.00386 m. The initial pressure is equal to 0.54Pa comparing with pressure responses from non-constant D model at the same positions.

Figure BA-2-b Dimensionless Pressure response which indicates the error to the constant actual flow of N_2 of 0.032 cm^3 (STP)/min at two positions x_1 = 0.44 m and x_2 = 2.22 m in a 2.34 m short tube with internal diameter of 0.00386 m. The initial pressure is equal to 0.54 Pa comparing with dimensionless pressure responses from non-constant D model at the same positions.

Figure BA-3-a Pressure responses to the constant actual flow of N_2 of 0.073 cm^3 (STP)/min at two positions x_1 = 0.44 m and x_2 = 2.22 m in a 2.34 m short tube with internal diameter of 0.00386 m. The initial pressure is equal to 0.54Pa comparing with pressure responses from non-constant D model at the same positions.

Figure BA-3-b Dimensionless Pressure response which indicates the error to the constant actual flow of N_2 of 0.073 cm^3 (STP)/min at two positions x_1 = 0.44 m and x_2 = 2.22 m in a 2.34 m short tube with internal diameter of 0.00386 m. The initial pressure is equal to 0.54 Pa comparing with dimensionless pressure responses from non-constant D model at the same positions.

Figure BA-4-a Pressure responses to the constant actual flow of N_2 of 0.12 cm^3 (STP)/min at two positions x_1 = 0.44 m and x_2 = 2.22 m in a 2.34 m short tube with internal diameter of 0.00386 m. The initial pressure is equal to 0.73 Pa comparing with pressure responses from non-constant D model at the same positions.

Figure BA-4-b Dimensionless Pressure response which indicates the error to the constant actual flow of N_2 of 0.12 cm^3 (STP)/min at two positions x_1 = 0.44 m and x_2 = 2.22 m in a 2.34 m short tube with internal diameter of 0.00386 m. The initial pressure is equal to 0.73 Pa comparing with dimensionless pressure responses from non-constant D model at the same positions.

Figure BA-5-a Pressure responses to the constant actual flow of N_2 of 0.22 cm^3 (STP)/min at two positions x_1 = 0.44 m and x_2 = 2.22 m in a 2.34 m short tube with internal diameter of 0.00386 m. The initial pressure is equal to 1.27 Pa comparing with pressure responses from non-constant D model at the same positions.

Figure BA-5-b Dimensionless Pressure response which indicates the error to the constant actual flow of N_2 of 0.22 cm^3 (STP)/min at two positions x_1 = 0.44 m and x_2 = 2.22 m in a 2.34 m short tube with internal diameter of 0.00386 m. The initial pressure is equal to 1.27 Pa comparing with dimensionless pressure responses from non-constant D model at the same positions.

Figure BB-1-a Effect of initial pressure, pressure responses to actual flow of 0.024 cm3 (STP)/min in 1/4" tube with length of 2.34 m at two different location x_1 = 0.44 m and x_2 = 0.222 m and initial pressure of 0.12 Pa. Comparison between the model with non-constant D and experimental data at the same conditions.

Figure BB-1-b Effect of initial pressure, dimensionless pressure responses to actual flow of 0.024 cm3 (STP)/min in 1/4" tube with length of 2.34 m at two different location x_1 = 0.44 m and x_2 = 0.222 m and initial pressure of 0.12 Pa. Comparison between the model with non-constant D and experimental data at the same conditions.

APPENDIX C

Figure CB-4- Pressure responses at two positions in ¼" tube with a length of 2.36 m and initial pressure of 23.84 Pa to determine transport properties of N2 in PPO membrane. The feed pressure is 206800 Pa and temperature is 23 ^{0}C.

Figure CB-5- Pressure responses at two positions in ¼" tube with a length of 2.36 m and initial pressure of 100.75 Pa to determine transport properties of N2 in PPO membrane. The feed pressure is 206800 Pa and temperature is 23 ^{0}C.

Figure CB-6- Pressure responses at two positions in ¼" tube with a length of 2.36 m and initial pressure of 301.73 Pa to determine transport properties of N2 in PPO membrane. The feed pressure is 206800 Pa and temperature is 23 ^{0}C.

Figures CC-1- Pressure responses at two positions in ½" tube with a length of 3.65 m and initial pressure of 0.13 Pa to determine transport properties of N2 in PPO membrane. The feed pressure is 206800 Pa and temperature is 23 ^{0}C.

Figures CC-2- Pressure responses at two positions in ½" tube with a length of 3.65 m and initial pressure of 5.61 Pa to determine transport properties of N2 in PPO membrane. The feed pressure is 206800 Pa and temperature is 23 ^{0}C.

Figures CC-3- Pressure responses at two positions in ½" tube with a length of 3.65 m and initial pressure of 104.3 Pa to determine transport properties of N2 in PPO membrane. The feed pressure is 206800 Pa and temperature is 23 ^{0}C.

Figures CC-4- Pressure responses at two positions in ½" tube with a length of 3.65 m and initial pressure of 300.26 Pa to determine transport properties of N2 in PPO membrane. The feed pressure is 206800 Pa and temperature is 23 ^{0}C.

Figure CD-1- Experiment with accumulation tank and PPO membrane. The effect of feed pressure on pressure responses at two positions x1=0.18, x2=0.81 in ¼" stainless steel tube with a length of 2.36 m and initial pressure of 0.13 Pa and feed pressure of 30 PSI. The volume of tank is V=2250 cm3 attached at the end of the tube, T=23 ^{0}C.

Figures CD-2- experiment with accumulation tank and PPO membrane. The effect of feed pressure on pressure responses at two positions x1=0.18, x2=0.81 in ¼" stainless steal tube with a length of 2.36 m and initial pressure of 0.13 pa and feed pressure of 50 PSI. The volume of tank is V=2250 cm^3 attached at the end of tube, T= 23 ^{0}C.

Figures CD-3- experiment with accumulation tank and PPO membrane. The effect of feed pressure on pressure responses at two positions x1=0.18, x2=0.81 in ¼" stainless steal tube with a length of 2.36 m and initial pressure of 0.13 pa and feed pressure of 90 PSI. The volume of tank is V=2250 cm^3 attached at the end of tube, T= 23 ^{0}C.

Figures CD-4- experiment with accumulation tank and PPO membrane. The effect of feed pressure on pressure responses at two positions x1=0.18, x2=0.81 in ¼" stainless steal tube with a length of 2.36 m and initial pressure of 0.13 pa and feed pressure of 110 PSI. The volume of tank is V=2250 cm^3 attached at the end of tube, T= 23 ^{0}C.

CHAPTER 1

Introduction

The time lag technique, originally developed by Daynes (1920), is the most common method for determining the diffusion coefficient of gas in porous and nonporous media. This technique involves a dynamic test in a constant volume (CV) system, in which a response to a step increase in pressure on one side of the tested medium (feed side) is monitored on the other side of the medium (permeate side) by a sensitive pressure sensor.

Figure 1 depicts a typical time lag experiment. Because of the resistance to gas transport in the tested medium, the pressure response immediately after initiation of the tests is not a linear function of time. The time lag of the tested medium (θ_m) is the intercept of the asymptote to the pressure response curve with the time axis. Knowing the volume of the permeate side of the CV system, the slope of the pressure response curve (dp/dt) allows determination of the gas flow rate (Q) through the tested medium.

The time lag experiments are always performed under transient conditions. This is because even when the pressure at the feed side is maintained constant, the pressure at the permeate side increases, and thus the driving force for the gas transport through the tested medium decreases as the experiment progresses. On the other hand, in practical systems the feed pressure is much greater than pressure increase at the permeate side, and a quasi steady condition, as in Fig. 1, is reached after the time corresponding to $2.5\theta_m$ (Crank and Park, 1968). If the tested medium is free of penetrant at the start of the experiment, the diffusion coefficient (D_m) is correlated with the time lag as follow (Daynes, 1920)

$$\theta_m = \frac{l_m^2}{6D_m} \tag{1}$$

where l_m is the thickness of the tested medium. Alternatively, the diffusion coefficient in the tested medium may be determined by considering the transient part of the pressure response curve in Fig. 1 using the correlations developed by Rogers *et al.* (1954).

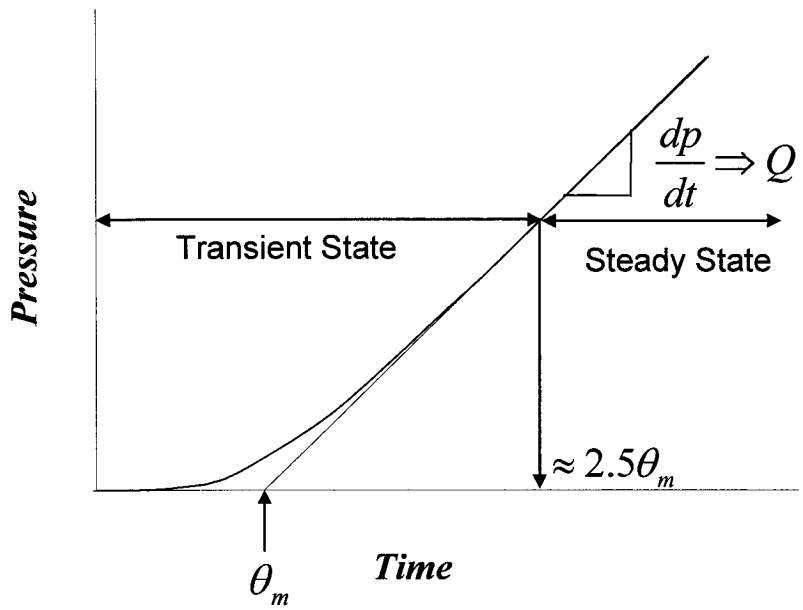

Figure 1. Pressure response in a typical time lag experiment.

The time lag technique requires the tested medium to be the only source of the resistance to gas transport in the system. A possibility of resistance to gas transport downstream from the tested medium was speculated by Kruczek and Matsuura (2000), who investigated gas permeability in sulfonated polyphynylene oxide membranes using a CV system described earlier by Mohammadi et al. (1995). The basis of this speculation was a 10% decrease in the gas

permeation rate resulting from only a 0.2% decrease in the pressure difference across the membrane (Kruczek and Matsuura, 2000).

The systematic studies of the resistance to gas transport downstream from the tested medium were started by Mr. R. Chapanian, who worked under the supervision of Dr. Kruczek from Sept. 2001 until Dec. 2003 (Chapanian, 2004). If there is any resistance downstream from the tested medium, it most likely arises from the gas transport in tubes of small cross sectional area. Consequently, Chapanian designed a simplified CV system consisting of a cylindrical tube, whose length and the internal diameter could be varied, and in which the pressure response was monitored at two different distances from the flow source simultaneously. The process of gas accumulation in the simplified CV is schematically presented in Fig. 2.

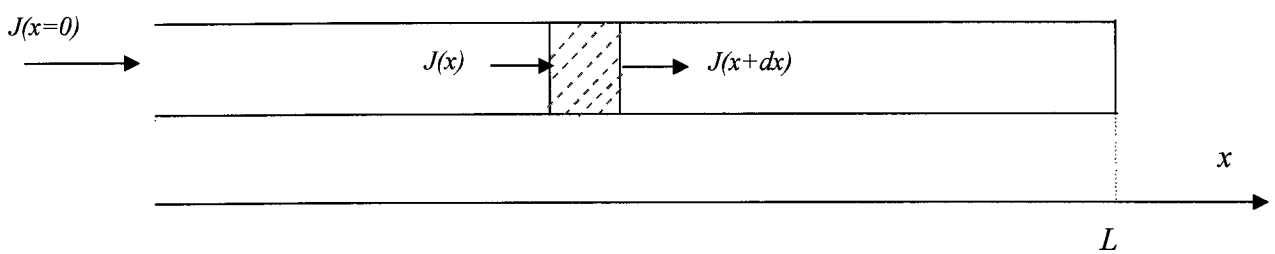

Figure 2 The process of accumulation in a simplified CV system, in which the outflow volume consists of a single tube.

The mass balance for a differential element of length *dx* in Fig. 2 can be expressed by:

$$J_x - J_{x+dx} = \frac{\partial c}{\partial t} dx \qquad (2a)$$

where J is the flux.

Dividing Eq. 2a by *dx* and letting *dx* approach to zero, leads to

$$\frac{\partial c}{\partial t} = -\frac{\partial J}{\partial x} \tag{2b}$$

Assuming that mass transfer in Fig 2 occurs by diffusion, the flux can be expressed using Fick's first law as follow:

$$J = -D\frac{\partial c}{\partial x} \tag{3}$$

where D is the diffusion coefficient of the gas in the tube.

At very low pressure (much lower than atmospheric pressure) and constant temperature that gas molecules are considered as rigid spheres, not exerting forces on one another, ideal gas law relates the gas pressure to its concentration as follow:

$$pV = NRT \;\Rightarrow c = \frac{N}{V} = \frac{p}{RT} \tag{4}$$

Substituting Eq. (4) into Eq. (3) leads to

$$J = -\frac{D}{RT}\frac{\partial p}{\partial x} \tag{5}$$

Assuming a constant diffusion coefficient of the gas in the tube, substitution of equations 4 and 5 into equation 2 leads to Fick's 2nd law of diffusion, a special case of the Stephan-Maxwell equations, as the governing partial differential equation (PDE)

$$\frac{\partial p(x,t)}{\partial t} = D\frac{\partial^2 p(x,t)}{\partial x^2} \tag{6}$$

where p is the pressure, t is the time, and x is the distance from the flow source. Before initiation of the flow, the pressure in the system is uniform (p_o), thus the initial condition for Eq. (6) is given by

$$p(x, t=0) = p_o = const. \tag{7}$$

The first boundary condition is expressed in terms of $J(x=0,t)$, i.e., the gas flux entering the tube

$$\frac{\partial p(x=0,t)}{dx} = -\frac{J(x=0,t)RT}{D} \tag{8}$$

Chapanian (2004) considered two different cases for $J(x=0,t)$. First, a constant gas flux entering the tube, which was realized by using a low-flow mass flow controller at the tube's entrance. Second, a time dependent gas flux entering the tube, which was realized by using a membrane at the tube's entrance and performing a typical time lag experiment. For the latter case, assuming a constant D_m, the applicability of Henry's law and the solution-diffusion mechanism (Zolandz and Fleming, 1992), the gas flux is given by (Barrer, 1939)

$$J(x=0,t) = \frac{p_f P_m A_m}{l_m A} + \frac{2p_f P_m A_m}{l_m A} \times \sum_{n=1}^{\infty} (-1)^n \exp\left(\frac{-n^2\pi^2 D_m t}{l_m^2}\right) \tag{9}$$

where P_m is the permeability coefficient of the gas in membrane, p_f is the feed pressure, and A_m and A are the membrane area and the internal cross section area of the tube, respectively. Regardless of the gas flux entering the tube, the second boundary condition (dead end system) for Eq. (6) is given by

$$\frac{\partial p(x=L,t)}{\partial x} = 0 \tag{10}$$

For the case of a constant gas flux entering the tube, Eq. (6) was solved analytically using the method of separation of variables. On the other hand, for the gas flux given by Eq. (9), the governing partial differential equation was solved numerically (Chapanian, 2004). Recently,

Kruczek et al. (2005) derived an expression for the time lag of the tube, which is valid for both a constant and time-dependent gas flux entering the tube.

The major limitation of the previous work by Chapanian was the assumption of a constant diffusion coefficient of the gas in tube. As a result, the obtained analytical and numerical solutions were valid for only a very short time after initiation of the flow into the system. This is because the diffusion coefficient of the gas in the tube depends on the pressure, which continuously increases as the gas accumulates in the tube. Therefore, to predict the pressure response without any time restriction, it is necessary to allow for the diffusion coefficient to vary with the pressure, which results in modification of the governing PDE

$$\frac{\partial p(x,t)}{\partial t} = \frac{\partial}{\partial x}\left(D \frac{\partial p(x,t)}{\partial x} \right) \tag{11}$$

This thesis consists of three papers, which are presented in Chapters 2, and 3, respectively. The first two papers are the extension of the Chapanian's project. In the first paper (Chapter 2, part I) the case of a constant gas flux at the tube entrance is considered, and in the second paper (Chapter 2, part II) the case of a time-dependent gas flux given by Eq. (9) is considered. The diffusion coefficient of gas in the tube is allowed to vary with pressure according to the empirical model of Knudsen (Loeb, 1961). The solution of the governing PDE is obtained numerically using a finite difference method in both cases.

Knudsen flow occurs when a gas molecule collides much more frequently with the walls of tube rather than with other gas molecules and diffusion coefficient of the gas is independent from gas pressure. Such conditions exits when the mean free path of gas molecules (λ) is much larger than the radius of the tube. Usually when $r/\lambda < 0.1$, it is assumed that gas transport is

governed by Knudsen diffusion (Kruczek et al. 2005). The conditions for Knudsen flow regime for N_2 molecules at 300 K in a tube having r = 0.193 cm (1/4" tube) is fulfilled at $p < 0.49$ Pa and for ½" tube it is fulfilled at $p < 0.185$ Pa (Kruczek et al. 2005).

At relatively high pressures, at which the collisions between gas molecules are much more frequent than collisions between gas molecules and the walls of the tube, the diffusion coefficient is directly proportional to pressure (Loeb, 1961).

$$D = \frac{pr^2}{8\eta} \tag{12}$$

At intermediate pressures, i.e. in a slip flow regime, in which the collisions with other gas molecules and the walls of tube are equally frequent, the diffusion coefficient can be estimated from the empirical model of Knudsen (Loeb, 1961)

$$D = \frac{pr^2}{8\eta} + \frac{2}{3} r \sqrt{\frac{8RT}{\pi M}} \left(\frac{1 + C_1 p}{1 + C_2 p} \right) \tag{13}$$

In comparison to Chapanian's project a small leak into the system was eliminated. As a result, the experiments were performed at the initial pressures as low as 0.13 Pa. For comparison, the lowest initial pressure achieved by Chapanian was 4.13 Pa. In addition, a bypass of a membrane cell was installed. This allowed direct evacuation of a feed side compartment rather than indirect evacuation through a membrane. As a result, not only much lower initial pressures were realized, but also the evacuation time prior to time lag experiments was reduced from five days in case of the Chapanian's project to several hours in the current work. All the experimental data presented in the first two papers were generated by me.

In the third paper (Chapter 3), we considered a more realistic geometry for the permeate side, in which the CV system consists of a tube and an accumulation tank at the end of the tube. Schematically, the process of gas accumulation in the modified CV system is presented in Fig. 3.

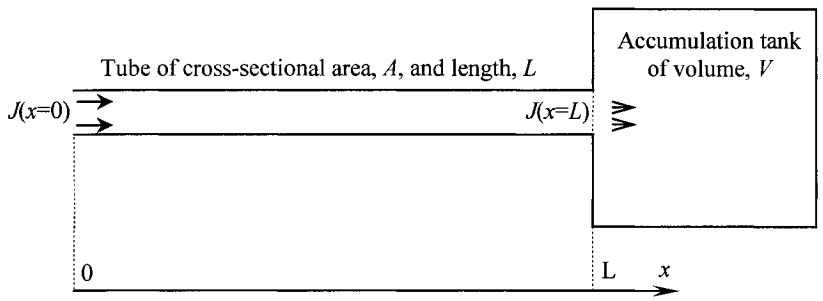

Figure 3 The process of accumulation in a CV system, in which the outflow volume consists of a tube and an accumulation tank attached at the end of the tube.

It is assumed that because of a relatively large internal diameter of the accumulation tank, there is no resistance to gas accumulation in the tank and the tank is well mixed (applicability of ideal gas law), the pressure in the tank will, at any time, be uniform and equal to the pressure at the end of the tube.

$$p_{\tan k}(x,t) = p_{tube}(x = L,t) \tag{14}$$

Then the rate of pressure increase in the tank is equal to the rate of pressure increase at the end of the tube.

$$\frac{dp(\text{tank})}{dt} = J(x = L,t)A\frac{RT}{V} = \frac{\partial p(x = L)}{\partial t} \tag{15}$$

The gas flux leaving the tube is given by the Fick's 1st law of diffusion

$$J(x = L,t) = -\frac{D}{RT}\frac{\partial p(x = L,t)}{dx} \tag{16}$$

Consequently, the incorporation of the tank at the end of the tube affects only the second boundary condition of Eq. (6)

$$\frac{\partial p(x = L,t)}{\partial t} = -\frac{DA}{V}\frac{\partial p(x = L,t)}{\partial x} \qquad (17)$$

All experiments in the system depicted in Fig. 3 were performed using a membrane cell. Thus the first boundary condition, the gas flux entering the tube, is given by Eq. (9). To obtain an analytical expression illustrating the effect of the tank's volume on the experimental time lag, the diffusion coefficient of gas in the tube was assumed constant and governing differential equation along with the boundary conditions were transformed into a Laplace's domain. Then, the concept of an asymptotic solution was utilized (Carslaw and Jaeger, (1959). Because of complexity of the analytical procedure, I was working on it along with Drs. Kruczek and Frisch, and my colleague S. Lashkari. On the other hand, all the experimental data presented in the third paper were generated by me.

It also important to emphasize that I also solved the governing differential equation for the case described depicted in Fig. 3, in which the gas flux entering the tube is constant. Because of the space and time limits, this work is not included in my thesis. A manuscript summarizing this work is currently under preparation.

References

Barrer, R. M., "Permeation, diffusion and solution of gases in organic polymers", Trans. Faraday Soc., 35, 628-643, (1939).

Carslaw, H. S. and J.C. Jaeger, "Conduction of Heat in Solids", Oxford at the Clarendon Press, 2nd Edition (1959), p. 402.

Chapanian, R., "Resistance to gas transport in high vacuum tubes and its implications for the measurement of permeability, diffusivity and solubility of gases polymeric films and membranes", M.A.Sc. Thesis, University of Ottawa, Ottawa, ON (2004).

Daynes, H. A., "The process of diffusion through a rubber membrane", Proc. R. Soc., A97, 286-307, (1920).

Kruczek, B., H. L. Frisch and R. Chapanian, "Analytical solution for the effective time lag of a membrane in a permeate tube collector in which Knudsen flow regime exists", J. Membrane Sci., 256, 57-65, (2005).

Kruczek B. and T. Matsuura, "Limitations of a constant-pressure type testing system in determination of gas transport properties of hydrophilic films", J. Membrane Sci. 177:129-142 (2000).

Loeb, L. B., "The Kinetic Theory of Gases," Dover Publications, Inc. New York, NY (1961), pp. 278-300.

Rogers, W. A., R. S. Buritz and D. Alpert, "Diffusion coefficient, solubility, and permeability for helium in glass", J. Appl. Phys., 25, 868-875, (1954).

Tabe Mohammadi, A., T. Matsuura and S. Sourirajan, "Design and construction of gas permeation system for the measurement of low permeation rated and permeate compositions", J. Membrane Sci., 98 (1995) 281.

Zolandz, R., Fleming, G.K., "Gas permeation", in: Sirkar, K. K. and W. S. W. Ho (Eds.), Membrane Handbook, Van Nostrand Reinhold, New York, NY (1992), pp. 25-35.

CHAPTER 2

Effects of Resistance to Accumulation of Gases in Vacuum Tubes. Part I. Error in Measurement of Gas Flow Rate by the Pressure Rise Technique

R. Chapanian, F. Shemshaki and B. Kruczek*

Department of Chemical Engineering
University of Ottawa
161 Louis Pasteur Street
Ottawa, ON K1N 6N5, Canada
Fax: (613) 562-5172
Phone: (613) 562-5800 ext. 6302
E-mail: kruczek@eng.uottawa.ca

*** To whom correspondence should be addressed.**

Abstract

Accumulative flow of gases into vacuum tubes has been studied, and a mathematical model based on Fick's 2nd law of diffusion has been developed to describe the pressure response in vacuum tubes to a constant flow rate of gases. Assuming that the diffusion coefficient of the gas in the tube is constant the analytical expression for the pressure response, as a function of the position in tube, was obtained. The obtained expression, which predicts the existence of a non-linear response immediately after commencing the flow, was verified in short-term experiments involving a constant flow of the gas via a low-flow mass flow controller into a vacuum tube, in which the pressure response was monitored simultaneously by two pressure transducers positioned at different distances from the mass flow controller. As time progresses the analytical model fails because the assumption of constant diffusion coefficient in the vacuum tube is no longer valid. Assuming the dependence of the diffusion coefficient on pressure according the empirical model of Knudsen, the governing partial differential equation was solved numerically. The numerical solution accurately predicts the pressure response in the tube without any time restriction. Since the diffusion coefficient of a gas in the tube generally increases with pressure, the non-linear response exists even a long time after initiation of the flow.

Key words: Very low gas flow rates, Constant volume systems, Diffusion, Diffusion coefficient of gas in tube.

Introduction

Gas flow rate is defined as the number of moles (N) of a particular gas species passing through a system at a given time, and the primary measurement is based on an equation of state. For the level of accuracy of flow measurements the ideal gas suffice (Arkilic et al., 1998)

$$pV = NRT \tag{1}$$

where p is the absolute pressure, V is the volume of the system, R is the universal gas constant, and T is the absolute temperature. A primary measurement can then be made and the flow rate is given by

$$Q = \frac{dN}{dt} = \frac{d}{dt}\left(\frac{pV}{RT}\right) \tag{2}$$

where Q is the molar flow rate. If V and T are constant, the flow rate becomes

$$Q = \frac{V}{RT}\frac{dp}{dt} \tag{3}$$

A technique which relies on Eq. (3) is commonly referred to as a constant-volume (CV) method. The CV method represents an indirect way of measuring of gas flows. On the other hand, techniques in which V varies while p is constant, i.e. constant-pressure (CP) methods, allow for a direct measurement of gas flow. In case of low flows, in the order of 10^{-9} mol/s or less, the measurements are usually performed using the CV method, because the CP methods such as piston displacement flow meters fail, or require sophisticated modifications (McCulloh et al., 1987). Low flows are important for performance characterization of nuclear and chemical vessels (Tison, 1994) and for the purpose of calibrating low-flow rate sensors, which might be required for specialized semiconductor processing (Arkilic et al., 1998). Low flows are also very common in applications involving characterization of materials for membrane separation.

The accuracy of the flow rate determined from Eq. (3) depends on the resolution of a pressure sensor. A flow rate of 10^{-9} mol/s accumulating in a 100 x 10^{-6} m^3 tank at ambient temperature for one minute increases the tank's pressure by only 1.5 Pa. If the tank were at atmospheric pressure, such a small rate of pressure increase would require an absolute pressure sensor with a dynamic range of six orders. This is why the measurements of low flows are typically performed at high vacuum. Another advantage of high vacuum is minimization of errors due to a temperature drift in CV systems (Arkilic et al., 1998).

Although not explicitly stated, Eq. (3) implies that there is no resistance to gas accumulation in the system. To define the resistance to gas accumulation, consider the following example. A CV system is initially at uniform pressure; there is no flow into the system. Suddenly, a flow is initiated at a fixed point of the system and as the gas accumulates the pressure in the system increases. There are three possible scenarios after initiation of the flow into the system,

1. The pressure increases but at any time it is uniform within the system;
2. A pressure difference develops and accumulation of the gas continues under a constant pressure difference within the system;
3. Accumulation of the gas occurs under a variable pressure difference within the system.

The conditions of no resistance to gas accumulation exist only in the first case. In the third case, the *dp/dt* will depend on a distance from the flow source, and thus the flow rate determined using Eq. (3) may be associated with an error. The same will be true in the second case before a constant pressure difference develops.

The situation in which a gas starts to flow into a fixed volume, which is initially at high vacuum, occurs, for example, during characterization of gas transport properties of semi-

permeable membranes in CV systems (Barrer, 1939). In extreme cases when turbo-molecular pumps are employed, the experiments may be performed at initial pressures in the order of 10^{-7} Pa (Sanchez et al., 2001). Without a turbo molecular pump the initial pressures are typically in the order of 10^{-1} Pa. It is well known that to maximize the conductance (minimize the resistance) of conduits they should be as short and wide-bored as possible. This is particularly true in case of flows at high vacuum (Chambers, 2005).

There are numerous references in the open literature in which the application of CV systems in membrane characterization is described; however, the information on the actual system configuration is rather limited. Generally, to accommodate membranes with different permeability coefficients it is a common practice to use systems having adjustable volume for gas accumulation. This is accomplished by connecting accumulation tanks having different volumes to a main gas line, which is typically a ¼" or ½" tube. Depending on the gas flow through the membrane one, two or more such tanks may be incorporated into the tube. As the number of accumulation tanks increases the length of tube must also increase. Interestingly, there seems to be no concern with possible resistance effects in the membrane literature, which is indicated by a general lack of information on the length and size of tubes in CV systems.

Assuming that accumulation is a diffusive process characterized by a constant diffusion coefficient, Kruczek et al. (2005) considered a pressure response to a gas flow in a closed cylindrical tube. Using Laplace transforms and the concept of asymptotic solution (Carslaw and Jaeger, 1959) they derived an expression for the time lag in the tube, which implies that gas accumulation occurs under a constant pressure difference within the tube. The final solution, however, does not predict that time required for the development of constant pressure difference within the tube, i.e., the time frame during which the flow rate calculated using Eq. (3) might be

associated with an error. The existence of time lag in the tube also implies potential problems in characterizing semi-permeable membranes in CV systems.

The purpose of this series of papers is to investigate the practical implications of a non negligible resistance to accumulation of gases in a simplified CV system consisting of a straight cylindrical tube. In Part I, an expression for the error in the flow rate determined from Eq. (3) is derived. To simplify the analysis, it is assumed that the flow into the system is constant. The derived expression is compared with the experimental data obtained in a system in which the pressure response is simultaneously monitored at two different distances from the tube entrance, i.e. from the flow source. The effects of the initial pressure and the actual flow rate into the tube are discussed. In Part II the effect of resistance to gas accumulation in the tube on the experimentally measured diffusion, permeability, and solubility coefficients of gas in a polymeric film is demonstrated, and a procedure for correcting the resulting errors is developed and discussed.

Theory

Mathematical Description of the Problem

In a simplest case, the outflow volume of a CV system can be modeled as a straight cylindrical tube of the length L and the internal radius r. Initially the tube is at uniform pressure (p_o)

$$p(x,t=0) = p_o \tag{4}$$

At $t > 0$, the gas starts to flow into the tube at its open end at a constant rate.

$$Q(x=0,t) = const. \tag{5}$$

Assuming that accumulation is a diffusive process, the following partial differential equation (PDE) is applicable

$$\frac{\partial p(x,t)}{\partial t} = \frac{\partial}{\partial x}\left(D \frac{\partial p(x,t)}{\partial x} \right) \tag{6}$$

where D is the diffusion coefficient of the gas in tube. It is important to emphasize that the diffusion coefficient in this analysis is directly proportional to conductance, which is a common parameter used in characterization of tubes by vacuum physicists (Chambers, 2005). The diffusion coefficient in Eq. (6) varies with pressure; therefore, it appears inside the brackets. The initial condition for Eq. (6) is given by Eq. (4). The first boundary condition for Eq. (6) is expressed in terms $Q(x = 0, t)$ using Fick's 1st law of diffusion

$$\frac{\partial p(x = 0,t)}{\partial x} = -\frac{Q(x = 0,t)}{\pi r^2} \frac{RT}{D} \tag{7}$$

where r is the internal radius of the tube. Using the heat transfer analogy, the closed end of the tube ($x = L$) is "perfectly insulated" and thus the pressure difference at the closed end of the tube is always zero. Consequently, the second boundary condition for Eq. (6) is given by

$$\frac{\partial p(x = L,t)}{\partial x} = 0 \tag{8}$$

Evaluation of the Diffusion Coefficient in Tube

When a gas molecule collides much more frequently with the walls of tube rather than with other gas molecules, i.e. the internal radius of the tube (r) is much smaller than the mean free path of gas molecules (λ), the diffusion coefficient is independent of pressure (Loeb, 1961)

$$D = \frac{2}{3} r \sqrt{\frac{8RT}{\pi M}} \tag{9}$$

where M is the molecular weight of the gas. The diffusion coefficient given by Eq. (9) is often referred as a Knudsen diffusion coefficient. The conditions at which Eq. (9) is valid are referred to as a Knudsen flow regime. They exist at high vacuum, because the mean free path of gas molecules is inversely proportional to the pressure

$$\lambda = \frac{RT}{\sqrt{2}\pi d^2 N_A}\frac{1}{p} \tag{10}$$

where d is the molecular diameter, and N_A is the Avogaro's number.

At relatively high pressures, at which the collisions between gas molecules are much more frequent than the collisions between gas molecules and the walls of tube, the diffusion coefficient is directly proportional to the pressure (Loeb, 1961)

$$D = \frac{pr^2}{8\eta} \tag{11}$$

where η is the dynamic viscosity of the gas. The diffusion coefficient given by Eq. (11) is often referred to a diffusion coefficient in a Poiseuille flow regime.

At intermediate pressures, i.e. in a slip flow regime, in which the collisions with other gas molecules and the walls of tube are equally frequent, the diffusion coefficient can be estimated from the empirical model of Knudsen (Loeb, 1961)

$$D = \frac{pr^2}{8\eta} + \frac{2}{3}r\sqrt{\frac{8RT}{\pi M}}\left(\frac{1+C_1 p}{1+C_2 p}\right) \tag{12}$$

where C_1 and C_2 are constants, which are determined by solving the following set of equations:

$$\frac{C_1}{C_2} = \frac{3\zeta\sqrt{\frac{\pi M}{RT}}p}{8\sqrt{2}\eta} \tag{13}$$

$$C_2 - C_1 = 0.6117\sqrt{\frac{M}{RT}}\frac{r}{\eta} \tag{14}$$

where ζ is the coefficient of slip, which is evaluated using the Maxwell's deduction from the kinetic theory of gases (Niven, 1965):

$$\zeta = \frac{\eta}{p}\sqrt{\frac{\pi RT}{2M}}\left(\frac{2-f}{f}\right) \tag{15}$$

where f is a fraction of gas molecules, which lose the momentum as a result of adsorption and desorption at the walls of tube. While f depends on the nature of gas and tube surface, it is usually close to unity (Stacy, 1923, and Van Dyke 1923). With f =1, the constants C_1 and C_2 become:

$$C_1 = 0.8768\sqrt{\frac{M}{RT}}\frac{r}{\eta} \tag{16}$$

$$C_2 = 1.4885\sqrt{\frac{M}{RT}}\frac{r}{\eta} \tag{17}$$

Regardless of the value of f, at very low pressures Eq. (12) approaches to Eq. (9), while at very high pressures Eq. (12) approaches to Eq. (11). Therefore, the empirical model of Knudsen may be used for the prediction of the diffusion coefficient of gas in a wide range of pressures.

Fig. 1 presents the plots of the diffusion coefficient of N_2 at 23°C as function of pressure in two standard stainless steel tubes having the internal radii of 0.193 cm and 0.510 cm, respectively, determined form the empirical model of Knudsen with f = 1. The horizontal dashed lines in Fig. 1, which represent the corresponding Knudsen diffusion coefficients determined from Eq. (9), are included for comparison. It should be pointed out that the empirical model of Knudsen predicts a minimum diffusion coefficient, which occurs in the slip flow regime. As the internal diameter of the tube increases the minimum diffusion coefficient shifts to lower pressures.

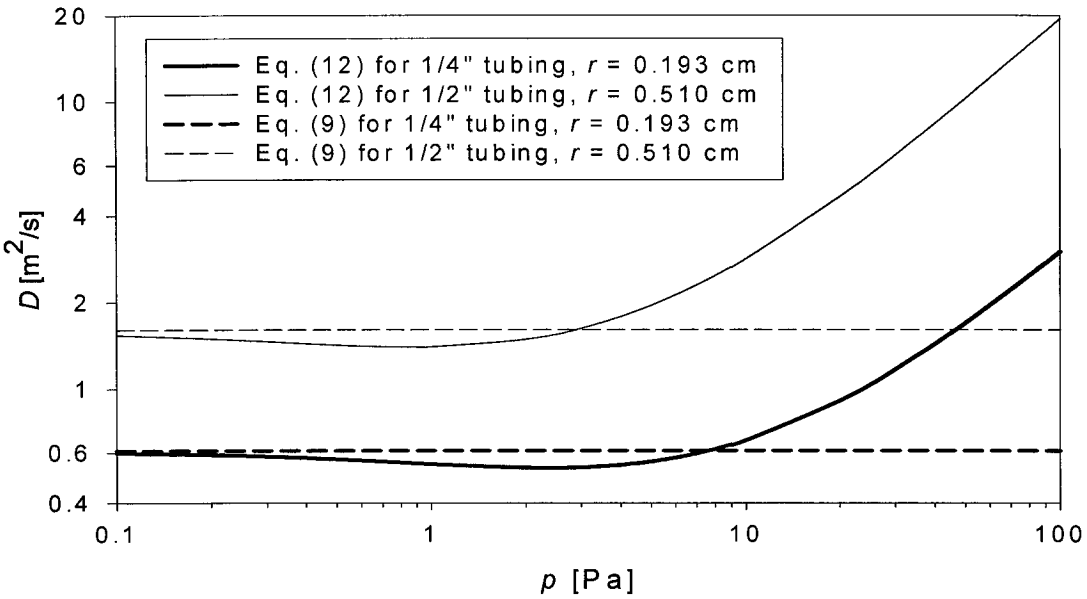

Figure 1. Effect of pressure on the diffusion coefficient of N_2 at 23°C in standard stainless steel tubes according to the empirical model of Knudsen (Loeb, 1961) - solid lines. Dashed lines indicate the corresponding coefficients in the Knudsen flow regime.

Experimental Set up and Procedure

The schematic diagram of the experimental set-up is presented in Fig. 2. It is composed of two parts, the feed part and the vacuum part, which are separated by a low-flow mass flow controller (MFC). The gas flowing through the MFC (MKS model M-200S) comes from a compressed nitrogen cylinder via an ultra high purity ceramic filter F (Swagelock model SS-SCF3-VR4-P-30).

The vacuum part consists of ¼" stainless steel tubing (Swagelock SS-T4-S-049-20) and several manually operated diaphragms (Swagelock model SS-DSVCR4) equipped with VCR fittings. In addition, the vacuum part is equipped with a buffer tank, a vacuum pump (Edwards model RV3), and two pressure absolute transducers (MKS model 627B11TBC1B) having a linear range from 0 to 13 33.2 Pa with a 0.27 x 10^{-1} Pa reading accuracy. The first pressure

transducer (P_1) is installed 0.44 m from the MFC and the second pressure transducer (P_2) is installed 2.23 m from the MFC. The total length the ¼" tube in the vacuum part is 3.76 m, while the active length, which is indicated as a thick line in Fig. 2, is 3.60 m. The active length of tubing may be decreased to 2.32 m by closing the valve V3. The volume associated with the difference between the total and the active lengths of tubing is considered to be a part of dead volume in the vacuum part. In addition, the dead volume includes the volumes associated with valves, fittings, and pressure transducers.

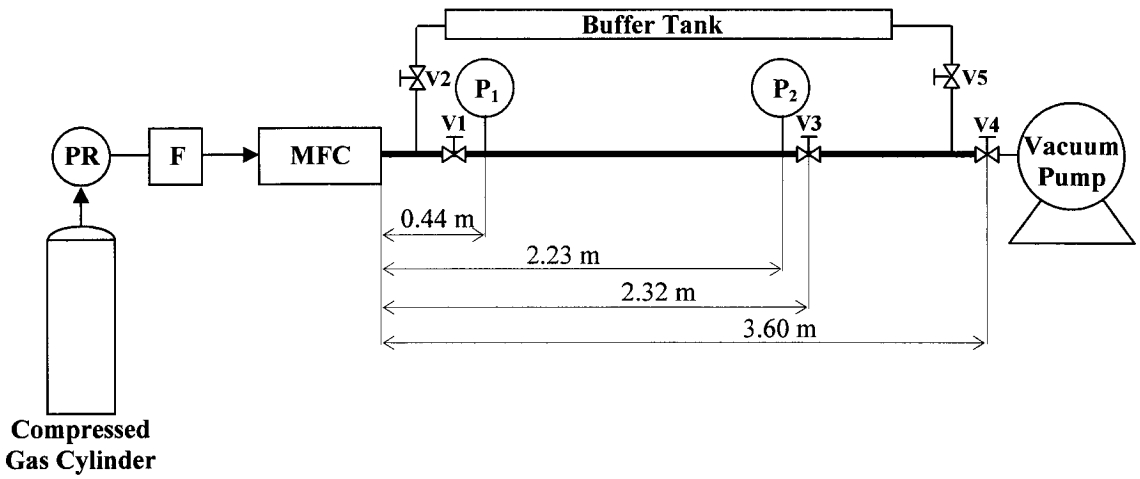

Figure 2 Schematic diagram of the experimental constant volume system. MFC is low-flow mass flow controller (MKS model M-200S), P_1 and P_2 are the absolute pressure transducers (MKS model 627B11TBC1B); F is the ultra high purity ceramic filter (Swagelock model SS-SCF3-VR4-P-30); PR is double stage pressure regulator; V*i* are the manually operated diaphragms (Swagelock model SS-DSVCR4).

With V3 open, the total volume of the vacuum part, as determined by a gas expansion technique, is 80.4 x 10^{-6} m^3. On the other hand, the volume of the active length of the ¼" tube (I.D. = 0.386 cm) is 42.1 x 10^{-6} m^3. The difference of 38.3 x 10^{-6} m^3 is the dead volume of the vacuum part. With V3 closed the total, active and dead volumes are 55.4 x 10^{-6} m^3, 27.1 x 10^{-6} m^3 and 28.3 x 10^{-6} m^3, respectively. The volume of the buffer tank is 8.69 x 10^{-3} m^3.

Before each experiment the tubes and the buffer tank were evacuated to a desired absolute pressure after which V4 was closed and the system was let to stabilize for several minutes. The experiments were performed at different initial absolute pressures ranging from 0.13 Pa to 300 Pa. Following a short stabilization period, the pressure in the vacuum part was monitored for at least an hour before initiating the flow. Any pressure rise during that time would be a leak. According to leak tests performed before each experiment, the leak rate was less than 5 x 10^{-7} cm^3/min, and thus was considered to be negligible. The experiments were started by setting a non-zero flow through the MFC with V1 and V5 closed, and V2 open. Depending on the set flow, it required from 2 to 15 s for the flow to stabilize, i.e., to reach the constant flow rate. During this period the gas was flowing into the buffer tank. It is important to indicate that according to the manufacturer's specification, the maximum flow rate through the MFC was 0.20 cm^3(STP)/min, with a control ability of 1 - 100% of the full scale. However, the actual flow rates of the gas through the MFC were considerably greater than the corresponding set flow rates. For example, for the set value of 0.002 cm^3 (STP)/min, which at 23°C corresponds to 0.0022 cm^3/min, the actual flow rate was 0.028 cm^3/min. The difference between the actual and set flows was decreasing with increase in the set flow. For the maximum set flow of 0.200 cm^3(STP)/min, which at 23°C corresponds to 0.217 cm^3/min, the actual flow rate was 0.227 cm^3/min.

Once the flow rate through the MFC stabilized, V2 was closed and at the same time V1 was opened. The dynamic pressures recorded by the pressure transducers and the flow rate through the MFC were recorded by a personal computer equipped with a LabView software. All experiments were performed at room temperature of 23 ± 0.5°C.

Results and Discussion

Simplification of the Governing PDE and Analytical Solution

The conditions for Knudsen flow regime, in which the diffusion coefficient is independent of pressure, exist when $r/\lambda < 0.1$. For a tube having $r = 0.193$ cm this requirement is fulfilled at $p < 0.49$ Pa. On the other hand, in a slip flow regime D varies with p, however the dependence of D on p, as shown in Fig. 1, is rather weak, even at pressures significantly greater than those for which $r/\lambda < 0.1$. For $r = 0.193$ cm, the diffusion coefficient does not differ more than 10% from the Knudsen diffusion coefficient up to 10 Pa. Therefore, it is not unreasonable to assume a constant diffusion coefficient in the tube, in case of which the governing PDE becomes Fick's 2nd law of diffusion

$$\frac{\partial p(x,t)}{\partial t} = D\frac{\partial^2 p(x,t)}{\partial x^2} \tag{18}$$

Eq. (18) may be solved analytically by the method of separation of variables (Haberman, 1983), and the solution is given by the following expression,

$$p(x,t) = p_o + \frac{Q(x=0,t)RT}{V}\left\{\left(t + \frac{(L-x)^2}{2D} - \frac{L^2}{6D}\right) - 2\sum_{n=1}^{\infty}\frac{(-1)^n}{\lambda_n^2}e^{-n^2\pi^2\tau}\cos\left[n\pi\left(1-\frac{x}{L}\right)\right]\right\} \tag{19}$$

where $\lambda_n = \frac{n\pi}{L}$ and τ is a dimensionless time defined as

$$\tau = \frac{Dt}{L^2} \tag{20}$$

The differentiation of Eq. (19) with respect to t gives the following expression,

$$\frac{dp}{dt} = \frac{Q(x=0,t)RT}{V}\left\{1 + 2\sum_{n=1}^{\infty}(-1)^n e^{-n^2\pi^2\tau}\cos\left[n\pi\left(1-\frac{x}{L}\right)\right]\right\} \tag{21}$$

For large τ the second term in the brackets on the right hand side is negligible, and Eq. (21) becomes Eq. (3). On the other hand, for small τ the second term in the brackets on the right hand side cannot be ignored, and thus *dp/dt* is not directly proportional to $Q(x=0,t)$. Consequently, for small τ the flow rate determined using Eq. (3) would be associated with an error. Since the first term in the brackets on the right hand side of Eq. (21) is unity, the relative error in the flow rate determined using Eq. (3) is given by the second term

$$\textit{Relative Flow Rate Error } (\%) = 100 \times \left\{ 2\sum_{n=1}^{\infty} (-1)^n e^{-n^2\pi^2\tau} \cos\left[n\pi\left(1-\frac{x}{L}\right)\right]\right\} \qquad (22)$$

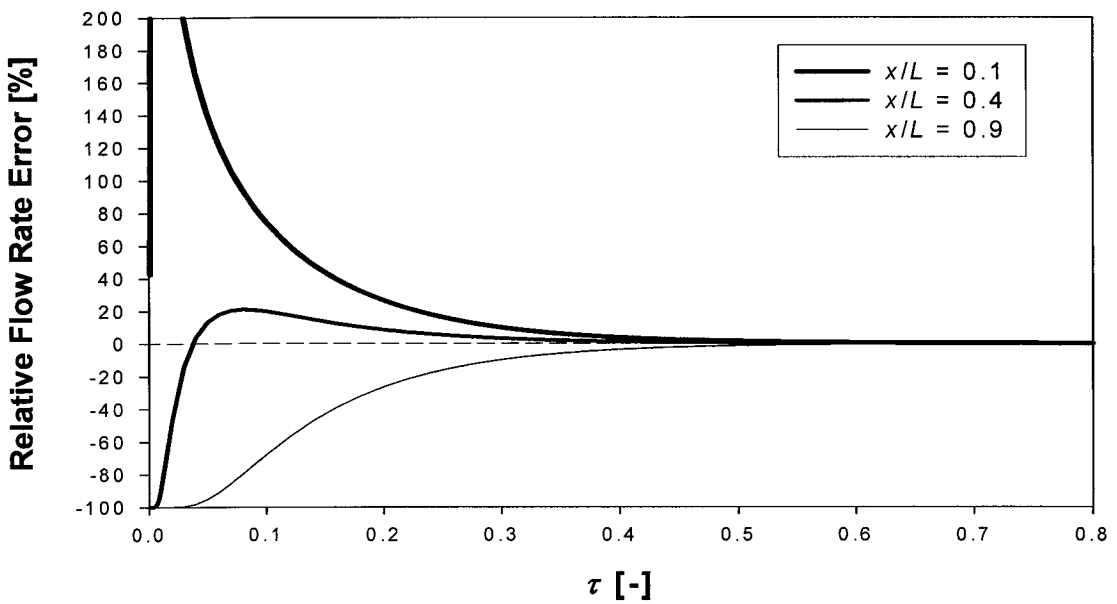

Figure 3 Application of the analytical solution for the pressure response in tube to predict the relative error in the flow rate determined from the rate of pressure rise as a function of dimensionless time at different dimensionless distances from the flow source.

Fig. 3 presents the plots of the relative error as a function of τ at three different locations corresponding to *x/L* of 0.1, 0.4 and 0.9, respectively. The negative error of 100% at given τ and

x/L, i.e., the zero flow rate, indicates that gas molecules entering the collection tube did not reach the given location. Although not shown in Fig. 3 even at $x/L = 0.1$ there is a negative error for $\tau < 0.00084$. Generally, for any $x/L < 0.5$ (e.g., $x/L = 0.4$) after being negative the error becomes positive and then approaches to zero. On the other hand, for $x/L \geq 0.5$ (e.g., $x/L = 0.9$) the error never becomes positive. While the value of the negative error is limited to -100%, there is no such limit for the positive error. For example, at $x/L = 0.1$ and $\tau = 0.006$, *Relative Error* = 280%. The error rapidly decreases with increase of τ, and for $\tau > 0.53$, the error becomes less than 1% at any x/L.

The actual time for which $\tau > 0.53$ depends on the diffusion coefficient and the length of tube. For N_2 at 0.13 Pa and 23°C in the tube having $r = 0.193$ cm, $D = 0.60$ m^2/s. Therefore, the conditions for $\tau > 0.53$ exist after 11.5 s when $L = 3.60$ m and after 4.9 s when $L = 2.32$ m. Since τ is inversely proportional to L^2, the time frame for a non linear pressure response decreases quickly with the length of tube. Also, because of an direct relationship between the diffusion coefficient and the radius of the tube, for a given tube length the time frame for a non linear pressure response decreases with increase of tube radius.

Experimental Results and Application of the Model

Fig. 4 presents the comparison of the experimental and theoretical pressure responses at 0.44 m ($x/L = 0.12$) and 2.23 m ($x/L = 0.62$) from the tube entrance to a constant flow of N_2 and the corresponding difference between these pressures, which will be referred to as a pressure gradient. The theoretical pressure responses were determined using Eq. (19) with the diffusion coefficient evaluated at the initial pressure of 0.13 Pa. It can be noticed that immediately after

initiation of flow the pressure at x/L = 0.12 (p_1) becomes greater than the pressure at x/L = 0.62 (p_2) i.e., a pressure difference starts to develop within the tube.

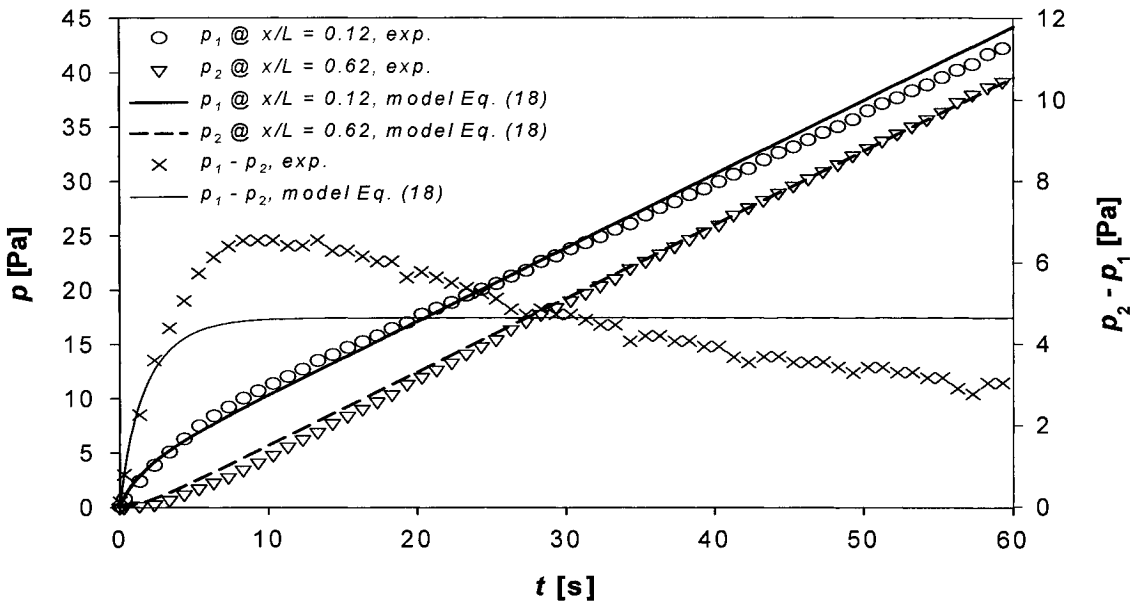

Figure 4 Comparison of the theoretical and experimental pressure responses in the ¼" tube at two different distances from the MFC. The theoretical pressure response was generated using a constant diffusion coefficient in tube D = 0.60 m^2/s. Other parameters: $Q(x=0,t)$ = 0.073 cm^3/min, L = 3.60 m, V = 80.4 x 10^{-6} m^3, T = 296 K.

It can be noticed during the first three seconds the pressure difference is well predicted by the theoretical model, but then the experimental pressure difference becomes greater than the theoretical one. The theoretical pressure difference increases during the first 10 s of the experiment, after which it remains constant. On the other hand, after reaching a maximum value of 6.5 Pa 8 s from the initiation of the flow, the experimental pressure difference gradually decreases as the experiment progresses. Consequently, 30 s after the initiation of the flow, the theoretical pressure difference becomes greater than the experimental one.

Fig. 5 presents the experimental pressure responses to similar flow rates of N_2 in two tests performed at different initial pressures, and the corresponding pressure differences. The maximum pressure difference of 6.5 Pa in the test performed at the initial pressure of 0.13 Pa is greater than the corresponding value of 3.7 Pa for the initial pressure of 25 Pa. In the tests performed at initial pressures greater than 25 Pa (not shown in Fig. 5) the maximum pressure difference continues to decrease. For example, in the experiment at the initial pressure of 104 Pa the maximum difference between p_1 and p_2 is just 1.4 Pa. A decrease in the maximum pressure difference with an increase in the initial pressure is consistent the relationship between the diffusion coefficient in the tube and the pressure. In other words, since the diffusion coefficient increases with pressure, the resistance to gas accumulation in the tube is lower at higher initial pressures.

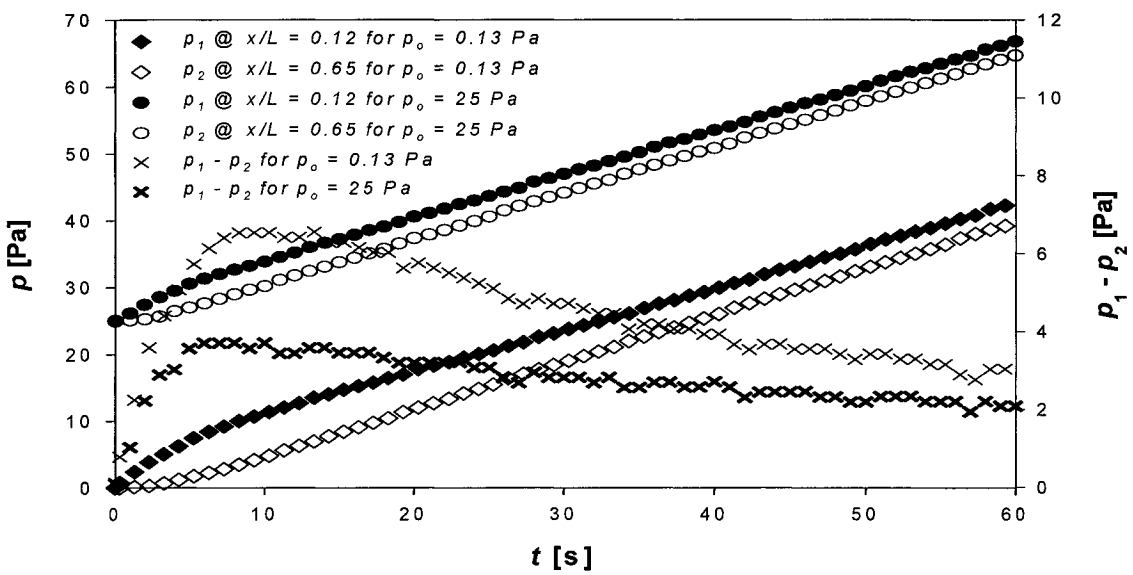

Figure 5 Effect of initial pressure in the ¼" tube of length L = 3.60 m on the pressure responses at two different distances from the MFC to the constant flow $Q(x=0,t)$ = 0.028 cm^3/min.

Fig. 6 presents the experimental pressure responses in two tests performed at similar initial pressures but using different flow rates of N_2 into the tube, and the corresponding pressure differences in the two tests. In the test in which $Q(x=0,t)$= 0.073 cm^3/min the maximum pressure difference is 13.1 Pa, while in the test in which $Q(x=0,t)$= 0.028 cm^3/min it is just 6.5 Pa. According to Eq. (19), the pressure difference within the tube is directly proportional to $Q(x=0,t)$; therefore an increase in the maximum pressure difference with the gas flow rate entering the tube is expected. On the other hand, increasing $Q(x=0,t)$ by a factor of 2.6 resulted in only doubling of the maximum difference between p_1 and p_2. To explain this apparent inconsistency it is necessary to point out that the maximum pressure differences in the experiments with $Q(x=0,t)$= 0.073 cm^3/min and $Q(x=0,t)$= 0.028 cm^3/min occur at 7 s and 8 s after initiation of the flow, respectively. As the pressure increases the diffusion coefficient in the tube increases and thus the pressure difference must gradually decrease as the time progresses, which is evident in all experiments shown in Figs. 4-6.

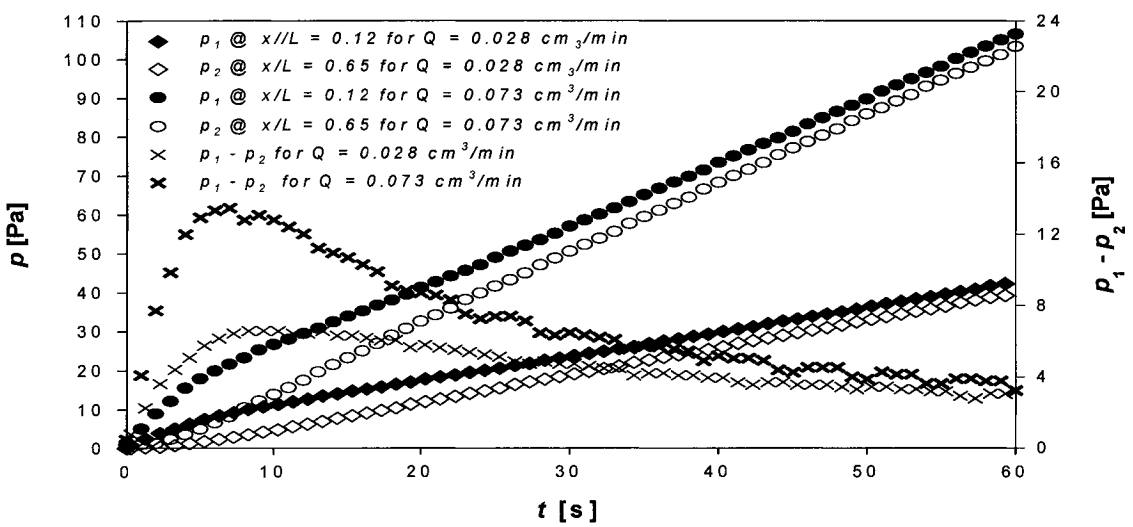

Figure 6 Effect of the flow entering the ¼" tube of length L = 3.60 m on the pressure responses at two different distances from the MFC. The initial pressure in both experiments, p_o < 0.5 Pa.

Therefore, although the pressure difference within the tube is directly proportional to the gas flow rate entering the tube, because of an increase in the diffusion coefficient with pressure, the "complete" pressure difference may not develop when the flow rate entering the tube is relatively high.

The mathematical model summarized by Eqs. (19) and (21) is valid provided that the pressure in the tube does not increase significantly from the value that existed before initiation of the flow. Therefore, the above equations are valid for a short time after initiation of the flow, in particular when the flow rate entering the tube is relatively low. To predict the pressure response without any time restrictions, one needs to solve Eq. (6) rather than its simplified version given by Eq. (18). Because of a dependence of D on p, Eq. (6) can only be solved numerically.

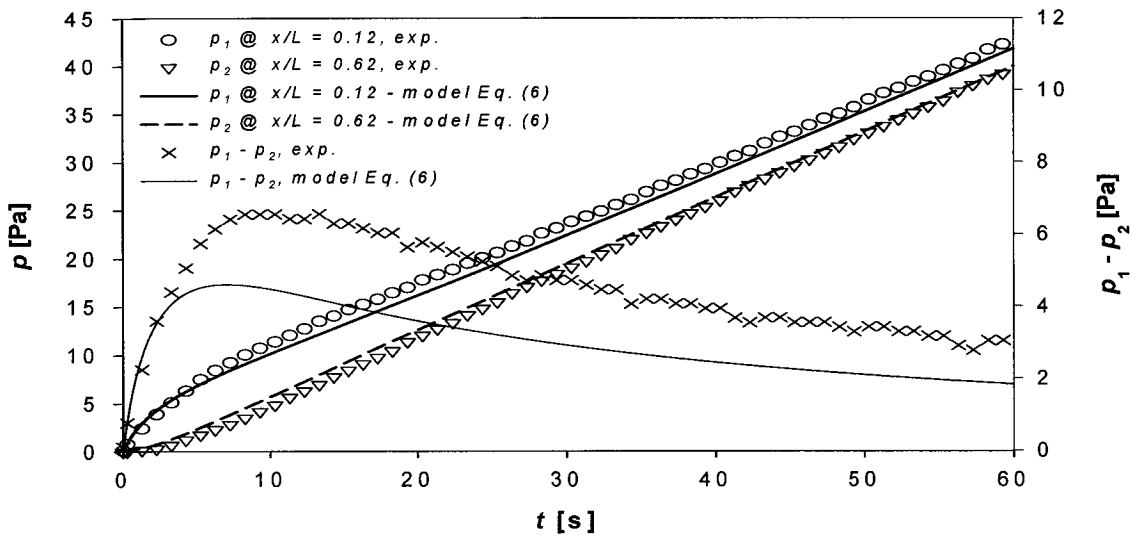

Figure 7 Comparison of the theoretical and experimental pressure responses in the ¼" tube at two different distances from the MFC. The theoretical pressure response was generated by solving numerically Eq. (4) in which D varies with pressure according to the empirical model of Knudsen. Parameters for the model: $Q(x=0,t)$ = 0.028 cm^3/min, L = 3.60 m, V = 80.4 x 10^{-6} m^3, T = 296 K, p_o = 0.13 Pa, f = 1.

Fig. 7 presents the comparison of the experimental and the theoretical pressure responses at $x/L = 0.12$ and $x/L = 0.62$ to a constant flow of N_2 and the corresponding pressure differences.

The theoretical pressure responses were obtained by solving numerically Eq. (6) with the diffusion coefficient varying according to the empirical model of Knudsen. It is evident that allowing D to vary with p improves the fit between the experimental and theoretical pressure responses. Although the maximum experimental pressure difference (6.5 Pa) is greater than the maximum theoretical pressure difference (4.5 Pa), the shape of both differences as a function of time is similar. The fact that the theoretical pressure difference is lower than the experimental pressure difference indicates that the model underestimates the actual resistance to gas accumulation in the tube.

There could be at least two possible reasons for this. First, if the actual diffusion coefficient of the gas in the tube were less than that predicted by the empirical model of Knudsen then the resistance effects would increase. The evaluation of D, requires the numerical value of f, which was assumed to be unity (though $0 \leq f \leq 1$). However, if f were < 1, D would increase rather than decrease. Therefore, underestimation of the resistance effects by the model is not the result of the assumed value of f. It is important to note that unlike the Knudsen and Poiseuille flow regimes, in which the respective diffusion coefficients are predicted from the first principles, the evaluation of the diffusion coefficient in the slip flow region is always associated with an uncertainty.

Secondly, in derivation of the model it was assumed that the gas accumulates in a straight cylindrical tube. However, as shown in Fig. 2, in addition to an active length of tube, which constitutes an active volume of the system, there was also a dead volume associated with the valves, pressure transducers and tubing connecting the main line with the buffer tank. The

presence of dead volume, which is unavoidable in practical systems, may be responsible for an additional resistance not accounted by the model.

Figs. 8a and 8b present the theoretical relative error in the flow rate determined from Eq. (3) as a function of time for two different flows. The error in Fig. 8 is determined from the following equation

$$Relative\ Flow\ Rate\ Error(\%) = 100 \times \left(\frac{(dp/dt)_t}{(dp/dt)_\infty} - 1 \right) \tag{23}$$

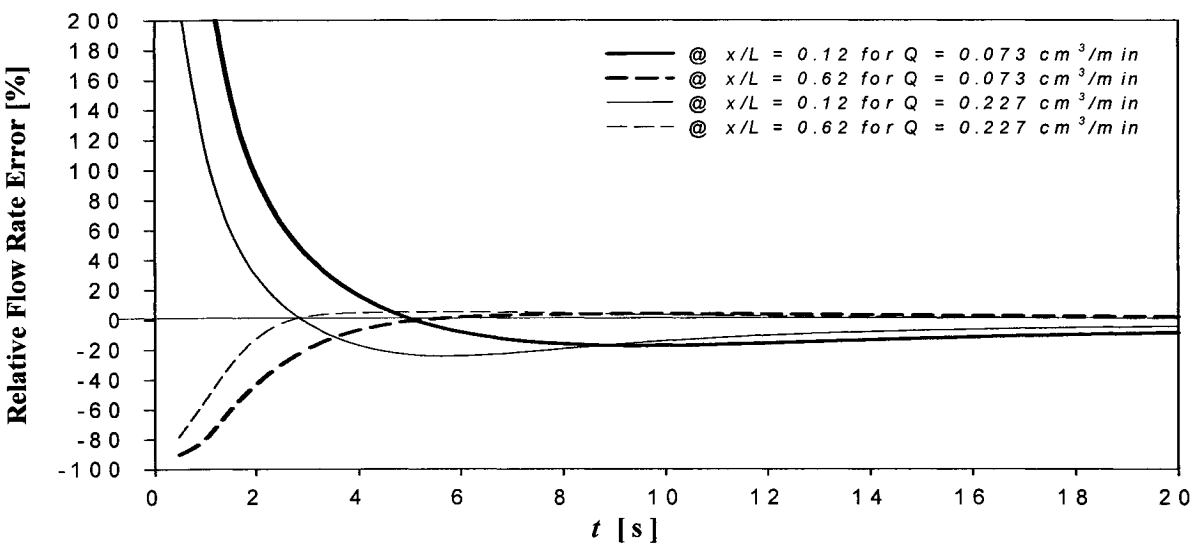

Figure 8.a Effect of time on a theoretical error in flow rate determined from the rate of pressure rise at two different distances from the MFC and for two different flow rates entering the tube. Parameters for the model: L = 3.60 m, V = 80.4 x 10^{-6} m^3, T = 296 K, p_o = 0.13 Pa, f = 1. Figure 8a shows the period between 0 and 20 s from the flow initiation.

The $(dp/dt)_t$ is the rate of pressure increase, at a given x/L, at time t, and $(dp/dt)_\infty$ is the rate of pressure increase that would exist if there were no resistance to gas accumulation. If $p_1 - p_2 > 0$, the $(dp/dt)_t$ is not constant. Once $p_1 - p_2 = 0$, $(dp/dt)_t = (dp/dt)_\infty$ = *constant*, provided

that $Q(x=0,t)$ = *constant*. In the actual experiments the pressure responses at 0.44 m and 2.23 m from the MFC become indistinguishable at pressures exceeding 5 00 Pa, i.e. after a relatively long time from initiation of the flow.

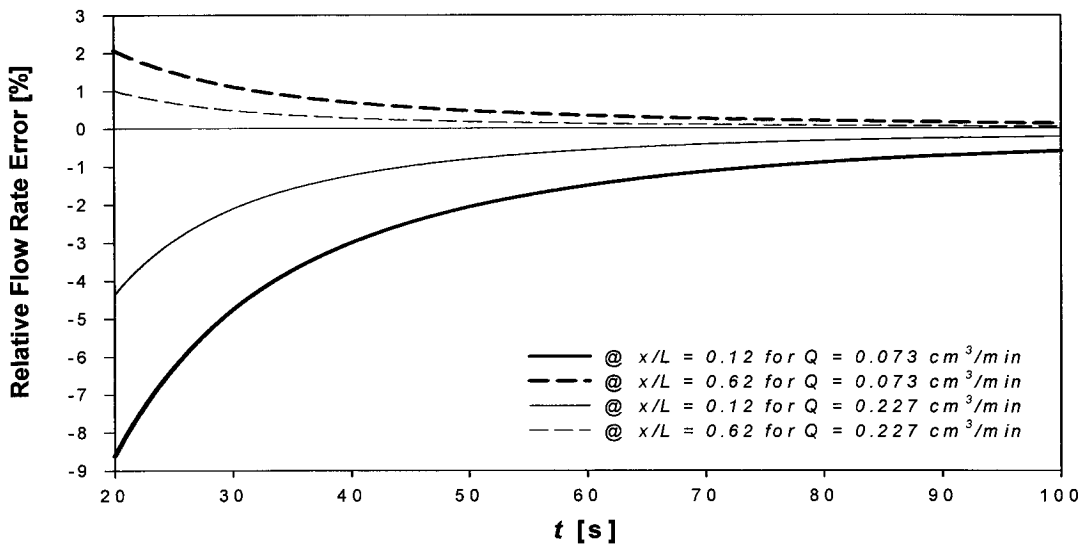

Figure 8.b Effect of time on a theoretical error in flow rate determined from the rate of pressure rise at two different distances from the MFC and for two different flow rates entering the tube. Parameters for the model: L = 3.60 m, V = 80.4 x 10^{-6} m^3, T = 296 K, p_o = 0.13 Pa, f = 1. Figure 8b shows the period between 20 and 100 s from the flow initiation.

It is important to note that, if D were constant, the relative error in the flow rate would be independent of the actual flow rate entering the tube. Moreover, as shown in Fig. 3, the error would practically disappear at $\tau > 0.53$, corresponding to $t > 11.5$ s for L = 3.60 m and D = 0.60 m^2/s. However, since D depends on p, the error depends on $Q(x=0,t)$. Moreover, even after 100 s from the initiation of the flow, the error is still present in both positions (Fig. 8b). As shown in Fig. 8a, immediately after initiation of the flow, there is a large positive error at x/L = 0.12. This positive error rapidly decreases with time, and changes sign reaching a maximum negative value

within several seconds. On the other hand, immediately after initiation of the flow there is a large negative error at $x/L = 0.65$. This negative error also rapidly decreases with time, and changes sign reaching the maximum positive value within several seconds. The time for the change depends on the flow rate entering the tube; the larger the flow the faster the sign changes. The magnitude of the maximum positive and negative errors depends on the flow rate; the larger the flow, the larger the maximum relative error. At longer times, the error in both ends of the tube asymptotically approaches zero, with errors at a given time being inversely related to the flow (Fig. 8b).

Conclusions

Pressure responses in a closed cylindrical tube, initially at uniform vacuum, to constant flows entering the tube have been studied at different distances. The system under investigation is relevant to applications involving CV systems for measurement and monitoring low flows and characterization of porous and non porous media in CV systems.

Assuming that accumulation is a diffusive process governed by Fick's 2nd law and a constant diffusion coefficient in tube, the governing PDE has been solved analytically. The diffusion coefficient, however, is a function of pressure and the analytical solution is applicable only for a short time after initiation of the flow into the tube. Immediately after initiation of the flow a pressure difference starts to develop within the tube leading to a nonlinear pressure response, i.e. to a significant error in the flow rate determined from the rate of pressure rise, which is well predicted by the analytical solution. The pressure difference within the tube reaches a maximum value and then it gradually decreases as the pressure in tube increases. Therefore, there are two distinct periods of nonlinear pressure response, before and after the

maximum pressure difference within the tube is reached. The first period, depending on the actual flow and the initial pressure lasts for several seconds, while the second one may last for several minutes. The magnitude of an error in the flow rate determined from the rate of pressure rise in the second period, depending on the distance from the flow source, can attain more than 20% and gradually decreases as the time progresses.

The existence of two distinct nonlinear periods in the pressure response to the flow results from a specific dependence of the diffusion coefficient on pressure as predicted by the transition from high vacuum (Knudsen flow regime) to low vacuum (Poiseuille flow regime) conditions. To predict the pressure response in the tube without any time restriction the dependence of the diffusion coefficient on pressure according to the empirical model of Knudsen has been assumed and the governing PDE has been solved numerically. The resulting theoretical pressure responses closely describe of the experimental pressure responses; however, the maximum theoretical pressure difference within the tube is lower than the experimental one indicating that the theoretical model underestimates the actual resistance to accumulation in the tube. This discrepancy is attributed to the presence of dead volume, which is unavoidable in real systems, and which is not accounted by the theoretical model.

Acknowledgement

The authors gratefully acknowledge the financial support for this project provided by the Natural Science and Engineering Research Council of Canada. The corresponding author expresses gratitude to Dr. M. Rodriguez for his valuable comments on this manuscript.

Nomenclature

C_1: Constant defined by Eq. (13), (Pa^{-1})

C_2: Constant defined by Eq. (14), (Pa^{-1})

d: Molecular diameter, (m)

D: Diffusion coefficient of gas in tube, (m^2/s)

f: Fraction of gas molecules that lose momentum as a result of adsorption and desorption at the walls of tube - assumed to be unity, (-)

L: Length of the collector tube, (m)

M: Molecular weight, (kg/mol)

N: Number of moles, (mol)

N_A: Avogaro's number, (mol^{-1})

p: Pressure, (Pa)

Q: Gas flow rate, (mol/s), or (cm^3/min)

r: Internal radius of tube, (m)

R: Universal gas constant, (J/mol·K)

t: Time, (s)

T: Absolute temperature, (K)

x : Position within the collector tube, (m)

Greek Symbols:

λ: Mean free path of gas molecules, (m)

η: Dynamic viscosity of the gas, (kg/m·s)

τ: Dimensionless time defined by Eq. (20), (-)

ζ: Coefficient of slip, (m)

References

Arkilic, E. B., M. A Schmidth and K. S. Breuer, "Sub-nonomol per second flow measurement near atmospheric pressure", Experiments in Fluids 25, 37-41 (1998).

Barrer, R. M., "Permeation, diffusion and solution of gases in organic polymers", Trans. Far. Soc., 35, 628-643, (1939).

Carslaw, H. S. and J.C. Jaeger, "Conduction of Heat in Solids", Oxford at the Clarendon Press, 2nd Edition (1959), p. 402.

Haberman, R., "Elementary Applied Partial Differential Equations with Fourier Series and Boundary Value Problems", Prentice-Hall Inc. (1983), pp. 28-123.

Kruczek, B., H. L. Frisch and R. Chapanian, "Analytical solution for the effective time lag of a membrane in a permeate tube collector in which Knudsen flow regime exists", J. Membrane Sci., 256, 57-65 (2005).

McCulloh, K. E., C. R. Tilford, C. D. Ehrlich and F. G. Long, Low-range flowmeters for use with vacuum and leak standards", J. Vac. Sci. Tech. A, 5, 376-381, (1987).

Loeb, L. B., "The Kinetic Theory of Gases," Dover Publications, Inc. New York, NY (1961), pp. 278-300.

Niven, W. D., "The Scientific Papers of James Clerk Maxwell", Dover Publications, New York, NY (1965), pp. 703-712.

Sanchez, J., C.L. Gijiu, V. Hynek, O. Muntean and A. Julbe, "The application of transient time-lag method for the diffusion coefficient estimation on zeolites composite membranes", Sep. Purification Tech., 25, 467-474, (2001).

Stacy, L. J., "A determination by the constant deflection method of the value of the coefficient of slip for rough and for smooth surfaces in air", Phys. Rev., 21, 239-249, (1923).

Van Dyke, K. S., "The coefficients of viscosity and slip of air and of carbon dioxide by the rotating cylinder method", Phys. Rev., 21, 250-265, (1923).

Captions for Figures

Figure 1 Effect of pressure on the diffusion coefficient of N_2 at 23°C in standard stainless steel tubes according to the empirical model of Knudsen (Loeb, 1961) - solid lines. Dashed lines indicate the corresponding coefficients in the Knudsen flow regime.

Figure 2 Schematic diagram of the experimental constant volume system. MFC is low-flow mass flow controller (MKS model M-200S), P_1 and P_2 are the absolute pressure transducers (MKS model 627B11TBC1B); F is the ultra high purity ceramic filter (Swagelock model SS-SCF3-VR4-P-30); PR is double stage pressure regulator; V*i* are the manually operated diaphragms (Swagelock model SS-DSVCR4).

Figure 3 Application of the analytical solution for the pressure response in tube to predict the relative error in the flow rate determined from the rate of pressure rise as a function of dimensionless time at different dimensionless distances from the flow source.

Figure 4 Comparison of the theoretical and experimental pressure responses in the ¼" tube at two different distances from the MFC. The theoretical pressure response was generated using a constant diffusion coefficient in tube D = 0.60 m^2/s. Other parameters: $Q(x = 0, t) = 0.073$ cm^3/min, L = 3.60 m, $V = 80.4 \times 10^{-6}$ m^3, T = 296 K.

Figure 5 Effect of initial pressure in the ¼" tube of length L = 3.60 m on the pressure responses at two different distances from the MFC to the constant flow $Q(x = 0, t) = 0.028$ cm^3/min.

Figure 6 Effect of the flow entering the ¼" tube of length L = 3.60 m on the pressure responses at two different distances from the MFC. The initial pressure in both experiments, $p_o <$ 0.5 Pa.

Figure 7 Comparison of the theoretical and experimental pressure responses in the ¼" tube at two different distances from the MFC. The theoretical pressure response was generated by solving numerically Eq. (4) in which D varies with pressure according to the empirical model of Knudsen. Parameters for the model: $Q(x=0,t)=$ 0.028 cm^3/min, L = 3.60 m, V = 80.4 x 10^{-6} m^3, T = 296 K, p_o = 0.13 Pa, f = 1.

Figure 8 Effect of time on a theoretical error in flow rate determined from the rate of pressure rise at two different distances from the MFC and for two different flow rates entering the tube. Parameters for the model: L = 3.60 m, V = 80.4 x 10^{-6} m^3, T = 296 K, p_o = 0.13 Pa, f = 1. Figure 8a shows the period between 0 and 20 s from the flow initiation; Figure 8b shows the period between 20 and 100 s from the flow initiation.

.

Abstract

The time lag technique has been widely used for the determination of diffusion coefficient of gases in porous and non-porous media. In case of solution-diffusion membranes this concept is even more appealing because in addition to the diffusion coefficient, the permeability and solubility coefficients can be determined from a single gas permeation experiment. In this paper, the effects of resistance to accumulation of gases in cylindrical vacuum tubes on the experimentally determined diffusion, permeability and solubility coefficients are evaluated. The resistance effects are well predicted by modeling the accumulation as a diffusive process governed by Fick's 2^{nd} law of diffusion with the diffusion coefficient of the gas downstream from the membrane predicted by the empirical model of Knudsen. A procedure has been developed to correct errors in the experimentally determined transport coefficients for the case of the permeating gas that accumulates in a straight cylindrical tube.

Key words: Resistance to Gas Accumulation, Time Lag, Diffusion Coefficient, Polyphenylene Oxide

Introduction

The mechanism of gas transport through practical polymeric gas separation membranes is exclusively described by the solution-diffusion mechanism. In this model the permeability coefficient (P_m) is a fundamental property of materials, which is expressed as a product of a thermodynamic factor (S_m) called the solubility coefficient, and a kinetic parameter (D_m) called diffusion coefficient (Zolandz and Fleming, 1992)

$$P_m = S_m D_m \tag{1}$$

The diffusion coefficient of a gas in a homogeneous membrane is determined experimentally using the concept of time lag. A common experimental technique involves the procedure in which the inflow and outflow volumes of a constant volume (CV) system are evacuated to the absolute vacuum or to the lowest possible pressure so that the membrane is degassed initially. The inflow volume is then instantaneously pressurized and the resulting pressure response at the permeate side of membrane is monitored. If the membrane is initially free from the diffusing gas and after pressurization the concentration of the gas is constant at the feed face of membrane and zero at the permeate face of membrane, D_m is correlated with the time lag of membrane (θ_m) by the following equation

$$\theta_m = \frac{l_m^2}{6D_m} \tag{2}$$

where l_m is the membrane thickness. The time lag of the membrane is the intercept of the asymptote of the pressure response curve with the time axis. Equation (2) was first deducted by Daynes (1920).

The permeability coefficient is evaluated from the slope (dp/dt) of the asymptote used for the determination of θ_m

$$P_m = \frac{V v_{STP} l_m}{R T A_m p_f} \frac{dp}{dt} \tag{3}$$

The V is the outflow volume, v_{STP} is the volume of one mole of gas at standard temperature and pressure, R is the universal gas constant, T is the absolute temperature, A_m is the membrane area, and p_f is the feed pressure. It is important to note that p_f in Eq. (3) represents the pressure difference across the membrane. This implies that the pressure at the permeate side of membrane is zero. Knowing D_m and P_m, allows determination of S_m from Eq. (1). Thus, the three gas transport coefficients can be evaluated based on the asymptote of the pressure response curve in a single gas permeation experiment (Barrer, 1939).

The accuracy of the time lag given by Eq. (2) depends on the accuracy of the slope of the asymptote. It has been suggested that steady state flow is achieved, to a good approximation, after three time lags (Crank and Park, 1968). On the other hand, after three time lags the assumption of zero concentration at the permeate face of membrane may no longer be valid. Rogers *et al.* (1954) developed the analysis for the determination of the diffusion coefficient from the pressure response before the steady flow is attained, but even then the assumption of zero concentration at the permeate face of membrane requires an infinitely large outflow volume. The mathematical solution when the outflow volume is finite and thus the concentration varies with time at the permeate face of membrane was obtained by Paul and Dibenedetto (1965). Jenkins *et al.* (1970) showed that the assumption of steady state flow after three time lags leads to a systematic overestimation of D_m by c.a. 4% even when the outflow volume is infinitely large. Frisch

(1962) considered permeation with non-Fickian diffusion and provided an analytical evaluation of the asymptotic solution where numerical techniques would otherwise be required. Rutherford and Do (1997) reviewed the time lag technique and summarized solutions of the diffusion equation for different boundary conditions.

In all these landmark papers referenced above it was assumed that the entire resistance to gas transport during the gas permeation experiment comes from the tested medium. The possibility of resistance to gas transport downstream from the tested medium was recently considered by Kruczek et al. (2005). Assuming that gas accumulation is a diffusive process characterized by a constant diffusion coefficient and that the process takes place is a closed cylindrical tube, they derived the following expression for an experimental time lag (θ_{exp})

$$\theta_{exp} = \theta_m + \frac{L^2}{6D} - \frac{(L-x)^2}{2D} \tag{4}$$

where L is the length of tube, x is the distance from the membrane, and D is the diffusion coefficient of the gas in tube. It is evident from Eq. (4) that if a tube is long and D is small, θ_{exp} may be different from θ_m and the difference, i.e. an error in time lag, depends on the location of a pressure sensor. The assumption of constant D implies that the slope of asymptote does not depend on the distance from the membrane. However, as shown in Part I, the slope of the asymptote should increase with the distance from the membrane (Chapanian et al., 2005). If so, Eq. (4) would not accurately predict the experimental time lag, making impossible the accurate correction of the resistance effects.

The purpose of Part II of this series is to experimentally demonstrate the effects of the resistance to accumulation of gas in a long cylindrical tube on the diffusion,

permeability and solubility coefficients of gas in membrane determined by the time lag method. It is also desired to develop an analytical procedure that would allow correcting the errors resulting from the resistance effects in the above transport coefficients.

Mathematical Description of the Process

The mathematical description of the problem with membrane is similar to the mathematical description of the problem with a mass flow controller (Chapanian et al., 2005). Thus, the governing partial differential equation (PDE), the initial and boundary conditions are given by the following equations

$$\frac{\partial p(x,t)}{\partial t} = \frac{\partial}{\partial x}\left(D \frac{\partial p(x,t)}{\partial x} \right) \tag{5}$$

$$p(x,t=0) = p_o \tag{6}$$

$$\frac{\partial p(x=0,t)}{\partial x} = -\frac{Q(x=0,t)}{\pi r^2} \frac{RT}{D} \tag{7}$$

$$\frac{\partial p(x=L,t)}{\partial x} = 0 \tag{8}$$

With a mass flow controller replaced by a membrane cell, the gas flow entering the tube, which must be the same as the gas flow emerging from the membrane, will not be constant. The gas flow emerging from the membrane depends on the membrane properties and the boundary conditions for the membrane.

Assuming a constant diffusion coefficient of the gas in membrane (D_m), the concentration of the gas in membrane (c) after a step increase in feed pressure is governed by Fick's second law of diffusion

$$\frac{\partial c(x',t)}{\partial t} = D_m \frac{\partial^2 c(x',t)}{\partial x'^2} \tag{9}$$

where x' is the distance from the feed-face of the membrane. In the simplest case, if before pressurization both sides of the membrane were degassed, and during the experiment the pressure in the permeate collector tube was increasing only slightly, the following initial and boundary conditions would be applicable (Barrer 1939),

$$c(x', t = 0) = 0 \tag{10}$$

$$c(x' = 0, t) = c_f = \frac{p_f P_m}{D_m} = const. \tag{11}$$

$$c(x' = l_m, t) \approx 0 \tag{12}$$

where c_f is the gas concentration at the feed face of the membrane after initiation of the experiment.

Solving Eq. (8) by the separation of variables leads to the following expression (Barrer, 1939)

$$c(x',t) = \frac{p_f P_m}{D_m}\left(1 - \frac{x'}{l_m}\right) - 2\frac{p_f P_m}{D_m \pi} \times \sum_{n=1}^{\infty} \frac{1}{n} \sin\left(\frac{n\pi x'}{l_m}\right) \exp\left(-\frac{D_m n^2 \pi^2 t}{l_m^2}\right) \tag{13}$$

The gas flow emerging from the membrane and hence the gas flow entering the tube can be expressed using Fick's first law of diffusion

$$Q(x = 0, t) = Q(x' = l_m, t) = -D_m A_m \frac{\partial c}{\partial t}(x' = l_m, t) \tag{14}$$

Differentiation of Eq. (13) and substitution of the resulting expression into Eq. (14) leads to

$$Q(x = 0, t) = \frac{p_f P_m A_m}{l_m} + \frac{2 p_f P_m A_m}{l_m} \times \sum_{n=1}^{\infty} (-1)^n \exp\left(\frac{-n^2 \pi^2 D_m t}{l_m^2}\right) \tag{15}$$

Substitution of Eq. (15) into Eq. (7) gives the final expression of the first boundary condition for Eq. (5).

$$\frac{\partial p(x=0,t)}{dx} = -\frac{RTA_m p_f P_m}{D\pi r^2 l_m}\left\{1+2\sum_{n=1}^{\infty}(-1)^n \exp\left(\frac{-n^2\pi^2 D_m t}{l_m^2}\right)\right\} \qquad (16)$$

The diffusion coefficient of the gas in tube (D) can be estimated from the empirical model of Knudsen, as illustrated in Part I of this series (Chapanian et al., 2005).

Experimental

Fig. 1 presents the schematic diagram of the CV system used for the determination of the diffusion, permeability, and solubility coefficients of gas in membrane. A membrane is sandwiched between the two cylindrical parts of a stainless steel membrane cell. The effective area for gas permeation in the cell, A_m = 9.08 x 10^{-4} m^2.

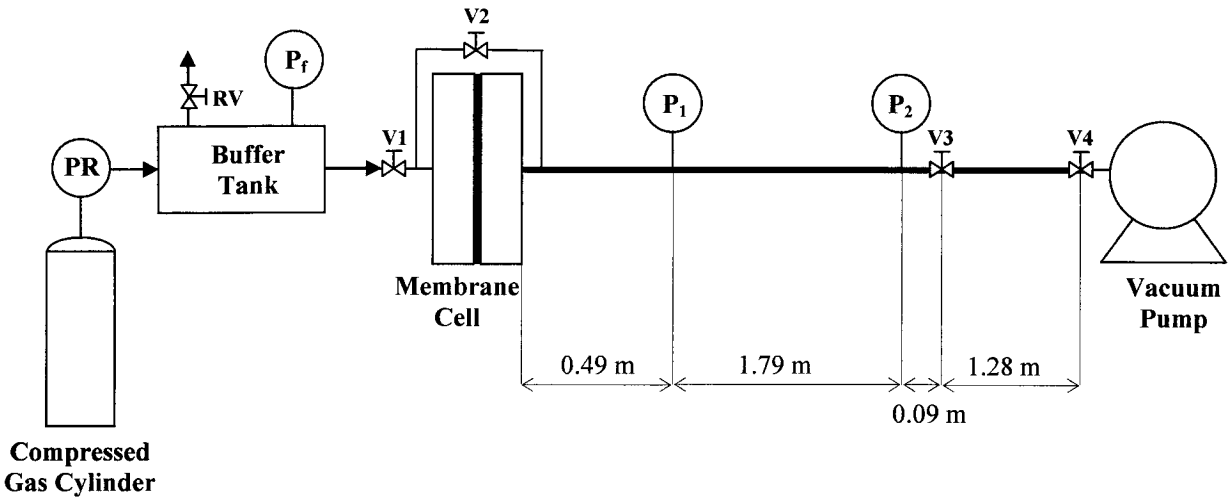

Figure 1 Schematic diagram of the experimental CV system. P_1 and P_2 are the MKS pressure transducers (model 627B11TBC1B); P_f is the absolute pressure transducer; PR is the pressure regulator, and RV is the relief valve.

The inflow volume consists of a standard ¼" stainless steel tubing and a buffer tank of volume 26.50×10^{-3} m^3, which can be pressurized up to 931 kPa using a gas from a compressed gas cylinder. The buffer tank is equipped with a relief valve (RV) and an absolute pressure gauge (P_f) having a 0 - 1207 kPa range and a 6.9 kPa reading accuracy. The reading of this pressure gauge during the gas permeation experiment is considered to be the pressure at the upstream face of the membrane (p_f). The upstream pressure is adjusted manually by a pressure regulator (PR) and the relief valve.

The outflow volume is similar to that used in Part I (Chapanian et al., 2005); it consists of a ¼" stainless steel tube (Swagelock SS-T4-S-049-20) and is equipped with two absolute pressure transducers, a rotary vacuum pump (Edwards model RV3), and several two-way manually operated valves (Swagelock model SS-DSVCR4) with VCR fittings. The pressure transducers P_1 and P_2 (MKS model 627B11TBC1B) have a linear range from 0 to 1333 Pa with a 0.0267 Pa reading accuracy and the maximum error corresponding to 0.12 % of the read pressure; they are connected to a personal computer equipped with a LabView software. The first pressure transducer (P_1) is installed 0.49 m from the membrane cell and the second pressure transducer (P_2) is installed 2.28 m from the membrane cell. The total length the ¼" tube in the outflow volume, which includes a bypass line up to V2, is 3.77 m, while the active length, which is indicated as a thick line in Fig. 1, is 3.65 m. The active length of tubing may be decreased to 2.37 m by closing the valve V3. With V3 open, the total volume of the vacuum part, as determined by a gas expansion technique, is 83.6×10^{-6} m^3. With V3 closed the total volume is 58.7×10^{-6} m^3. The corresponding active volumes are 42.7×10^{-6} m^3 and 27.7×10^{-6} m^3. The difference

between the total volume and the active volume is a dead volume, which constitutes of volumes associated with the membrane cell, valves, fittings, and pressure transducers.

A membrane, which was utilized as a medium to provide time lag in the pressure response, was a solution-cast high molecular weight polyphenylene oxide (PPO) film prepared by the complete evaporation of solvent. The film had an average thickness $l_m = 39.5 \times 10^{-6}$ m.

Before each experiment the system was evacuated, during which all valves except V1 were opened. Once the desired vacuum was reached V4 was closed and the system was let to stabilize, after which V2 was closed. The actual gas permeation experiments did not start until one hour after closing V2, and since no pressure increase was detected during this period before any experiment, it was concluded that the outflow volume was leak-free. The experiments were performed at the initial pressures ranging from 0.13 Pa to 300 Pa. With V1 closed, the pressure in the buffer tank was set at $p_f = 206.8 \pm 6.9$ kPa in every experiment. The experiments were initiated by opening V1. After pressurization of the membrane the data was collected for 5 minutes with a frequency of one data set per 1 s. The temperature during experiments was not controlled; however, it remained relatively constant at 23°C ± 1°C.

Results and Discussion

Error in experimentally determined D_m, P_m and S_m

Fig. 2 presents the progress of one of the gas permeation experiments. The figure shows the pressure responses at 0.49 m (p_1) and 2.28 m (p_2) from the membrane cell in the ¼" tube of the total length of 3.65 m and the corresponding difference between these

pressures, which will be referred to as a pressure gradient. The outflow volume was initially at 0.13 Pa; therefore, the Knudsen flow regime existed at the beginning of this experiment (Chapanian et al, 2005).

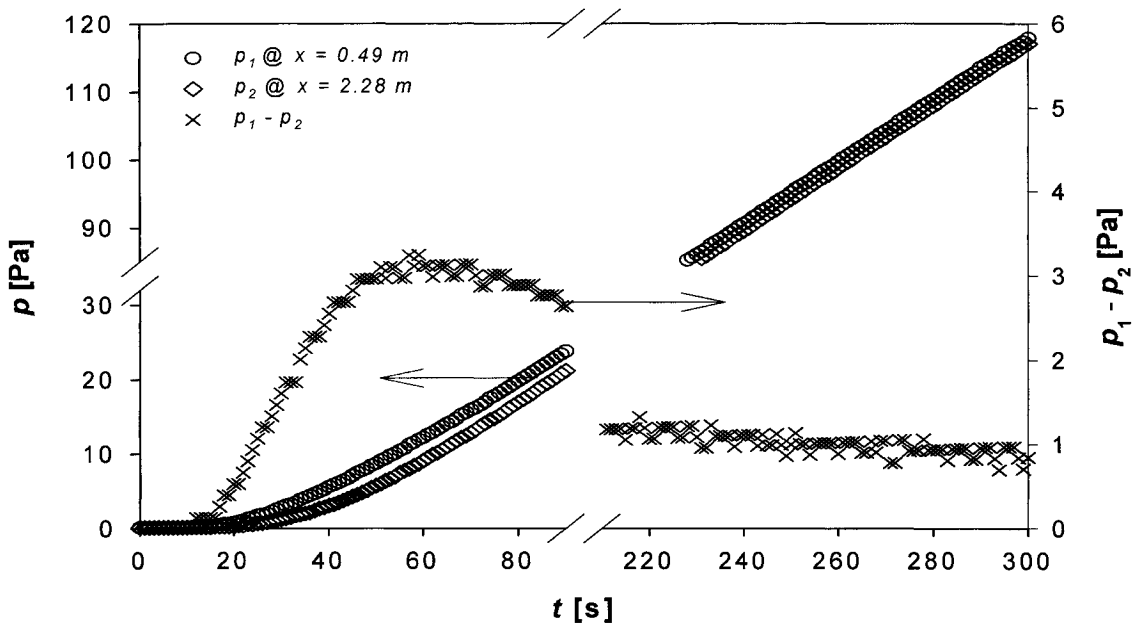

Figure 2 Progress of N_2 permeation experiment through PPO membrane monitored at two different distances from the membrane in a standard ¼" stainless steel tube of length L = 3.65 m. Initial pressure, p_o = 0.13 Pa; feed pressure p_f = 206.8 kPa; temperature T = 23°C.

It can be noticed that after 18 s from the initiation of the experiment, the pressures recorded by the two pressure transducers start to differ from each other, that is a pressure difference within the tube starts to develop. After 60 s from the initiation of the experiment the pressure difference reaches the maximum value exceeding 3.2 Pa, and as the experiment progresses the pressure difference decreases. In the period between 220 s and 300 s, the pressure difference decreases from 1.2 Pa to 1.0 Pa.

Different pressure responses at different distances from the membrane are direct consequence of the resistance to accumulation of N_2 in the collector tube. The resistance to accumulation prevents uniform distribution of gas molecules downstream from the membrane leading to a higher concentration (pressure) of gas near the membrane. It is important to note that unlike the experiments in which a mass flow controller was used (Chapanian et al., 2005); the gas flow into the tube was gradually increasing before reaching a constant value given by the first term on the right hand side of Eq. (15). Thus, a step increase in flow rate from zero to a finite value is not a necessary condition for the resistance effects to be observed.

Fig. 3 presents the analysis of the experiment depicted in Fig. 2. The straight lines in Fig. 3 are the asymptotes. These asymptotes are used for the determination of time lag at the two positions. The experimental time lag depends on the time frame of the asymptote equation.

It is a common practice to determine the slope of the asymptote based on the pressure response after the time corresponding to three time lags. This is because after the three time lags the gas flow rate through the membrane should be within 1% of the steady state value (Crank and Park, 1969). On the other hand, as time progresses the pressure in the outflow volume increases and the boundary condition given by Eq. (12) may no longer be valid. Therefore, the upper end of the time frame for the determination of the asymptote should not be much greater than the time corresponding to three time lags.

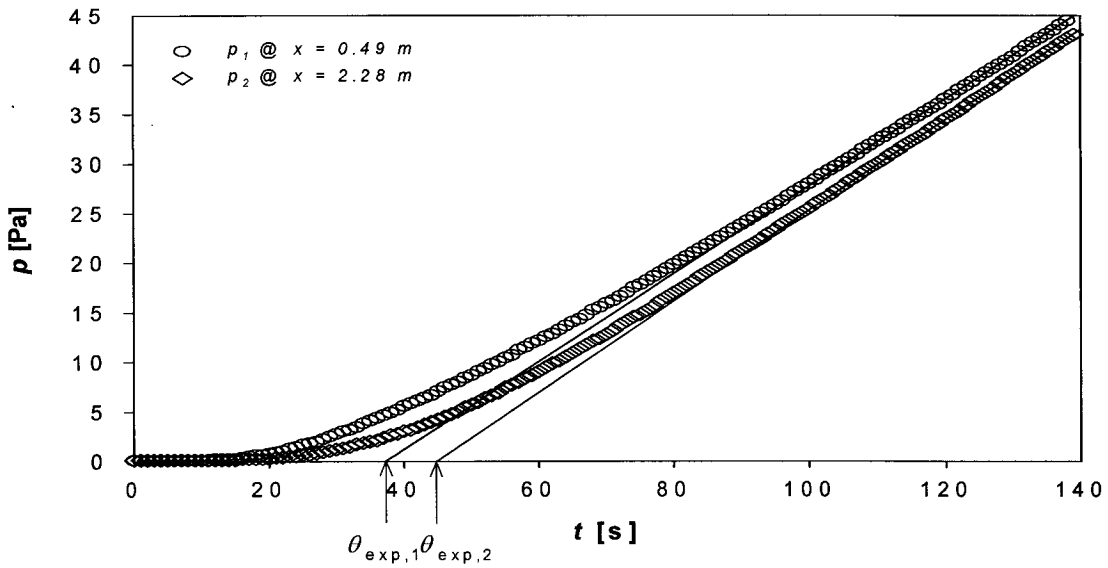

Figure 3 Determination of the experimental time lag at different distances from the membrane. Gas: N_2; polymer: PPO; tube of length L = 3.65 m; initial pressure p_o = 0.13 Pa; feed pressure p_f = 206.8 kPa; temperature T = 23°C.

The asymptotes in Fig. 3 were determined by linear regression of pressure values between the three and four experimental time lags. This required the following iterative procedure. An arbitrary time frame was chosen and a linear regression was performed on the corresponding pressure values. Using the resulting slope and intercept of the asymptote, the time lag was evaluated. The times corresponding to the lower and upper limits of the chosen time frame were then divided by the time lag. The procedure continued until the lower and upper limits of chosen time frame corresponded to the three and four time lags, respectively.

For the experiment depicted in Fig. 3, the experimental time lag based on p_1, $\theta_{exp,1}$ = 37.5 s, while the experimental time lag based on p_2, $\theta_{exp,2}$ = 45.1 s. Therefore,

according to Eq. (2), the diffusion coefficient of N_2 in the membrane is 6.93 x 10^{-12} m^2/s based on p_1, and 5.76 x 10^{-12} m^2/s based p_2. There is also a difference in the permeability coefficients determined from the asymptotes at different distances from the membrane cell. The permeability coefficients of N_2 in the membrane are 7.07 x 10^{-17} m^3(STP)/s·m·Pa and 7.33 x 10^{-17} m^3(STP)/s·m·Pa based on p_1 and p_2, respectively. Knowing D_m and P_m the solubility coefficient may be determined from Eq. (1). The solubility coefficients of N_2 in the membrane determined using the respective values of D_m and P_m are 1.02 m^3(STP)/m^3·Pa and 1.27 m^3(STP)/m^3·Pa. The relative difference between the solubility coefficients at the two positions is greater than the relative difference between the diffusion coefficients. This is because the former is magnified by the difference between the permeability coefficients at the two positions.

Table 1 summarizes the experimental D_m, P_m and S_m based on the pressure responses at 0.49 m and 2.28 m from the membrane cell, respectively, determined in tests at different initial pressures and with different active lengths of the tube. In addition, the table presents the diffusion coefficient of N_2 in the tube evaluated at the initial pressure from the empirical model of Knudsen (Chapanian et al., 2005). In all experiments, the slopes of the asymptotes at the two distances from the membrane were determined using the criteria discussed above, i.e. considering the pressure responses in the time frame between the three and four experimental time lags. It is important to emphasize that all experiments summarized in Table 1 were performed using the same membrane.

Table 1 Summary of the analysis of the permeation experiments with a ¼" tube in the outflow volume. Membrane: PPO film of thickness 39.5 μm; gas: N_2; feed pressure: 206.8 kPa; temperature: 23°C.

p_o [Pa]	D_o [m^2/s]	L [m]	x [m]	Slope [Pa/s]	θ_{exp} [s]	D_m x 10^{12} [m^2/s]	P_m x 10^{17} m^3(STP)/s·m·Pa	S_m x 10^6 m^3(STP)/m^3·Pa
0.13	0.60	3.65	0.49	0.442	37.5	6.93	7.07	1.02
			2.28	0.458	45.1	5.76	7.33	1.27
1.33	0.54	3.65	0.49	0.461	35.5	7.33	7.37	1.01
			2.28	0.477	43.1	6.04	7.64	1.26
5.50	0.57	3.65	0.49	0.451	37.3	6.98	7.22	1.04
			2.28	0.466	44.2	5.88	7.45	1.27
22.6	0.97	3.65	0.49	0.466	37.1	7.02	7.45	1.06
			2.28	0.478	42.5	6.12	7.64	1.25
105	3.12	3.65	0.49	0.470	38.0	6.84	7.52	1.10
			2.28	0.473	40.1	6.48	7.57	1.17
295	8.16	3.65	0.49	0.473	39.1	6.65	7.57	1.14
			2.28	0.473	40.0	6.51	7.57	1.16
0.13	0.60	2.37	0.49	0.640	39.5	6.59	7.19	1.09
			2.28	0.649	42.5	6.11	7.29	1.19
1.30	0.54	2.37	0.49	0.637	39.8	6.54	7.16	1.10
			2.28	0.646	42.5	6.13	7.26	1.19
5.70	0.57	2.37	0.49	0.642	40.1	6.49	7.21	1.11
			2.28	0.649	42.7	6.10	7.29	1.20
23.8	1.01	2.37	0.49	0.643	39.7	6.55	7.23	1.10
			2.28	0.648	41.6	6.25	7.28	1.17
101	3.03	2.37	0.49	0.633	42.0	6.19	7.11	1.15
			2.28	0.635	43.0	6.04	7.13	1.18
301	8.34	2.37	0.49	0.635	42.5	6.13	7.13	1.16
			2.28	0.633	42.6	6.10	7.11	1.17

In all tests D_m determined from the pressure response monitored at 0.49 m from the membrane cell is greater than D_m determined from the pressure response monitored at 2.28 m from the membrane cell, whereas the opposite occurs for P_m. This is consistent with an increase in the asymptote's slope with the distance from the flow source reported in Part I (Chapanian et al., 2005). For each experiment presented in Table 1, S_m values obtained from the sensor further from the membrane are higher.

The differences between the respective transports parameters at different distances from the membrane cell depend on the initial pressure and the active length of tube. For a given initial pressure, these differences are greater in the longer tube. This is because the resistance, which is the reason for these differences, increases with the length of tube. For a given tube length the differences between the respective transport parameters are generally similar in the experiments performed at initial pressures up to 5.7 Pa. A weak dependence of these differences on the initial pressure may be explained by a relatively constant diffusion coefficient of N_2 in the ¼" tube between 0.13 Pa and to 5.7 Pa. The resistance in the tube is inversely proportional to the diffusion coefficient of the gas in the tube. On the other hand, for the experiments performed at 20, 100 and 300 Pa, the differences between the respective transports parameters at different distances from the membrane cell are inversely related to the initial pressure because of a strong dependence of D on p in this pressure range (Chapanian et al., 2005). At 300 Pa, i.e. in the Poiseuille flow regime, the diffusion coefficient of N_2 is large and the differences between the respective transport coefficients become very small or disappear.

The existence of two different numerical values for a given transport coefficient, i.e. a dependence of transport coefficient on the distance from the membrane cell, is an

indication of a possible error due to resistance to gas accumulation downstream from the membrane cell.

Determination of single values for D_m, P_m and S_m from two pressure responses

For the simplest configuration, in which the outflow volume consists of a cylindrical tube, the errors in the experimental time lag and hence D_m and S_m may partly be corrected by applying Eq. (4). Application of Eq. (4) offers only a partial correction because it does not allow correcting P_m. Moreover, since the slope of the asymptote increases with the distance from the membrane cell and the time lag is the intercept of the asymptote with the time axis, the experimental time lag near the membrane cell should be lower than θ_{exp} given by Eq. (4) and the experimental time lag near closed end of the tube should be greater than θ_{exp} given by Eq. (4). Therefore, to accurately correct the errors in the transport coefficients due to resistance to gas accumulation in the tube it is necessary to apply the solution of the governing PDE, in which the variation of the diffusion coefficient of the gas in tube with pressure is properly incorporated.

The solution of Eq. (4) requires the numerical values of D_m and P_m, which are being sought. Therefore, in order to find these values an iterative procedure is required. For arbitrary chosen D_m and P_m, a theoretical pressure response is generated and then compared with the corresponding experimental pressure response. The combination of D_m and P_m for which the difference between the theoretical and experimental pressure responses is minimized represents the set of sought parameters. Since the pressure responses were monitored at two different distances from the membrane cell, the sum of the differences at the two positions should be minimized.

The selection of D_m and P_m for generation of theoretical pressure response is not completely arbitrary. In general, as shown in Table 1, the slope of the asymptote at 0.49 m is greater than at 2.28 m, but the difference does not exceed 5%. As an experiment progresses the difference between the rates of pressure increase at the two positions decreases. For example, for the membrane depicted in Fig. 2 the slope of the asymptote at 2.28 m is 3.6% greater than at 0.49 m. On the other hand, between 220 s and 300 s the slope at 2.28 m is just 0.6% greater than at 0.49 m. Moreover, considering the results presented in Part I, it may be assumed that the corresponding slope at further distance should be closer to expected value when there is no resistance (Chapanian et al., 2005). Therefore, the value of P_m required for generation of the theoretical pressure response was determined using the slope at 2.28 m in the time frame between 220 s and 300 s from the initiation of the experiment.

The range of D_ms for the generation of the theoretical pressure response is limited by the values determined at 0.49 m and 2.28 m. For example, for the first experiment listed in Table 1 the actual D_m must be greater than 5.76×10^{-12} m^2/s but less than 6.93×10^{-12} m^2/s. The range of possible D_ms may be further decreased by applying Eq. (4) to evaluate θ_m. For $D = 0.60$ m^2/s, $L = 3.65$ m, $x = 0.49$ m and $\theta_{exp} = 37.5$ s, the corrected time lag of membrane is $\theta_m = 42.2$ s, which corresponds to $D_m = 6.16 \times 10^{-12}$ m^2/s. On the other hand, for $D = 0.60$ m^2/s, $L = 3.65$ m, $x = 2.28$ m and $\theta_{exp} = 45.1$ s, $\theta_m = 43.0$ s, which corresponds to $D_m = 6.05 \times 10^{-12}$ m^2/s. Therefore, the actual D_m must be greater than 6.05×10^{-12} m^2/s but less than 6.16×10^{-12} m^2/s.

Fig. 4 presents the comparison of the experimental pressure responses and the theoretical pressure responses during the first 140 s of the experiment depicted in Fig. 2.

The theoretical pressure responses were generated with D_m = 6.05 x 10^{-12} m^2/s and P_m = 7.35 x 10^{-17} m^3(STP)/s·m·Pa.

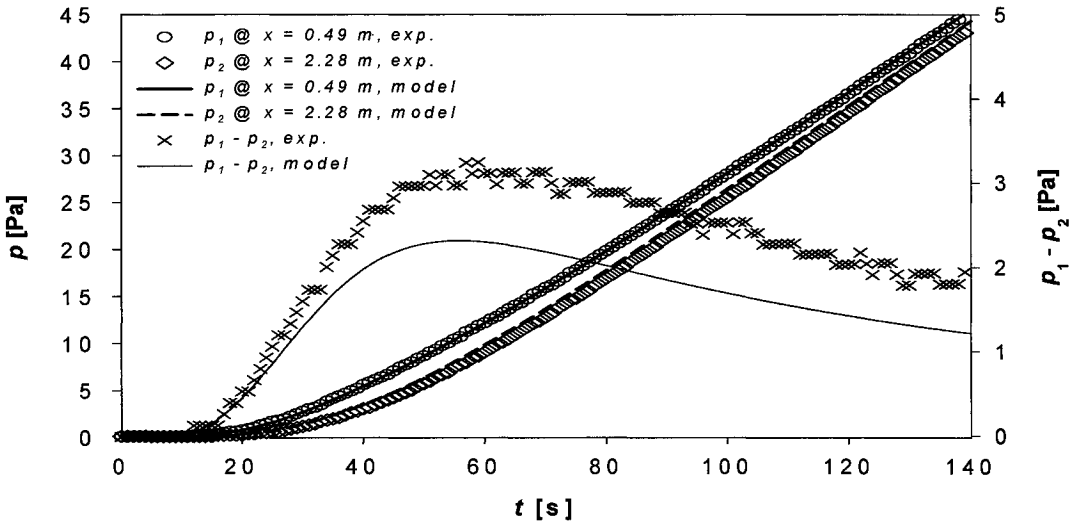

Figure 4 Modeling of the of N_2 permeation experiment through the PPO film at two different positions in the standard ¼" stainless steel tube using D_m = 6.05 x 10^{-12} [m^2/s] and P_m = 7.35 x 10^{-17} [m^3(STP)/s·m·Pa] determined by the least square method. Other parameters: tube length L = 3.65 m; initial pressure p_o = 0.13 Pa; feed pressure p_f = 206.8 kPa; temperature T = 23°C; membrane thickness l_m = 39.5 x 10^{-6} m.

It can be noticed that there is almost a perfect match between the theoretical and the experimental pressure responses at 0.49 m from the membrane cell. At 2.28 m, the model slightly overestimates the pressure response. As a result, for a given time the difference between the theoretical pressure responses is slightly lower than the corresponding difference between the experimental pressure responses.

Table 2 summarizes the determination of single values for D_m, P_m and S_m from the two pressure responses in each gas permeation test. The last column presents the sum of squared differences between the experimental and theoretical pressures determined every second over the first 185 s of each experiment. The difference between the experimental

and theoretical pressures at a given time represents an error. The smaller the sum the better the fit between the experimental and theoretical pressure responses. In addition, for each transport coefficient the average and standard deviation values from the respective experiments in the longer and shorter tubes are also included. The average sums in both positions are also provided.

With the exceptions of two experiments in the longer tube, the sum at 2.28 m is greater than the sum at 0.49 m, which indicates a generally better fit between the experimental and theoretical pressure responses at 0.49 m. Similarly to Fig. 4, the deviation between the theoretical and experimental pressures at 2.28 m is due to a slight overestimation of the pressure at a given time by the model. This indicates that the model slightly underestimates the resistance effects at this position (Chapanian et al., 2005).

Table 2 Summary of experimentally determined transport coefficients corrected for the resistance effects using variable-diffusion coefficient model.

p_o [Pa]	D_o [m^2/s]	L [m]	x [m]	P_m x 10^{17} m^3(STP)/s·m·Pa	D_m x 10^{12} [m^2/s]	S_m x 10^6 m^3(STP)/m^3·Pa	$\Sigma(p_{exp}-p_{th})^2$ [Pa]^2
0.13	0.60	3.65	0.49	7.35	6.05	1.21	66.3
			2.28				255.7
1.33	0.54	3.65	0.49	7.65	6.39	1.20	74.1
			2.28				333.9
5.50	0.57	3.65	0.49	7.46	6.20	1.20	59.2
			2.28				251.0
22.6	0.97	3.65	0.49	7.65	6.52	1.17	41.2
			2.28				25.7
105	3.12	3.65	0.49	7.63	6.68	1.14	31.3
			2.28				25.4
295	8.16	3.65	0.49	7.62	6.53	1.17	90.3
			2.28				273.1
Average values for the experiments in longer tube				**7.56±0.13**	**6.40±0.23**	**1.18±0.03**	**60.4**
							194.1
0.13	0.60	2.37	0.49	7.30	6.35	1.15	195.0
			2.28				433.2
1.30	0.54	2.37	0.49	7.27	6.30	1.15	187.7
			2.28				413.2
5.70	0.57	2.37	0.49	7.32	6.27	1.17	183.6
			2.28				420.0
23.8	1.01	2.37	0.49	7.32	6.39	1.15	208.4
			2.28				400.0
101	3.03	2.37	0.49	7.17	6.09	1.18	171.0
			2.28				273.0
301	8.34	2.37	0.49	7.17	6.11	1.17	207.8
			2.28				381.9
Average values for experiments in shorter tube				**7.26±0.07**	**6.25±0.12**	**1.16±0.01**	**192.3**
							386.9

Considering the sum of errors in different tube length configurations, it is evident that a better fit is obtained for the experiments in the longer tube. It is important to note that the prediction of a theoretical pressure response is based on a total rather than an active outflow volume, which implies that a dead volume does not contribute to the resistance downstream from the membrane. In reality however, the dead volume might contribute to the resistance, but its contribution is difficult to predict. The percentages of the dead volume in the total outflow volume in the configurations with tube lengths of 3.65 m and 2.37 m are 49% and 53%, respectively. A smaller fraction of the dead volume might explain a better fit between the experimental and theoretical pressure responses in the configuration with the longer tube.

For a given length of tube downstream from the membrane, the transport coefficients listed in Table 2 vary from experiment to experiment, and this variation does not correlate with the initial pressure. Therefore, the variation in the transport coefficients for a given configuration represents an experimental error, which is quantified by the respective standard deviation values. The main source of the experimental error in permeability coefficients arises from an uncertainty in the feed pressure ($p_f = 206.8 \pm 6.9$ kPa). On the other hand, the main source of the experimental error in the diffusion coefficient arises from a manual operation of V2, which could affect recording the "zero time". In terms of time, the larger of the two standard deviations in D_m reported in Table 2 corresponds to ± 1.5 s uncertainty in the zero time.

It can be noticed that the average transport coefficients determined in the longer tube configuration are slightly greater than the corresponding values from the shorter tube configuration. In case of the diffusion and solubility coefficients the difference between

the respective averages is smaller than the sum of the respective standard deviations. Therefore, the observed difference might be a result of the experimental error. On the other hand, the difference between the average permeability coefficients in the longer and shorter tube configurations is greater than the sum of the respective standard deviations. Thus, the difference cannot be explained by the experimental error; it most likely arises from a systematic error in the total volumes used for the evaluation of the permeability coefficients (83.6×10^{-6} m^3 for the longer tube and 58.7×10^{-6} m^3 for the shorter tube).

A difference between the transport coefficient in Table 1 and the corresponding single value in Table 2 indicates of an error due to resistance to gas accumulation. It is evident that the sign and the magnitude of this error depend on the position of the pressure sensor relative to the membrane. The errors at 0.49 m are greater than the errors at 2.28 m; also the errors at 0.49 m and 2.28 m have the opposite signs. The absolute relative errors in P_m, D_m, and S_m due to resistance to gas accumulation in the longer tube configuration are as high 4%, 15% and 16%, respectively. These errors decrease considerably in the shorter tube configuration. Therefore, to minimize the errors due to resistance to gas accumulation it would be recommended to minimize the length of tubing downstream from the membrane. On the other hand, as indicated in the introduction to Part I of this series, accommodation of membranes having a wide range of permeability coefficients might require an increased length of tubes downstream from the membrane.

It is important to emphasize that since the time lag of membrane is directly proportional to the square of its thickness (Eq. 2), a given resistance in the outflow volume would lead to a much larger relative error in the diffusion and solubility

coefficients of a thinner membrane. For example, if the thickness of tested film were 20 μm rather than 39.5 μm, the magnitude of the relative errors in the diffusion and solubility coefficients would increase by a factor of four. Moreover, a thinner membrane at a given feed pressure would lead to a larger permeation rate leading to a greater relative error in the permeability coefficients (Chapanian et al., 2005). The same would happen if for a given membrane thickness a higher feed pressure were used.

The transport coefficients of N_2 in PPO listed in Table 2 are comparable with those reported by Aguilar-Vega and Paul (1993) and Alentiev *et al.* (1998).

Conclusions

The effect of the resistance to accumulation of gas in a long cylindrical tube on the diffusion, permeability and solubility coefficients of the gas in membrane determined by the time lag method has been demonstrated experimentally. The resistance leads to a dependence of these transport coefficients on the position of the pressure sensor in the tube. In turn, this is an indication of possible errors in gas transport coefficients of membrane determined with the time lag technique. With the pressure sensors located at two different distances from the membrane, the magnitude of the differences between the respective coefficients decreases in the following order, solubility, diffusivity and permeability.

For the simplest configuration of the outflow volume consisting of a straight cylindrical tube a procedure for correcting errors due to resistance has been developed. The procedure involves solving numerically a partial differential equation that governs accumulation of the gas in tube, which takes into consideration the dependence of the

diffusion coefficient of the gas in tube on pressure. The comparison of the theoretical and experimental pressure responses indicates that the model slightly underestimates the actual resistance. This is attributed to an unaccounted contribution of a dead volume to the total resistance downstream from the membrane, which is unavoidable in real CV systems.

Acknowledgement

The authors gratefully acknowledge the financial support for this project provided by the Natural Science and Engineering Research Council of Canada.

Nomenclature

A_m: Membrane area, (m^2)

c: Concentration of gas in membrane, (mol/m^3)

c_f: Concentration of gas at the upstream face of the membrane, (mol/m^3)

D: Diffusion coefficient of gas in tube, (m^2/s)

D_m: Diffusion coefficient of gas in membrane, (m^2/s)

l_m: Membrane thickness, (m)

L: Length of permeate collector tube, (m)

p : Pressure, (Pa)

p_o : Initial pressure, (Pa)

p_f: Feed pressure, (Pa)

P_m: Permeability coefficient of gas in membrane, (m^3(STP)/m·Pa·s)

Q: Gas flow emerging from membrane and entering the tube, (m^3/s)

r: internal radius of tube, (m)

R: Universal gas constant, (J/mol·K)

S_m: Solubility coefficient of gas in membrane, (m^3(STP)/m^3·Pa)

t: Time, (s)

T: Absolute temperature, (K)

x : Position within the collector tube, (m)

x' : Position within the membrane, (m)

Greek Symbols:

θ_m: Time lag of membrane, (s)

θ_{exp}: Experimental time lag of membrane, (s)

References

Aguilar-Vega, M. and D. R. Paul, "Gas transport properties of polyphenylene ethers", J. Polym. Sci. Part B, 31, 1577-1589, (1993).

Alentiev, A., E. Drioli, M. Gokzhaev, G. Golemme, O. Ilinich, A. Lapkin, V. Volkov and Yu. Yampolskii, "Gas permeation properties of phenylene oxide polymers", J. Membrane Sci., 138, 99-107,(1998).

Barrer, R. M., "Permeation, diffusion and solution of gases in organic polymers", Trans. Faraday Soc., 35, 628-643, (1939).

Chapanian, R., F. Shemshaki and B. Kruczek, "Effects of resistance to accumulation of gases in vacuum tubes. Part I. Error in measurement of gas flow rate by the pressure rise technique", submitted to Can. J. Chem. Eng.

Daynes, H. A., "The process of diffusion through a rubber membrane", Proc. R. Soc., A97, 286-307, (1920).

Frisch, H. L., "Anomalous polymer-penetrant permeation", J. Chem. Phys., 37, 2408-2413, (1962).

Jenkins, R. C. L., P. M. Nelson and L. Spirer, "Calculation of the transient diffusion of a gas through a solid membrane into a finite outflow volume", Trans. Faraday Soc., 66, 1391-1401, (1970).

Kruczek, B., H. L. Frisch and R. Chapanian, "Analytical solution for the effective time lag of a membrane in a permeate tube collector in which Knudsen flow regime exists", J. Membrane Sci., 256, 57-65, (2005).

Paul, D. R. and T. DiBenedetto, "Diffusion in amourphous polymers", J. Polym. Sci. Part C, 10, 17-44, (1965).

Rogers, W. A., R. S. Buritz and D. Alpert, "Diffusion coefficient, solubility, and permeability for helium in glass", J. Appl. Phys., 25, 868-875, (1954).

Rutherford, S. W. and D. D. Do, "Review of time lag permeation technique as a method for characterization of porous media and membranes", Adsorption, 3, 283-312, (1997).

Zolandz, R., Fleming, G.K., "Gas permeation", in: Sirkar, K. K. and W. S. W. Ho (Eds.), Membrane Handbook, Van Nostrand Reinhold, New York, NY (1992), pp. 25-35.

Captions for Figures

Figure 1 Schematic diagram of the experimental CV system. P_1 and P_2 are the MKS pressure transducers (model 627B11TBC1B); P_f is the absolute pressure transducer; PR is the pressure regulator, and RV is the relief valve.

Figure 2 Progress of N_2 permeation experiment through PPO membrane monitored at two different distances from the membrane in a standard ¼" stainless steel tube of length L = 3.65 m. Initial pressure, p_o = 0.13 Pa; feed pressure p_f = 206.8 kPa; temperature T = 23°C.

Figure 3 Determination of the experimental time lag at different distances from the membrane. Gas: N_2; polymer: PPO; tube of length L = 3.65 m; initial pressure p_o = 0.13 Pa; feed pressure p_f = 206.8 kPa; temperature T = 23°C.

Figure 4 Modeling of the of N_2 permeation experiment through the PPO film at two different positions in the standard ¼" stainless steel tube using D_m = 6.05 x 10^{-12} [m^2/s] and P_m = 7.35 x 10^{-17} [m^3(STP)/s·m·Pa] determined by the least square method. Other parameters: tube length L = 3.65 m; initial pressure p_o = 0.13 Pa; feed pressure p_f = 206.8 kPa; temperature T = 23°C; membrane thickness l_m = 39.5 x 10^{-6} m.

Abstract

The expression for the time lag in a cylindrical tube, into which a gas at very low flow rate enters at one end while the other end is connected to a resistance-free accumulation tank, has been derived assuming that the gas transport in the tube is a diffusive process. Assuming a constant diffusion coefficient of the gas in tube allowed obtaining an analytical expression for the time lag using the concept of linear asymptotes and Laplace transformation of the governing partial differential equation. The obtained expression indicates that if the pressure response is monitored in the tube, the presence of the tank at the end of tube would lead to a negative time lag in the tube. The time lag becomes more negative as the distance from the tank increases and the volume of the tank increases while the cross-sectional area of the tube decreases.

The comparison of the model with the experimental data obtained in tests in which the pressure response to a step increase in feed pressure of membrane was monitored in the tube at two different distances from the membrane cell, indicates that the error due to resistance to gas transport in the tube on the experimental time lag of tested medium is even greater than that predicted by the model. This is because of the assumption of constant diffusion coefficient in tube, which does not allow predicting the experimentally observed increase in the slope of the asymptote with the distance from the membrane cell.

Key words: Time Lag, Diffusion Coefficient of Gas in Tube, Fick's 2nd Law of Diffusion

Introduction

The time lag method, which originates from the analysis of Daynes [1] is nowadays a basis of a generally accepted technique to assess the permeability and diffusion coefficients of gases in porous and nonporous media. The numerous refinements of the original time lag analysis have been made over the years, and are summarized by Rutherford and Do [2]. All these refinements are concerned with the boundary conditions and properties of tested medium; hence they can be referred to as "internal" refinements.

In our recent paper [3] we considered the effect of resistance to accumulation of gases downstream from the membrane on the experimentally measured time lag. Assuming that the gas permeating through the membrane accumulates in a straight cylindrical tube and that accumulation is a diffusive process characterized by a constant diffusion coefficient (D), we derived the following expression for the experimental time lag

$$\theta_{\exp} = \theta_m + \frac{L^2}{6D} - \frac{(L-x)^2}{2D} \tag{1}$$

where θ_m is the actual time lag of membrane, L is the length of the tube, and x is the distance from the membrane where the pressure response is monitored. Eq. (1) can be considered as an "external" refinement of the original time lag analysis. Another example of an external refinement is the correction factor proposed by Favre *et al.*, which accounts for a non-instantaneous pressurization of the inflow volume [4]. The non-instantaneous pressurization, which often occurs when testing organic vapors, leads a systematic overestimation of the time lag of membrane [4]. The correction of gas diffusion data reported by Sanchez *et al.* for the apparatus "delay times", which varied from 0.30 to

0.67 s [5], is also an example of the external refinement. It is not clear however how the delay times used by Sanchez *et al.* were established. The possibility of system resistance was also considered by Shishatskii *et al.* [6]. The resistance imposed by the system, which was referred to as a "time resolution", was examined by a sudden exposure of the outflow volume, initially at vacuum, to a pressure of 1,000 Pa and measuring the time for a pressure transducer to detect the increase in pressure. The authors concluded that the apparatus error in time lag determination was significantly lower than 1 s [6].

In this paper the effect of the resistance to gas transport in vacuum tube on the experimental time lag is investigated in the configuration, in which a cylindrical tube is followed a cylindrical accumulation tank, and the internal radius of the tank is much larger than the internal radius of the tube. The expression for the time lag is developed by using the concept of the asymptotic solution of the Laplace-transformed governing partial differential equation. The mathematical model is then verified experimentally in the configuration with and without the tank at the end of tube. In both cases the pressure response is monitored simultaneously by two pressure transducers installed on the tube at different distances from the membrane cell. The diffusion coefficient of the gas downstream from the membrane is evaluated using the empirical model of Knudsen.

Diffusion coefficient in cylindrical tubes

The diffusion coefficient of a single gas in cylindrical tubes over a wide range of pressures, which includes, Knudsen, slip, and Poiseuille flow regimes, may be predicted from the empirical model of Knudsen [7]

$$D = \frac{pr^2}{8\eta} + \frac{2}{3} r \sqrt{\frac{8RT}{\pi M}} \left(\frac{1 + C_1 p}{1 + C_2 p} \right) \tag{2}$$

where p is the absolute pressure, r is the internal radius of the tube, η is the dynamic viscosity of the gas, M is the molecular weight of the gas, R is the universal gas constant, T is the absolute temperature, and C_1 and C_2 are constants, which are determined by solving the following set of equations

$$\frac{C_1}{C_2} = \frac{3\zeta \sqrt{\frac{\pi M}{RT}} p}{8\sqrt{2}\eta} \tag{3}$$

$$C_2 - C_1 = 0.6117 \sqrt{\frac{M}{RT}} \frac{r}{\eta} \tag{4}$$

The coefficient of slip (ζ) is evaluated using the Maxwell's deduction from the kinetic theory of gases [8]

$$\zeta = \frac{\eta}{p} \sqrt{\frac{\pi RT}{2M}} \left(\frac{2 - f}{f} \right) \tag{5}$$

where f is a fraction of gas molecules, which lose the momentum as a result of adsorption and desorption at the walls of tube. While f depends on the nature of gas and tube surface, it is usually close to unity [9,10]. With f=1, solving simultaneously equations (3) and (4) leads to the following expressions for constants C_1 and C_2

$$C_1 = 0.8768 \sqrt{\frac{M}{RT}} \frac{r}{\eta} \tag{6}$$

$$C_2 = 1.4885 \sqrt{\frac{M}{RT}} \frac{r}{\eta} \tag{7}$$

At very low pressures, regardless of the value of f, Eq. (2) approaches the expression for the diffusion coefficient in the Knudsen flow regime

$$D = \frac{2}{3} r \sqrt{\frac{8RT}{\pi M}} \tag{8}$$

Equation (8) is valid when a gas molecule collides much more frequently with the walls of tube rather than with other gas molecules. Such conditions exist when the mean free path of gas molecules (λ) is much greater than the internal radius of the tube, i.e., $r/\lambda < 0.1$.

At high pressures, the second term of Eq. (2) approaches to unity and becomes much smaller than the first term; therefore at high pressures Eq. (2) approaches the expression for the diffusion coefficient in the Poiseuille flow regime

$$D = \frac{pr^2}{8\eta} \tag{9}$$

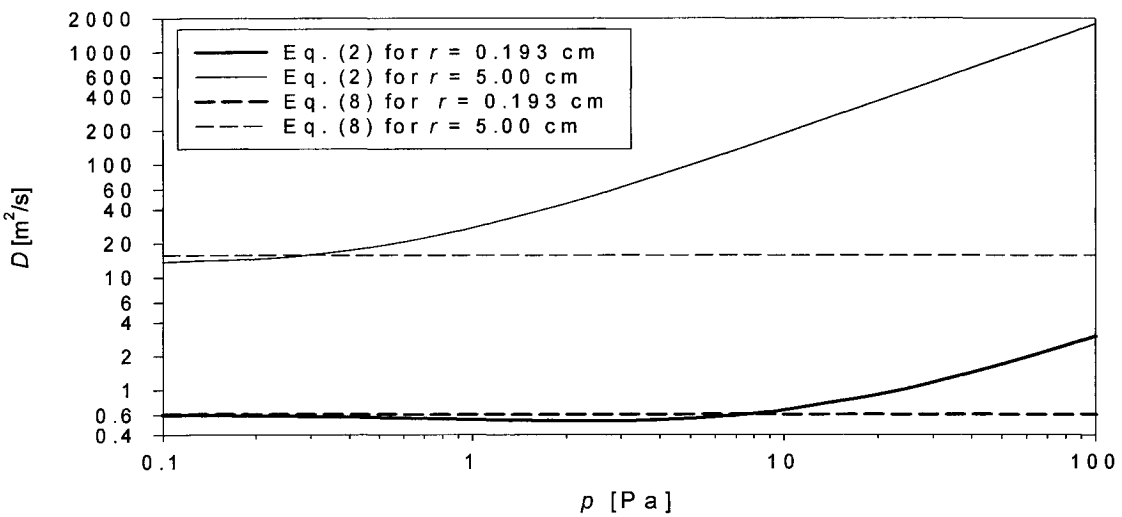

Figure 1. Effect of pressure on the diffusion coefficient of N_2 at 23°C in standard stainless steel tubes according to the empirical model of Knudsen [7] (solid lines). Dashed lines indicate the corresponding coefficients in pure Knudsen regime.

Assuming $f = 1$, Fig. 1 presents the graphical illustration of the empirical model of Knudsen, for the prediction of the diffusion coefficient of N_2 at 23°C in two cylindrical tubes of radii 0.193 cm and 5.0 cm.

The horizontal dashed lines in Fig. 1 represent the corresponding Knudsen diffusion coefficients. It should be noted that the tube radius not only affects the diffusion coefficient, but also the range of pressures, in which the diffusion coefficient is relatively constant. The smaller the radius, the larger the pressure range with a relatively constant D. For example, for 0.193 cm, the conditions for $r/\lambda < 0.1$, i.e., for the Knudsen flow regime, exist at $p < 0.49$ Pa. On the other hand, for the pressures up 10 Pa the diffusion coefficient does not differ more than 10% from the corresponding Knudsen diffusion coefficient.

Mathematical formulation of the problem

Figure 2 presents a simplified configuration of a constant volume system consisting of a cylindrical tube of length L and cross sectional area A, and a cylindrical tank of volume V. Initially, there is no flow of the gas, and the tube and the tank are at high vacuum. At time $t > 0$, the gas starts to flow into the tube at $x = 0$, and is accumulated in the tank. The gas flow at $x = 0$ may originate from any source, including membrane permeation.

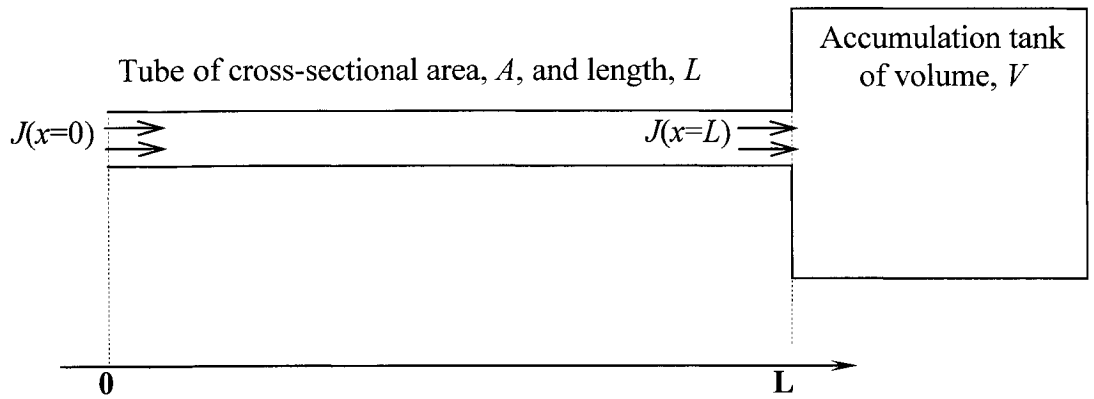

Figure 2. Simplified configuration of a constant volume system for the modeling purposes.

For low flow rates, for which the convective velocity of the gas in tube is very small, the gas transport in the tube occurs by diffusion. Thus, the pressure response in the tube following initiation of the flow is governed by the Fick's 2nd law of diffusion

$$\frac{\partial p(x,t)}{\partial t} = D\frac{\partial^2 p(x,t)}{\partial x^2} \tag{10}$$

Equation 10 implies that the diffusion coefficient is constant, which in case of a tube of internal radius of 0.193 cm shown in Fig. 1, is justified up to 10 Pa. It is important to emphasize that r = 0.193 cm represents the internal radius of a standard ¼" stainless steel tube. The accumulation of the gas in the tank is also a diffusive process; however, if the internal radius of the tank is large, the corresponding diffusion coefficient will be large, and the resistance to accumulation of the gas in the tank will be negligible.

Assuming no resistance to accumulation of the gas in the tank, the pressure in the tank will, at any time, be uniform and equal to the pressure at the end of tube, i.e. $p(\text{tank},t) = p(x = L,t)$. Consequently, the rates of pressure increase in the tank and at the end of tube will be the same. Assuming applicability of the ideal gas law, the rate of

pressure increase in the tank, and thus at the end of tube, may be expressed in terms of the gas flux leaving tube

$$\frac{dp(\text{tank})}{dt} = J(x = L,t)A\frac{RT}{V} = \frac{\partial p(x = L)}{\partial t} \tag{11}$$

The gas flux leaving the tube is given by the Fick's 1st law of diffusion

$$J(x = L,t) = -\frac{D}{RT}\frac{\partial p(x = L,t)}{dx} \tag{12}$$

Combining equations (11) and (12) yields the following expression

$$\frac{\partial p(x = L,t)}{\partial t} = -\frac{DA}{V}\frac{\partial p(x = L,t)}{\partial x} \tag{13}$$

Equation (13) represents one of two boundary conditions required for the solution of Eq. (10). The other boundary condition is expressed in terms of the gas flux entering the tube

$$\frac{\partial p(x = 0,t)}{dx} = -\frac{J(x = 0,t)RT}{D} \tag{14}$$

Before initiation of the flow the tube and the tank are at uniform pressure, thus the initial condition is expressed by

$$p(x,t = 0) = p_o = const. \tag{15}$$

Expression for time lag of the tube

The expression for the time lag of the tube may be obtained using the concept of the asymptotic solution [11] following the same procedure as in Ref. [3]. This procedure requires transformation of the governing partial differential equation using the Laplace transforms and then the solution of the transformed equation.

Application of the Laplace transform to Eq. (10) along with the initial condition given by Eq. (15) leads to the following ordinary differential equation

$$\frac{d^2\bar{p}}{dx^2} - q^2\bar{p} + \frac{p_o}{D} = 0 \tag{16}$$

where, $\bar{p} = \bar{p}(x,s) = \int_0^\infty e^{-st} p(x,t)dt$ and $q^2 = \frac{s}{D}$.

Equation (16) has the following particular solution

$$\bar{p}(x,s) = M\sinh(qx) + N\cosh(qx) + \frac{p_o}{s} \tag{17}$$

The constants M and N may be determined from the Laplace transforms of the boundary conditions, which are as follows

$$\frac{d\bar{p}(x=L)}{dx} = -\frac{V}{AD}(sp(x=L) - p_o) \tag{18}$$

$$\frac{d\bar{p}(x=0)}{dx} = -\frac{\bar{J}(x=0)RT}{D} \tag{19}$$

where $\bar{J} = \bar{J}(x,s) = \int_0^\infty e^{-st} J(x,t)dt$

Application of equations (18) and (19) leads to the following expressions for M and N

$$M = -\frac{\bar{J}(x=0)RT}{Dq} \tag{20}$$

$$N = -M\frac{\frac{A}{Vq}\cosh(qL) + \sinh(qL)}{\cosh(qL) + \frac{A}{Vq}\sinh(qL)} \tag{21}$$

Therefore, the final form of the particular solution is given by

$$\bar{p}(x,s) - \frac{p_o}{s} = \left(\frac{\bar{J}(x=0)RT}{\sqrt{Ds}}\right)\frac{\frac{A}{V}\sqrt{\frac{D}{s}}\cosh\left(\sqrt{\frac{s}{D}}(L-x)\right) + \sinh\left(\sqrt{\frac{s}{D}}(L-x)\right)}{\cosh\left(\sqrt{\frac{s}{D}}L\right) + \frac{A}{V}\sqrt{\frac{D}{s}}\sinh\left(\sqrt{\frac{s}{D}}L\right)} \tag{22}$$

According to the asymptotic solution concept [11], when the Laplace transform of any quantity has the form

$$\bar{y}(s) = \frac{f(s)}{s^2 \Delta(s)} \tag{23}$$

and $f(s)/\Delta(s)$ is regular at $s = 0$, the expression for time lag is given by the following equation

$$\theta = \frac{f(0)\frac{d\Delta}{ds}(0) - \Delta(0)\frac{df}{ds}(0)}{f(0)\Delta(0)} = \frac{\frac{d\Delta}{ds}(0)}{\Delta(0)} - \frac{\frac{df}{ds}(0)}{f(0)} \tag{24}$$

The determination of expressions for $f(s)$ and $\Delta(s)$ requires the expression for $\bar{J}(x = 0)$.

Constant flux at tube entrance

If the flux at the tube entrance is constant, i.e. $J(x = 0) = F$, then $\bar{J}(x = 0) = F/s$. Consequently, by equating the right hands sides of equations (22) and (23), it can be shown that the following expressions for $f(s)$ and $\Delta(s)$ are obtained

$$f(s) = FRT\left(\frac{A}{V}\cosh\left(\sqrt{\frac{s}{D}}(L-x)\right) + \sqrt{\frac{s}{D}}\sinh\left(\sqrt{\frac{s}{D}}(L-x)\right)\right) \tag{25}$$

$$\Delta(s) = \cosh\left(\sqrt{\frac{s}{D}}L\right) + \frac{A}{V}\sqrt{\frac{D}{s}}\sinh\left(\sqrt{\frac{s}{D}}L\right) \tag{26}$$

Evaluation of equations (25) and (26) and their first derivatives at $s = 0$, and substitution of the resulting expressions into Eq. (24) leads to the following expression for the experimental time lag

$$\theta_{\text{exp}} = \frac{\frac{L^2}{D}\left(\frac{L}{6} + \frac{V}{2A}\right)}{L + \frac{V}{A}} - \frac{(L-x)^2}{2D} - \frac{V(L-x)}{AD} \tag{26}$$

Time dependent flux at tube entrance

If the tube entrance represents the outlet of a membrane, and the membrane is subjected to a step increase in feed pressure, the gas flux entering the tube will depend on time, i.e., $J(x=0)=f(t)$. The exact dependence of the gas flux on time at the tube entrance depends on membrane properties, and the initial and boundary conditions for the membrane. In the simplest case, the permeability (P_m) and the diffusion (D_m) coefficients of the gas in membrane are independent of gas concentration (c), and the following initial and boundary conditions are assumed [1],

$$c(x',t=0)=0 \tag{27}$$

$$c(x'=0,t)=\frac{p_f P_m}{D_m}=const. \tag{28}$$

$$c(x'=l_m,t)\approx 0 \tag{29}$$

where p_f is the feed pressure, and l_m is the membrane thickness. The positions, $x'=0$ and $x'=l_m$ correspond to the feed and permeate faces of the membrane, respectively. For such specified conditions, it can be shown that the Laplace transform from the gas flux entering the tube is given by the following expression [3]

$$\bar{J}(x=0)=\frac{B}{\sqrt{s}\sinh\left(\sqrt{\frac{s}{D_m}}l\right)};\ \text{with},\ B=\frac{p_f P_m A_m}{A\sqrt{D_m}} \tag{30}$$

where, A_m is the membrane area.

Substituting Eq. (30) into Eq. (22) and then equating the right hand sides of equations (22) and (23) leads, after rearrangements, to the following expressions for $f(s)$ and $\Delta(s)$

$$f(s)=\frac{BRT}{\sqrt{D}}\left(\cosh\left(\sqrt{\frac{s}{D}}(L-x)\right)+\frac{V}{A}\sqrt{\frac{s}{D}}\sinh\left(\sqrt{\frac{s}{D}}(L-x)\right)\right) \tag{31}$$

$$\Delta(s)=\frac{V}{A\sqrt{D}}\frac{\cosh\left(\sqrt{\frac{s}{D}}L\right)\sinh\left(\sqrt{\frac{s}{D_m}}l_m\right)}{\sqrt{s}}+\frac{\sinh\left(\sqrt{\frac{s}{D}}L\right)\sinh\left(\sqrt{\frac{s}{D_m}}l_m\right)}{s} \tag{32}$$

Evaluation of equations (31) and (32) and their first derivatives at $s = 0$, and substitution of the resulting expressions into Eq. (24) leads to the following equation for the time lag

$$\theta_{\exp}=\theta_m+\frac{\frac{L^2}{D}\left(\frac{L}{6}+\frac{V}{2A}\right)}{L+\frac{V}{A}}-\frac{(L-x)^2}{2D}-\frac{V(L-x)}{AD} \tag{33}$$

where,

$$\theta_m=\frac{l_m^2}{6D_m} \tag{34}$$

It is important to note that Eq. (34) represents a well-know expression for the time lag of membrane, which is subject to the initial and boundary conditions specified by Eqs. (27-29), and for which Henry's law is applicable and the diffusion coefficient is independent of gas concentration [1]. Since the membrane and the tube are in series, regardless of the expression for $J(x=0)$, the above analysis should always lead to Eq. (33). Changing the properties of membrane and the initial and boundary conditions would result in a different expression for θ_m [2].

It is important to note that in the limiting case of $V = 0$, i.e. for the configuration without the tank, Eq. (33) simplifies to Eq. (1).

Experimental

Figure 3 presents the schematic diagram of the gas permeation system used in this project. A membrane is sandwiched between the two cylindrical parts of a stainless steel cell. The effective area for gas permeation in the cell, $A_m = 9.08 \times 10^{-4}$ m^2. The inflow volume consists of a standard ¼" stainless steel tubing and a buffer tank of volume 26.50×10^{-3} m^3, which can be pressurized up to 931 kPa using a gas from a compressed gas cylinder. The buffer tank is equipped with a relief valve (RV) and an absolute pressure gauge (P_f) having a 0 - 1207 kPa range and a 6.9 kPa reading accuracy. The reading of this pressure gauge during the gas permeation experiment is considered to be the pressure at the feed face of the membrane (p_f). This pressure is adjusted manually by a pressure regulator (PR) and the relief valve.

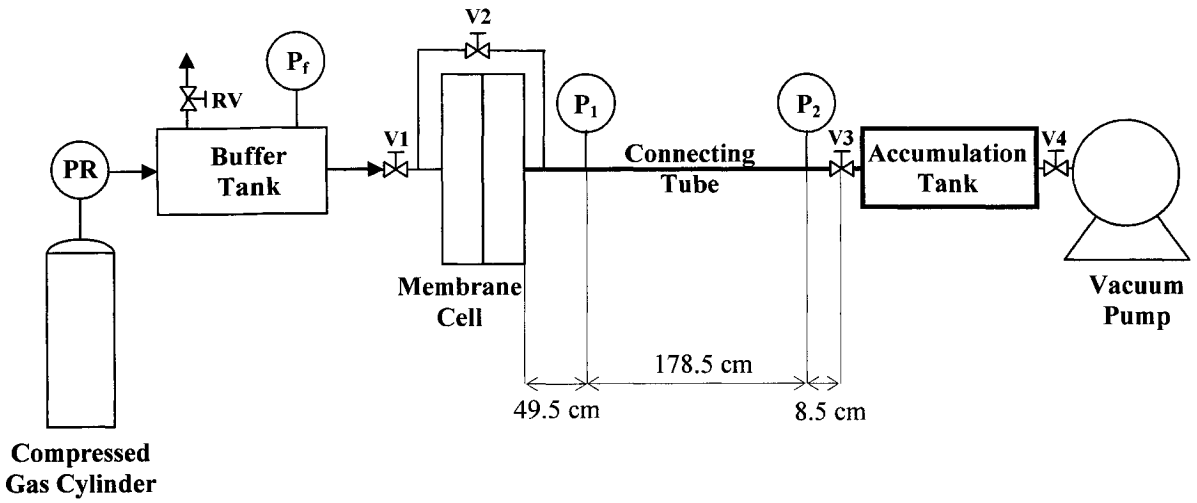

Figure 3. Schematic diagram of the experimental constant volume system. P_1 and P_2 are the MKS pressure transducers (model 627B11TBC1B); P_f is the absolute pressure transducer; PR is the pressure regulator, RV is the relief valve.

The outflow volume consists of a standard ¼" stainless steel tube of length L = 2.365 m and an accumulation tank of volume V = 2.250 x 10^{-3} m^3. The internal radius of the tube r = 0.193 cm, thus its cross-sectional area A = 1.17 x 10^{-5} m^2. The configuration of the outflow volume in Fig. 3 is typical for a constant volume system, except the length of the tube and the volume of the tank are exaggerated for illustration purposes. The outflow volume is equipped with two absolute pressure transducers, a rotary vacuum pump (Edwards model RV3), and several two-way manually operated valves (Swagelock model SS-DSVCR4) with VCR fittings. The pressure transducers P_1 and P_2 (MKS model 627B11TBC1B) have a linear range from 0 to 1 333 Pa with a 0.0267 Pa reading accuracy and the maximum error corresponding to 0.12 % of the read pressure; they are connected to a personal computer equipped with a LabView software. The pressure transducers are installed in the tube 0.495 m and 2.28 m from the membrane

cell. With V3 closed the outflow volume, as determined by a gas expansion technique, is 58.7 x 10^{-6} m^3. This volume includes dead volumes associated with valves, fittings, pressure transducers, and the membrane cell.

A membrane, which is utilized as a medium to provide time lag in the pressure response, is a solution-cast high molecular polyphenylene oxide (PPO) film prepared by complete evaporation of solvent, of thickness l_m = 39.5 x 10^{-6} m.

Before each experiment the system was evacuated, during which all valves except V1 were in the open position. Once the desired vacuum was reached V4 was closed and the system was allowed to stabilize for at least 30 minutes, after which V2 was closed. The experiments were performed at the same initial pressure of 0.13 Pa. With V1 closed, the pressure in the buffer tank was set at the desired level. The experiments were performed at four different feed pressures. The temperature during experiments was not controlled; however, it remained relatively constant at 23°C ± 1°C. The experiments were initiated by opening V1. After pressurization of the membrane the data was collected for at least 5 minutes with a frequency of one data set per 1 s.

Results and Discussion

Experiments without tank

Figure 4 presents the progress of the first 80 s of the gas permeation experiment in the configuration without the tank, i.e., with V3 closed. The pressure responses in Fig. 4 are monitored 0.495 m (p_1) and 2.280 m (p_2) from the membrane cell.

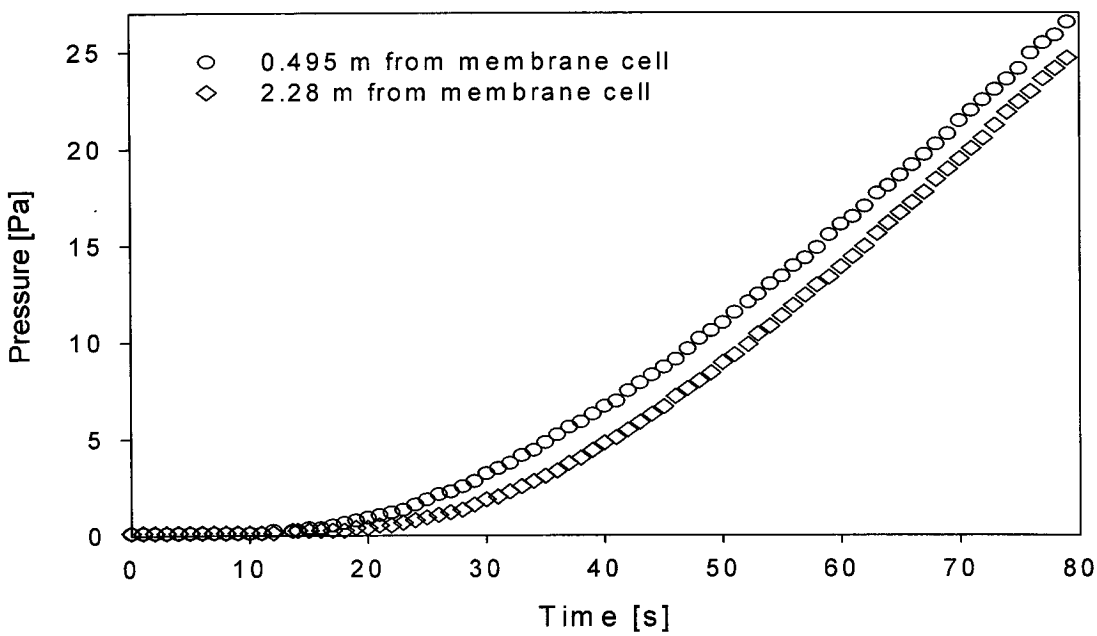

Figure 4. Progress of N_2 permeation experiment through PPO membrane monitored at two different distances from the membrane cell in a standard ¼" stainless steel tube of length L = 2.365 m. Initial pressure p_o = 0.13 Pa; feed pressure, p_f = 206.8 kPa; temperature, T = 23°C.

It can be noticed that 20 s after the initiation of the experiment, the pressures recorded by the two pressure transducers start to differ from each other. In the period between 42 s and 63 s the difference between p_1 and p_2 reaches the maximum value exceeding 2 Pa. As the experiment progresses $\Delta p = p_1 - p_2$ decreases. For example, at 100 s, 200 s and 300 s after initiation of the experiment the corresponding Δps are 1.38 Pa, 0.77 Pa, and 0.56 Pa, respectively. The difference between the pressure responses leads to a difference between the time lags. For the experiment depicted in Fig. 4, the experimental time lags based on p_1 and p_2, are $\theta_{exp,1}$ = 39.5 s and $\theta_{exp,2}$ = 42.5 s,

respectively. Thus, there is a difference of 3.0 s between the experimental time lags at the two positions.

Different pressure responses at different distances from the membrane leading to different time lags are direct consequence of the resistance to accumulation of N_2 in the tube. The resistance to accumulation prevents uniform distribution of gas molecules downstream from the membrane leading to a higher concentration of the gas near the membrane.

For the experiment depicted in Figure 4, $V = 0$, and Eq. (33) becomes Eq. (1). Knowing the diffusion coefficient of the gas in tube, Eq. (1) may be used for the prediction of the difference between the experimental time lags at different distances from the membrane. Assuming applicability of the empirical model of Knudsen, for N_2 at the initial pressure of 0.13 Pa and 23°C in the tube having $r = 0.193$ cm, $D = 0.60$ m^2/s. It therefore follows from Eq. (1) that for $L = 2.365$ m the difference between the experimental time lags at 2.28 m and 0.495 m from the membrane cell should be 2.9 s, which is in excellent agreement with the experimentally observed difference between the $\theta_{exp,2}$ and $\theta_{exp,1}$.

Knowing θ_{exp}, Eq. (1) may be used to determine the actual time lag of the membrane. For the experiment depicted in Fig. 4, for $x = 0.495$ m and $\theta_{exp} = 39.5$ s, $\theta_m = 40.9$ s. On the other hand, for $x = 2.28$ m and $\theta_{exp} = 42.5$ s, $\theta_m = 41.0$ s.

The error in time lag of membrane due to resistance to gas accumulation in the ¼" tube is evident. On the other hand, its magnitude is rather small. Moreover, as already mentioned the length of the tube in the system used in this study was exaggerated for the illustration purposes. Such a length of tubing in the actual gas permeation system would

represent inept apparatus design. Therefore, in a properly designed system the error in time lag of membrane due to resistance to accumulation of gas in tube should practically be negligible.

Experiments with tube and tank

Figure 5 presents the progress of the first 300 s of the gas permeation experiment similar to the one depicted in Fig. 4.

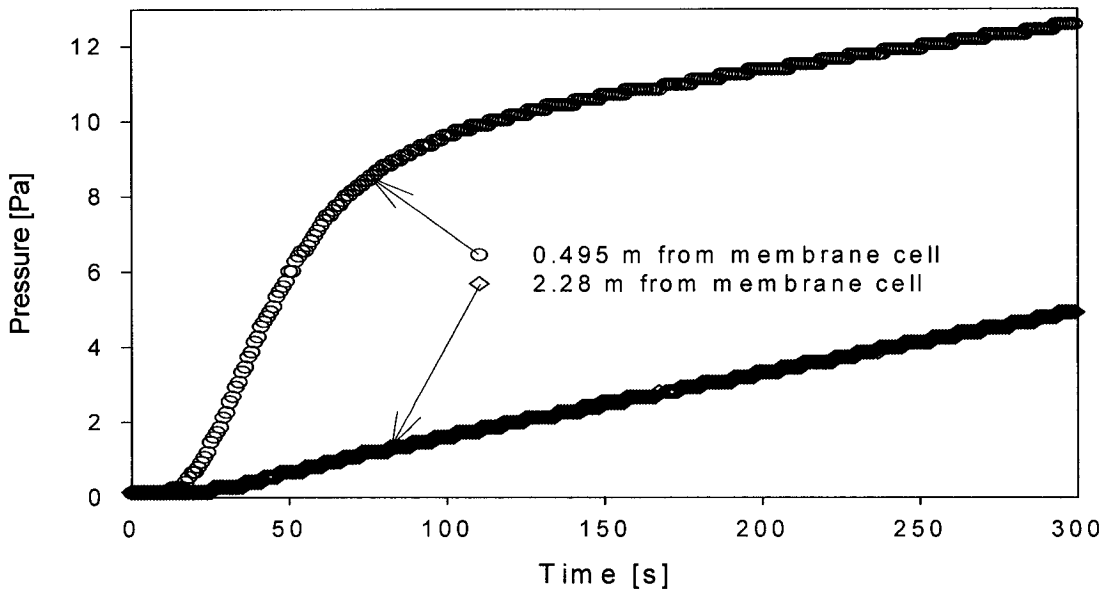

Figure 5. Progress of N_2 permeation experiment through PPO membrane monitored at two different distances from the membrane cell in a standard ¼" stainless steel tube of length L = 2.415 m in the configuration with a cylindrical tank of volume $V = 2.250 \times 10^{-3}$ m^3 attached at the end of the tube. Initial pressure p_o = 0.13 Pa; feed pressure, p_f = 206.8 kPa; temperature, T = 23°C.

The only difference between the experiments shown in Figs. 4 and 5 is the configuration of the outflow volume, while the membrane, the initial and feed pressures are the same.

The experiment presented in Fig. 5 was performed with open V3, thus, with the tank incorporated into the outflow volume. Opening V3 also increased the length of tubing by 5 cm, i.e., L = 2.415 m. Because of inclusion of the tank in the outflow volume, the rate of pressure rise in the experiment shown in Fig. 5 is much slower than that in Fig. 4, but most importantly the difference between the pressure responses at 0.495 m and 2.28 m from the membrane cell, which at 150 s reaches 8.2 Pa, is significantly greater than that in Fig. 4. As the experiment progresses, the difference between p_1 and p_2 slightly decreases; at 300 s this difference drops to 7.7 Pa. It can be noticed that between 150 and 300 s the pressure responses in both positions are linear, but not parallel to each other. Using the slopes of the pressure response between 150 and 300 s at the two positions the following experimental time lags are obtained: at 0.495 m, $\theta_{exp,1}$ = -677 s; at 2.28 m, $\theta_{exp,2}$ = 8.6 s. It should be remembered that actual time lag of membrane estimated based on the pressure responses shown in Fig. 4 and Eq. (1), θ_m = 41 s. Therefore, incorporation of the tank in the outflow volume results is very a large negative error in the experimental time lag, whose magnitude depends on the distance from the membrane cell.

The experimental results presented in Fig. 5 may be explained by considering the model given by Eq. (33). The large negative error is caused by the last term on the right hand side of Eq. (33), - $\frac{V(L-x)}{AD}$. Assuming θ_m = 41 s, the substitution of the numbers into Eq. (33) leads to the following predicted experimental time lags: at 0.495 m, $\theta_{exp,1}$ =

-577 s; at 2.28 m, $\theta_{exp,2}$ = 2.3 s. The predicted experimental time lags deviate considerably from the observed experimental time lags, particularly at the position closer to the membrane cell. The experimental time lags may also be used to evaluate the time lag of membrane using Eq. (33).

Table 1 summarizes the analysis of gas permeation experiments performed at different feed pressures in the configuration with the tank in the outflow volume.

Table 1. Summary of the analysis of the permeation experiments in the configuration with the tank in the outflow volume. Polymer: PPO; gas: N_2; initial pressure p_o = 0.13 Pa; temperature T = 23°C.

p_f [kPa]	x [m]	Slope [a] [Pa/s]	θ_{exp} [a] [s]	θ_m [b] [s]
207	0.495	0.0128	-677	-59.2
	2.280	0.0166	8.6	47.3
345	0.495	0.0186	-696	-78.2
	2.280	0.0265	0.8	39.5
620	0.495	0.0291	-667	-49.2
	2.280	0.0457	7.9	46.6
758	0.495	0.0349	-643	-25.2
	2.280	0.0560	8.1	46.8

[a] Based on the pressure response between 150 s and 300 s from the initiation of the experiment

[b] Evaluated from Eq. (33) using θ_{exp} and the following parameters: D = 0.60 m^2/s, L = 2.415 m, V = 2.25 x 10^{-3} m^3, A = 1.17 x 10^{-5} m^2

The table lists the slope of the asymptote, which is determined from the pressure response between 150 s and 300 s, the experimental time lag determined from the asymptote, and the time lag of membrane determined from the experimental time lag using Eq. (33). It should be pointed out that in every test the experimentally observed θ_{exp} at x = 0.495 m is much less than the predicted value of -577 s, and consequently the predicted θ_m is much less than the 41 s, i.e., the actual time lag of membrane. In fact, the predicted θ_m based on θ_{exp} at x = 0.495 m is a negative number in every experiment. On the other hand, θ_{exp} at x = 2.28 m is generally greater than 2.3 s and consequently θ_m, except for the experiment at 345 kPa, is slightly greater than 41 s. The discrepancy between the predicted θ_m and the actual time lag of membrane is a result of the assumption of constant D, which implies a constant slope of the asymptote. However, as shown in Table 1 the slope of the asymptote at x = 2.28 m is greater than the slope of the asymptote at x = 0.495 m, and the difference between the slopes at the two positions increases with feed pressure.

Assuming that the diffusion coefficient in the tube is constant, the slope of the asymptote is given by the following expression

$$\frac{dp}{dt} = \frac{A_m p_f P_m RT}{v_{STP} V_t l_m} \tag{35}$$

where v_{STP} is the volume of one mole of gas at standard temperature and pressure, and V_t is the total outflow volume. Since D depends on p, $\frac{dp}{dt}$ will be a function on x even after

disappearance of highly non-linear pressure response immediately after pressurization of the membrane.

The determination of $\frac{dp}{dt}$ as a function on x would require numerical solution of Eq. (10) in which D depends on p according to Eq. (2). On the other hand, the existence of a greater slope of the asymptote at x = 2.28 m than at x = 0.495 m can be explained qualitatively by considering the dependence of the diffusion coefficient on pressure shown in Fig. 1. For the ¼" tube and pressures greater than 2.4 Pa, the diffusion coefficient increases with pressure. As the gas accumulates in the outflow volume and the diffusion coefficient increases, the distribution of gas molecules must become more uniform leading to a decrease in the difference between p_1 and p_2. Thus, the slope of the asymptote will increase with the distance from the membrane cell, and at some distance it will be equal to the slope determined from Eq. (35).

The time lag is the intercept of the asymptote of the pressure response curve with the time axis. Therefore, if the slope of the asymptote is less than the slope determined from Eq. (35), the experimental time lag will decrease leading to underestimation of θ_m evaluated from Eq. (33). On the other hand, if the experimental slope of asymptote is greater than the slope determined from Eq. (35), the experimental time lag will increase leading to overestimation of θ_m evaluated from Eq. (33). The apparent closeness of θ_m evaluated from Eq. (33) at x = 2.28 m to 41 s indicates that the slope at x = 2.28 m is similar to that from Eq. (35). The dependence of the slope of the asymptote on the distance from the membrane cell magnifies the effects of resistance to gas transport in the tube predicted by Eq. (33).

As already mentioned, the length of tubing and the volume of the tank downstream from the membrane were exaggerated in this study, and in practical systems such a configuration of the outflow volume would represent an inept apparatus design. On the other hand, if the pressure transducer were installed on the tube, the effects of the resistance to gas transport in the tube would affect the experimental time lag even when the length of tube was minimized. For small L, the second and third terms on the right hand side of Eq. (33) are small. However, if $L - x > 0$, the fourth term might contribute significantly to the experimental time lag. The best solution, of course, would be to install the pressure transducer on the tank, which would eliminate the fourth term altogether. On the other hand, for a given volume of the tank, if ½" rather than ¼" tubes were used, A and D would increase minimizing the fourth term. Another way to minimize the fourth term would be to decrease the volume of the tank.

It is important to emphasize that the configuration in which the accumulation tank is located at the end of tube, i.e. at $x = L$, simplifies the mathematical analysis. If a tank were located at $x < L$, or if there were multiple tanks at different distances from the membrane cell, the analytical solution of the problem would not be possible. On the other hand, for any configuration of the outflow volume, the influence of resistance to gas transport downstream from the tested medium could be evaluated by solving numerically the resulting set of partial differential equations.

Conclusions

The effect of the presence of a resistance-free accumulation tank at the end of a tube on the experimental time lag has been modeled by assuming that the gas transport in

the tube is a diffusive process characterized by a constant diffusion coefficient. The latter assumption was necessary to obtain analytically the final expression for the experimental time lag by using the concept of the asymptotic solution. According to the proposed model, which is given by Eq. (33), if the pressure response is monitored in the tube, the resistance to gas transport in the tube would lead to underestimation of the time lag of tested medium. The magnitude of the error increases with the distance of the pressure transducer from the tank and the volume of the tank. The error also increases with decrease in the cross sectional area of tube.

The comparison of the model with the experimental data obtained in tests in which the pressure response to a step increase in feed pressure of membrane was monitored in the tube at two different distances from the membrane cell, indicates that the error due to resistance to gas transport in the tube on the experimental time lag of tested medium is even greater than that predicted by the model. This is because of the assumption of constant diffusion coefficient in tube, which does not allow predicting the experimentally observed increase in the slope of the asymptote with the distance from the membrane cell.

To minimize the error in the time lag of tested medium due to resistance to gas transport in the tube, the pressure response should be monitored in the tank. In this case, the resistance to gas transport in the tube would lead to an overestimation of the time lag of tested medium. However, in a well-designed system, in which the length of the tube is minimized while its cross sectional area is maximized, the positive error should be negligible.

Acknowledgement

The authors gratefully acknowledge the financial support for this project provided by the Natural Science and Engineering Research Council of Canada.

Nomenclature

A: Cross-sectional area of permeate collector tube (m^2)

A_m: Membrane area (m^2)

c: Concentration of gas in membrane (mol/m^3)

C_1: Constant in Eq. (2) defined by Eq. (3) (Pa^{-1})

C_2 Constant in Eq. (2) defined by Eq. (7) (Pa^{-1})

D: Diffusion coefficient of gas in tube (m^2/s)

D_m: Diffusion coefficient of gas in membrane (m^2/s)

f: Fraction of gas molecules that lose momentum as a result of adsorption and desorption at the walls of tube; assumed to be unity (-)

J: Gas flux within the tube (mol/m^2 s)

l_m: Membrane thickness (m)

L: Length of permeate collector tube (m)

M: Molecular weight (kg/mol)

p : Pressure (Pa)

p_f: Feed pressure (Pa)

p_o: Initial pressure (Pa)

P_m: Permeability coefficient of gas in membrane (mol/m Pa s)

r: internal radius of tube

R: Universal gas constant (J/mol K)

t: Time (s)

T: Absolute temperature (K)

x : Position within the tube (m)

x' : Position within the membrane (m)

Greek Symbols:

λ: Mean free path of gas molecules (m)

η: Dynamic viscosity of the gas (kg/m s)

θ_m: Actual time lag of membrane (s)

θ_{exp}: Actual time lag of membrane (s)

ζ: Coefficient of slip (m)

References

1. H.A. Daynes, The process of diffusion through a rubber membrane, Roy. Soc. Proc., A97 (1920) 286.
2. S.W. Rutherford and D.D. Do, Review of time lag permeation technique as a method for characterization of porous media and membranes, Adsorption, 3 (1997) 283.
3. B. Kruczek, H.L. Frisch and R. Chapanian, Analytical solution for the effective time lag of a membrane in a permeate tube collector in which Knudsen flow regime exists, J. Membr. Sci., 256 (2005) 57.

4. G E. Favre, N. Morlier, D. Roizard, Experimental evidence and implications of an imperfect upstream pressure step for the time lag technique, J. Membr. Sci., 207 (2002) 59.
5. J. Sanchez, C.L. Gijiu, V. Hynek, O. Muntean, A. Julbe, The application of transient time-lag method for the diffusion coefficient estimation on zeolites composite membranes, Sep. Purification Tech., 25 (2001) 467.
6. A.M. Shishatskii, Yu.P, Yampol'skii, K.-V Peinemann, Effects of film thickness and density on gas permeation parameters of glassy polymers, J. Membr. Sci., 112 (1996) 275.
7. L.B. Loeb, The Kinetic Theory of Gases, Dover Publications, Inc. New York, 1961, pp 278-300.
8. W.D. Niven, The Scientific Papers of James Clerk Maxwell, Dover publications, New York, 1965.
9. L.J. Stacy, A determination by the constant deflection method of the value of the coefficient of slip for rough and for smooth surfaces in air, Phys. Rev., 21 (1923) 239.
10. K.S.V. Dyke, The coefficients of viscosity and slip of air and of carbon dioxide by the rotating cylinder method, Phys. Rev., 21 (1923) 250.
11. H.S. Carslaw and J.C. Jaeger, Conduction of Heat in Solids, Oxford at the Clarendon Press, 2nd Edition, 1959, p. 402.

Figure Captions

Figure 1. Effect of pressure on the diffusion coefficient of N_2 at 23°C in standard stainless steel tubes according to the empirical model of Knudsen [7] (solid lines). Dashed lines indicate the corresponding coefficients in pure Knudsen regime.

Figure 2. Simplified configuration of a constant volume system for the modeling purposes.

Figure 3. Schematic diagram of the experimental constant volume system. P_1 and P_2 are the MKS pressure transducers (model 627B11TBC1B); P_f is the absolute pressure transducer; PR is the pressure regulator, RV is the relief valve.

Figure 4. Progress of N_2 permeation experiment through PPO membrane monitored at two different distances from the membrane cell in a standard ¼" stainless steel tube of length L = 2.365 m. Initial pressure p_o = 0.13 Pa; feed pressure, p_f = 206.8 kPa; temperature, T = 23°C.

Figure 5. Progress of N_2 permeation experiment through PPO membrane monitored at two different distances from the membrane cell in a standard ¼" stainless steel tube of length L = 2.415 m in the configuration with a cylindrical tank of volume $V = 2.250 \times 10^{-3}$ m^3 attached at the end of the tube. Initial pressure p_o = 0.13 Pa; feed pressure, p_f = 206.8 kPa; temperature, T = 23°C.

CHAPTER 4

Conclusion and Recommendations

The accumulation of gas in a single cylindrical tube and in a single cylindrical tube connected to a cylindrical tank of large internal diameter has been investigated. The above configurations represent simplified geometries for a constant volume (CV) system, which is widely used for the measurement and monitoring of low flows of gases, and for the characterization of porous and nonporous media using a time lag technique. The pressure response in the tube has been successfully predicted by treating gas accumulation as a diffusion process, in which the diffusion coefficient in the tube was predicted using the empirical model of Knudsen.

The mathematic analyses performed in this project have allowed quantifying the resistance to gas transport in the tube, and its consequences for the determination of the gas flow from the rate of the pressure increase in the tube, and for determination of the diffusion, permeability and solubility coefficients of gases in solution-diffusion membranes.

The resistance gas transport in the tube has been quantified using the concept of time lag in the tube. For the resistance effects to be observable in a single ¼" tube, the length of tube should exceed 1 m. On the other hand, inclusion of a resistance-free tank at the end of the tube magnifies dramatically the resistance in the tube. The following analytical expression for the time lag in the tube has been derived assuming a constant diffusion coefficient in Chapter 4.

$$\theta_{exp} = \frac{\frac{L^2}{D}\left(\frac{L}{6}+\frac{V}{2A}\right)}{L+\frac{V}{A}} - \frac{(L-x)^2}{2D} - \frac{V(L-x)}{AD} \quad (1)$$

where L and A are the length and internal cross section of the tube, D is the diffusion coefficient of the gas in the tube, V is the volume of the accumulation tank, and x is the distance of the pressure sensor from the flow source. In the limiting case of $V = 0$, i.e. no accumulation tank, the above equation simplifies to

$$\theta_{exp} = \frac{L^2}{6D} - \frac{(L-x)^2}{2D} \quad (2)$$

The actual resistance effects are greater than those predicted from the above equation because of variation of the diffusion coefficient in the tube with pressure.

The resistance to accumulation in the CV system could simply be avoided by not using any tubes downstream from the flow source. However, the literature survey indicates that in the last 40 years most CV systems utilized in membrane laboratories for the characterization of membranes contain tubes. The tubes downstream from the tested medium connect accumulation tanks of different volumes. The purpose of this is to vary the volume of a CV system, thus allowing a wide range of flows that could be tested in a given system. The example considered in Chapter 4, which represents the simplest arrangement for a tube/tank configuration, indicates that it might not be possible to avoid the resistance effects in tube/tank configurations. Consequently, the data reported in hundreds of papers published in last 40 years becomes questionable.

It is recommended for any researcher who uses a constant volume system having a tube/tank(s) configuration to quantify the resistance effects. This could be done by solving a set of appropriate partial differential equations, which each equation originating

from Fick's 2nd law of diffusion. The number of differential equations would depend on the actual geometry of the system, and of course the set of the partial differential equations would need to be solved numerically.

Another project arising from this work could be modification of a tube/tank configuration described in Chapter 4 by moving the tank along the tube. If the tank were located at $x_t \neq L$, there would be two partial differential equations; one for $0 < x < x_t$ and the other one for $x_t < x < L$. Adding a second tank to the line would result in addition partial differential equation.

CHAPTER 5

Uncertainty of Measurement

To measure the uncertainty of measurements three experiments with the same initial condition (the same initial pressure, temperature, and length of the tube) have been performed. Pure error variance (δ_i^2) for each experiment is calculated from the following equation:

$$\delta_i^2 = \frac{\sum_{i=1}^{N}(p_i - p^{avg})^2}{n-1} \qquad (1)$$

Where p_i is the pressure at t_i and a step time is one second, p^{avg} is the average pressure at t_i in n experiments at the same conditions (n=3), and N is the total number of points (N=t=522). Pooled error variance (δ_p^2) represents the total error variance between these three experiments and is calculated from following equation:

$$\delta_p^2 = \frac{\sum_{i=1}^{N}(n-1)\delta_i^2}{\sum_{i=1}^{N}(n_i - 1)} \qquad (2)$$

Figs. 1a and 1b represent the comparison of pressure responses at x=2.28 m from membrane cell in three experiments at the same initial pressure for the first 50 second and the last 50 second.

The pooled error variance for three experiments has been calculated and it is equal to $\delta^2 = 0.1997$ Pa^2 which leads to a standard deviation of $\delta = 0.447$ Pa for 522 points at each experiment, measuring pressures from 0.13 Pa to 93 Pa.

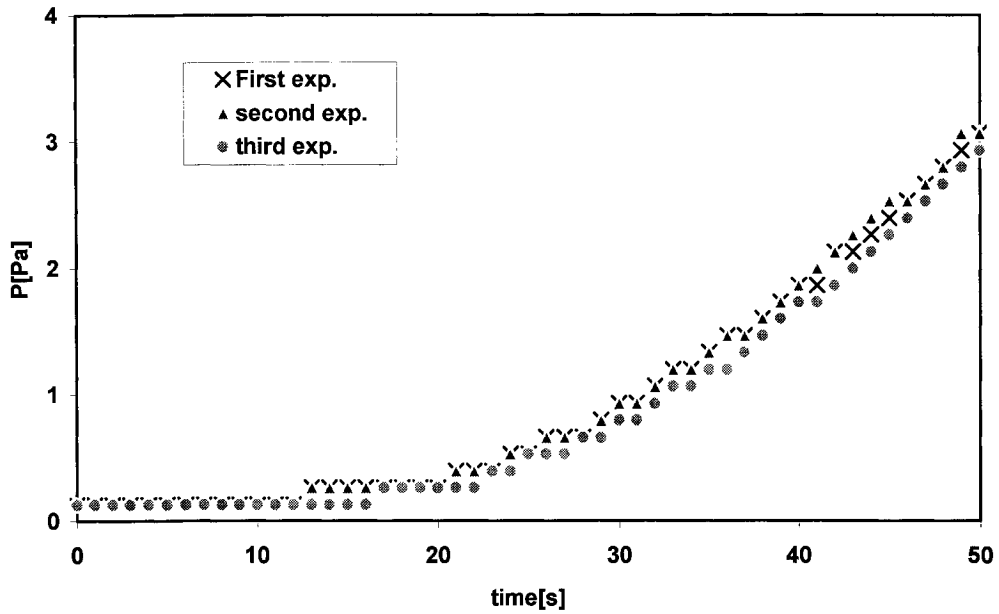

Figure 1a-Comparison of pressure response at x=2.28 m from membrane cell in three experiments at the same initial pressure at the first 50 second

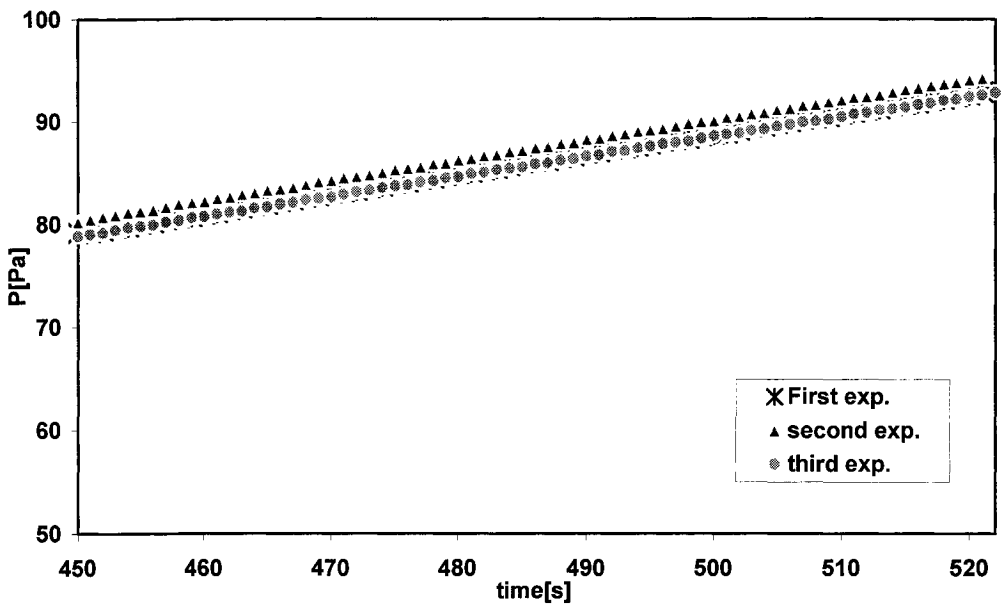

Figure 1b-Comparison of pressure response at x=2.28 m from membrane cell in three experiments at the same initial pressure at the last 50 second

APPENDIXES

APPENDIX A

This appendix provides all experiments with mass flow controller and long tube which contains two parts:

AA- Effect of flow

AB- Effect of initial pressure

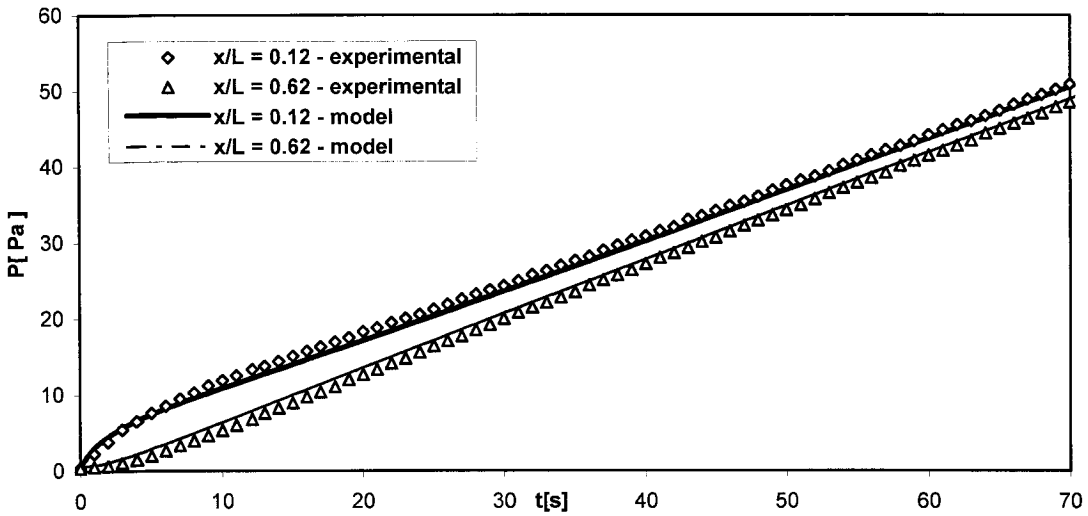

Figure AA-1- a Pressure responses to the constant set flow of N2 of 0.005 cm3(STP)/min at two positions x=0.44 m and x=2.22 m in a 3.60 m long tube with internal diameter of 0.00386 m. The initial pressure is equal to 0.4 Pa. Comparing with pressure responses from the non-constantat D model at the same positions.

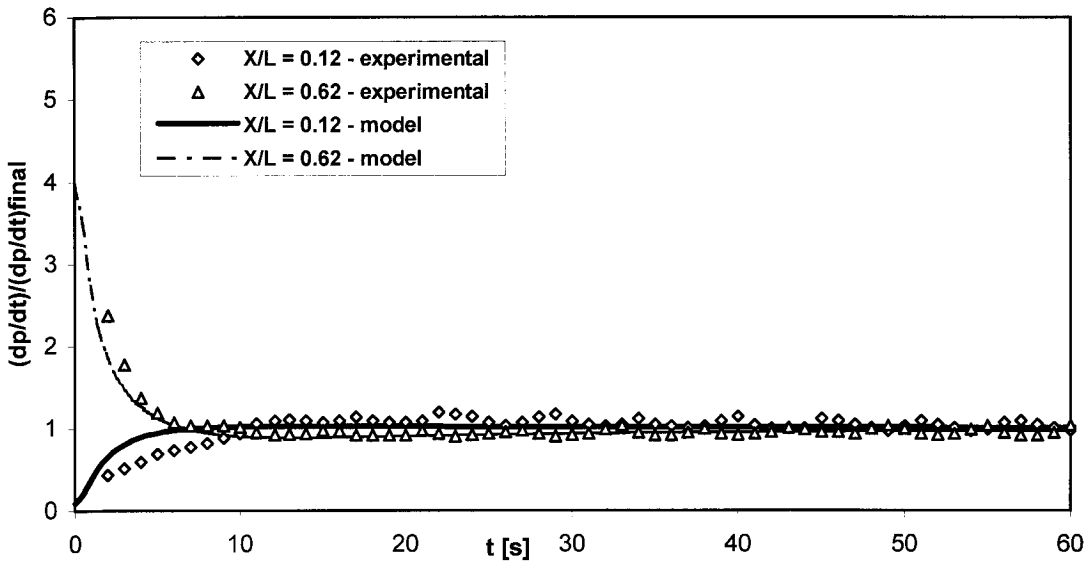

Figure AA-1-b Dimensionless Pressure response which indicates the error to the constant set flow of N2 of 0.005 cm3 (STP)/min at two positions x=0.44 m and x=2.22 m in a 3.60 m long tube with internal diameter of 0.00386 m. The initial pressure is equal to 0.4 Pa. Comparing with dimensionless pressure responses from the non-constant D model at the same positions.

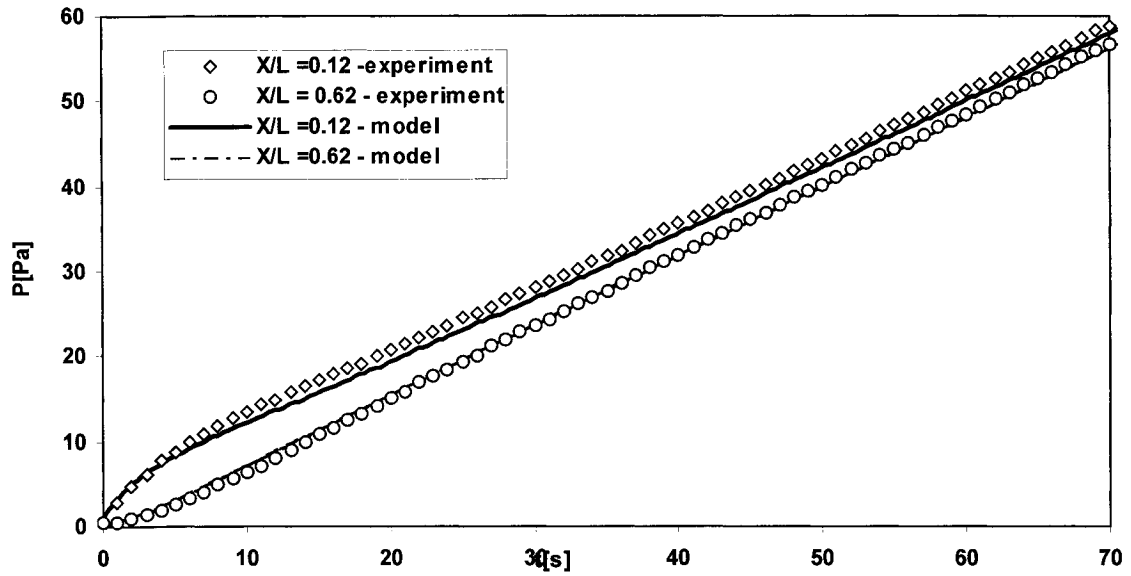

Figure AA-2- a Pressure responses to the constant set flow of N2 of 0.01 cm3 (STP)/min at two positions x=0.44 m and x=2.22 m in a 3.60 m long tube with internal diameterof 0.00386 m. The initial pressure is equal to 0.533 Pa. comparing with pressure responses from non-constant D model at the same positions.

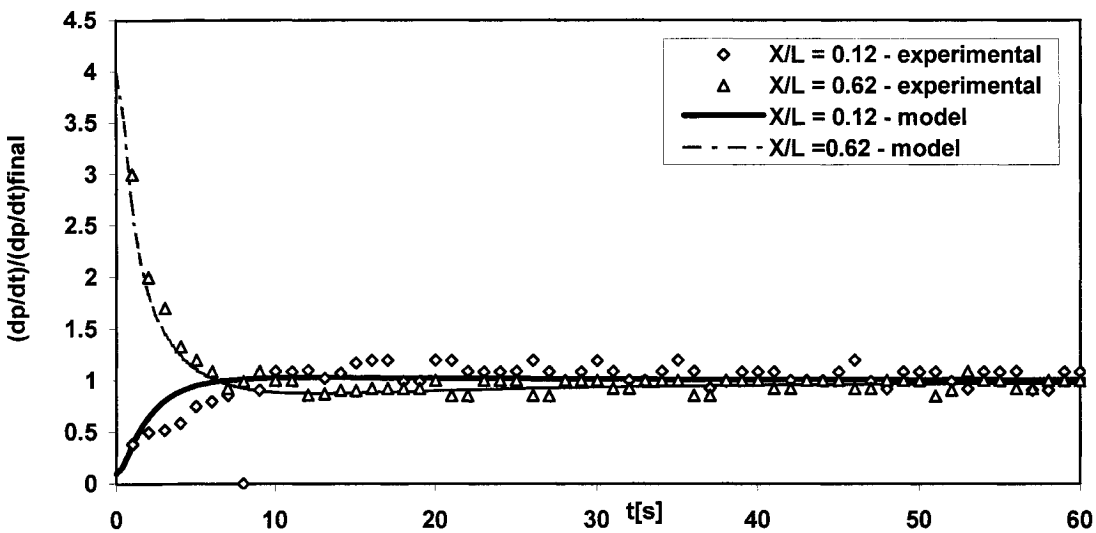

FigureAA-2-b Dimensionless Pressure response which indicates the error to the constant set flow of N2 of 0.01 cm3 (STP)/min at two positions x=0.44 m and x=2.22 m in a 3.60 m long tube with internal diameter of 0.00386 m. The initial pressure is equal to 0.533 Pa compare with dimensionless pressure responses from non-constant D model at the same positions.

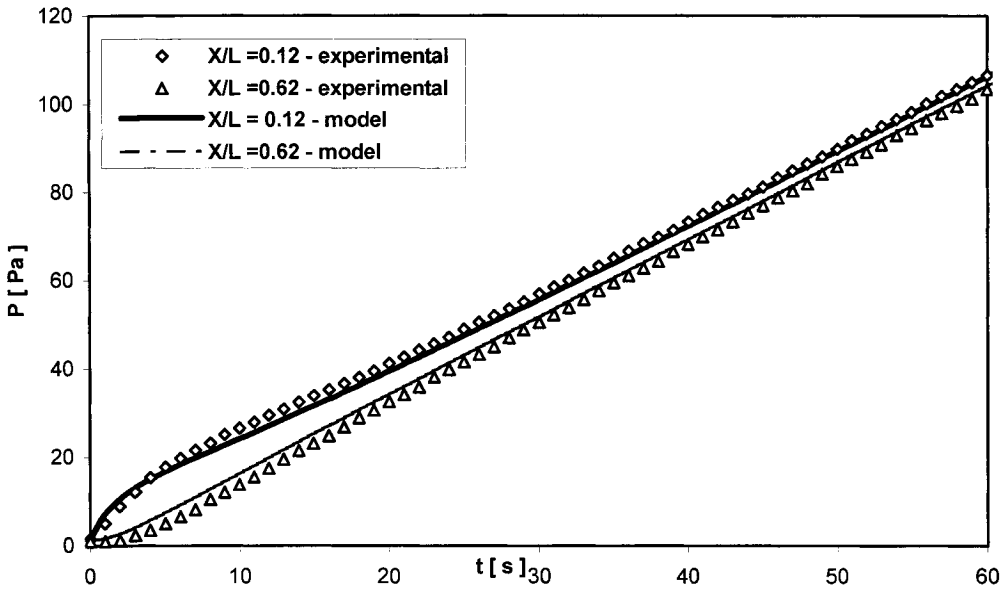

Figure AA-3- a Pressure responses to the constant set flow of N2 of 0.05 cm3 (STP)/min at two positions x=0.44 m and x=2.22 m in a 3.60 m long tube with internal diameter of 0.00386 m. The initial pressure is equal to 1.4 Pa. comparing with pressure responses from non-constant D model at the same positions.

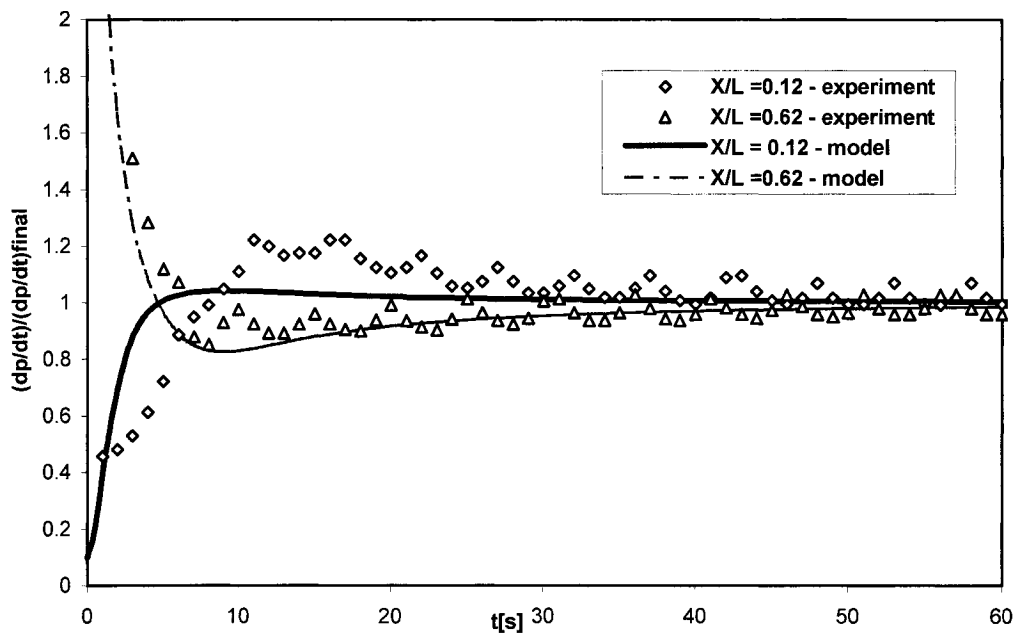

Figure AA-3-b Dimensionless Pressure response which indicates the error to the constant set flow of N2 of 0.05 cm3 (STP)/min at two positions x=0.44 m and x=2.22 m in a 3.60 m long tube with internal diameter of 0.00386 m. The initial pressure is equal to 1.4 Pa. comparing with dimensionless pressure responses from the non-constant D model at the same positions.

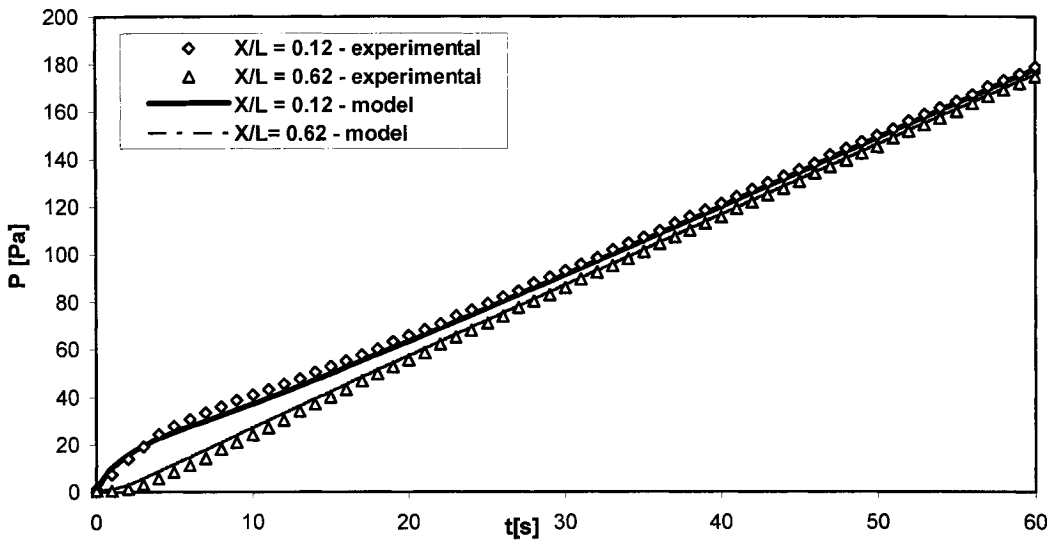

Figure AA-4- a Pressure responses to the constant set flow of N2 of 0.1 cm3 (STP)/min at two positions x=0.44 m and x=2.22 m in a 3.60 m long tube with internal diameter of 0.00386 m. The initial pressure is equal to 0.87 Pa. comparing with pressure responses from the non-constant at D model at the same positions.

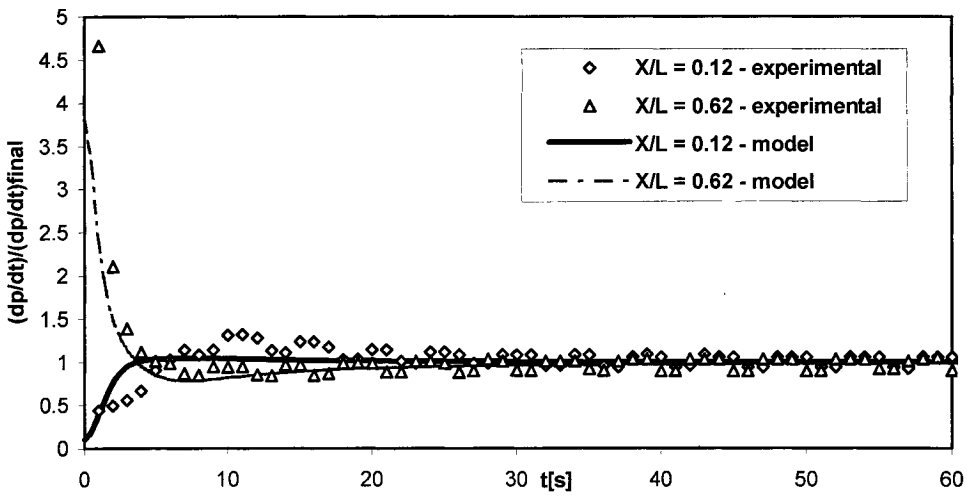

Figure AA-4-b Dimensionless Pressure response which indicates the error to the constant set flow of N2 of 0.1 cm3 (STP)/min at two positions x=0.44 m and x=2.22 m in a 3.60 m long tube with internal diameter of 0.00386 m. The initial pressure is equal to 0.87 Pa. comparing with dimensionless pressure responses from non-constant D model at the same positions.

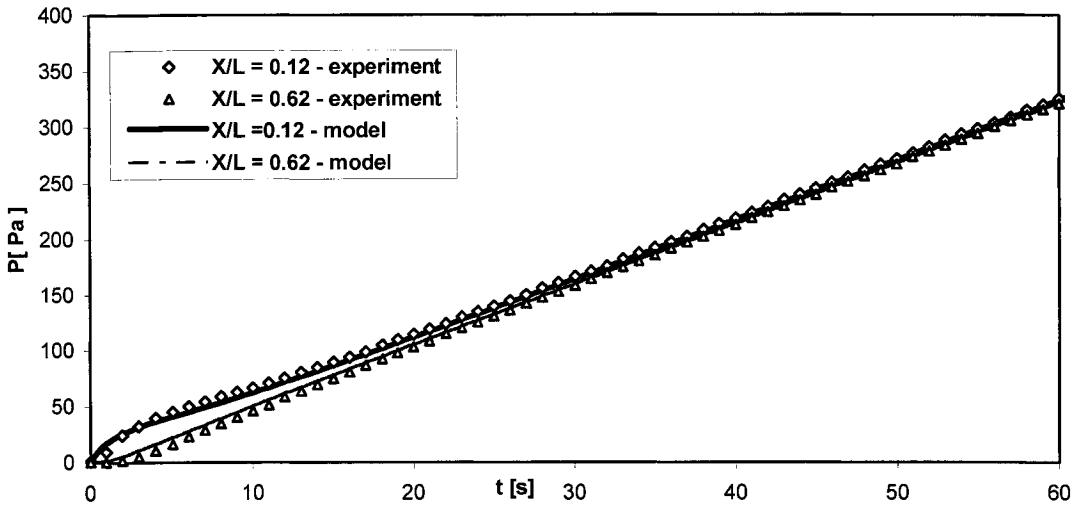

Figure AA-5- a Pressure responses to the constant set flow of N2 of 0.2 cm3 (STP)/min at two positions x=0.44 m and x=2.22 m in a 3.60 m long tube with internal diameter of 0.00386 m. The initial pressure is equal to 0.667 Pa. comparing with pressure responses from non-constant D model at the same positions.

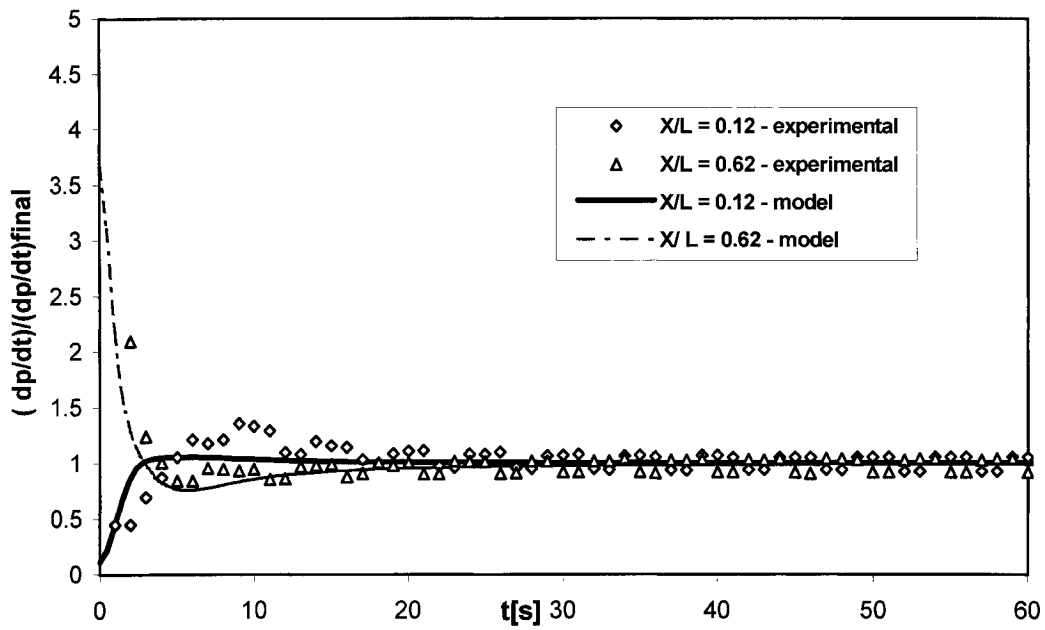

Figure AA-5-b Dimensionless Pressure response which indicates the error to the constant set flow of N2 of 0.2 cm3 (STP)/min at two positions x=0.44 m and x=2.22 m in a 3.60 m long tube with internal diameter of 0.00386 m. The initial pressure is equal to 0.667 Pa. comparing with dimensionless pressure responses from non-constant D model at the same positions.

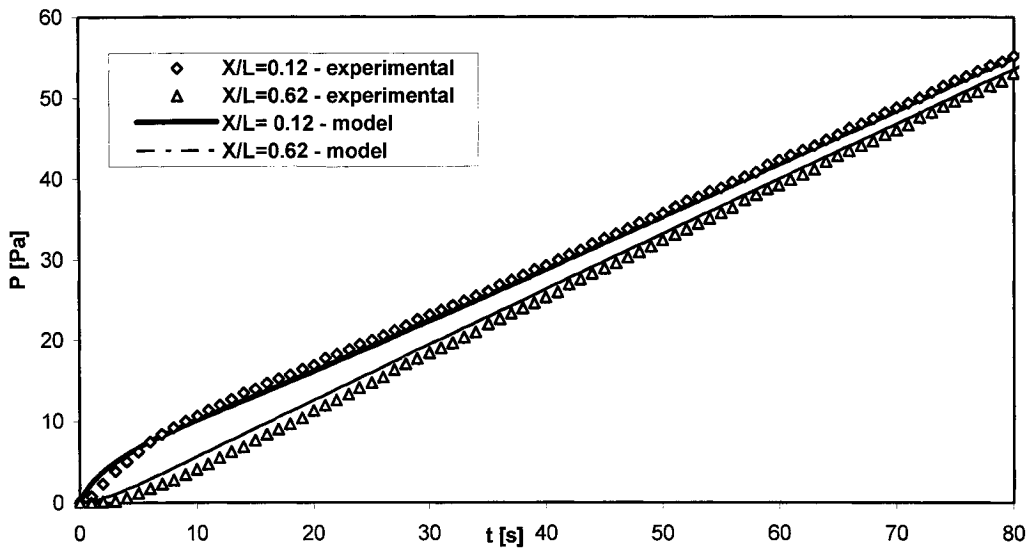

Figure AB-1-a Effect of initial pressure, pressure responses to actual flow of 0.024 cm3 (STP)/min in 1/4" tube with length of 3.6 m at two different location x1=0.44 m and X2=0.222 m and initial pressure of 0.13 Pa. Comparison between the model with constant D and the model with non-constant D and the experimental data at the same conditions.

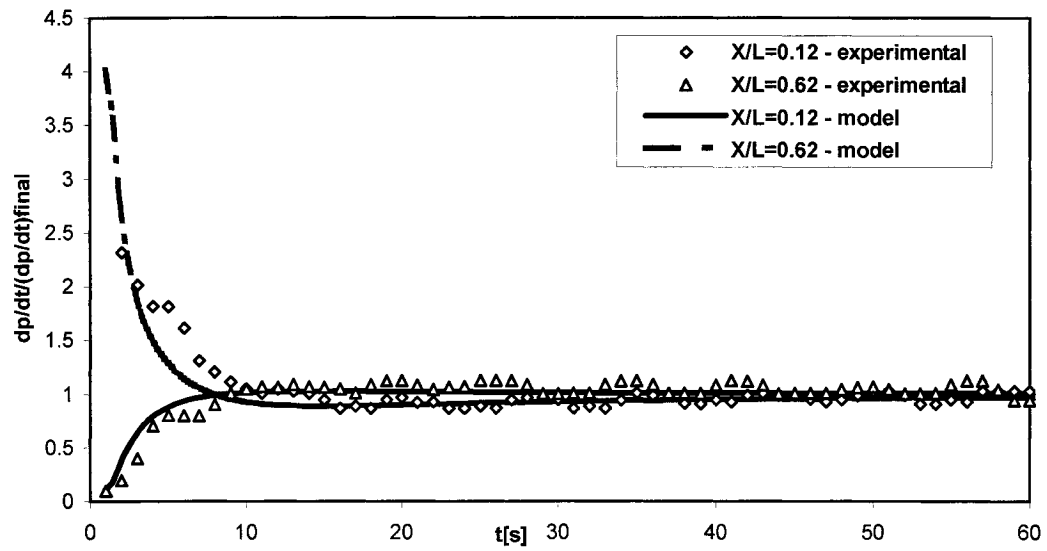

Figure AB-1-b The effect of initial pressure, dimensionless pressure responses to actual flow of 0.024 cm3 (STP)/min in 1/4" tube with length of 3.6 m at two different location x1=0.44 m and X2=0.222 m and initial pressure of 0.12 Pa.

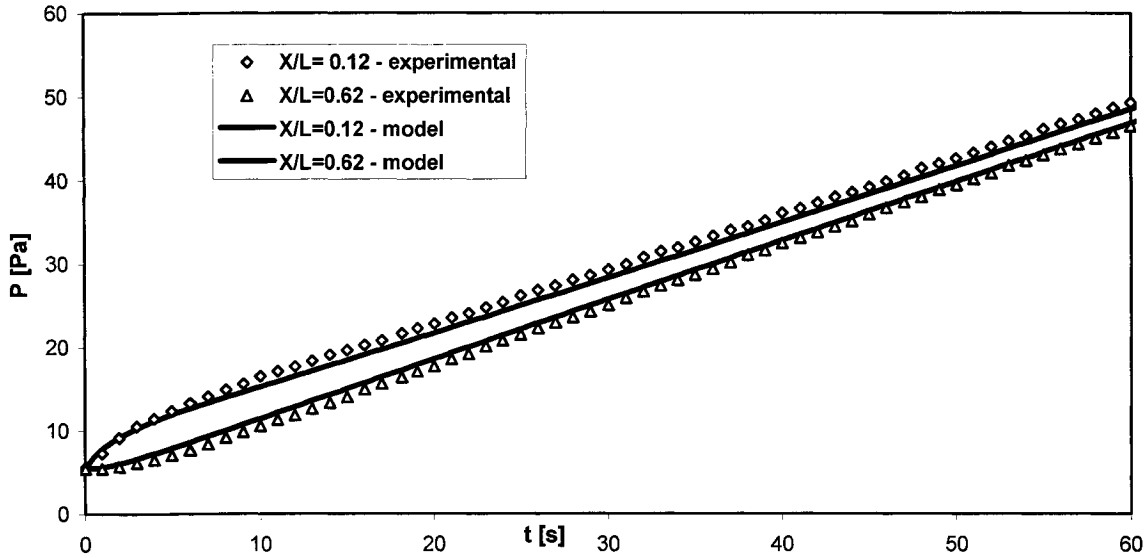

Figure AB-2-a Effect of initial pressure, pressure responses to actual flow of 0.024 cm3 (STP)/min in 1/4" tube with length of 3.6 m at two different location X1=0.44 m and X2=0.222 m and initial pressure of 5.57 Pa.

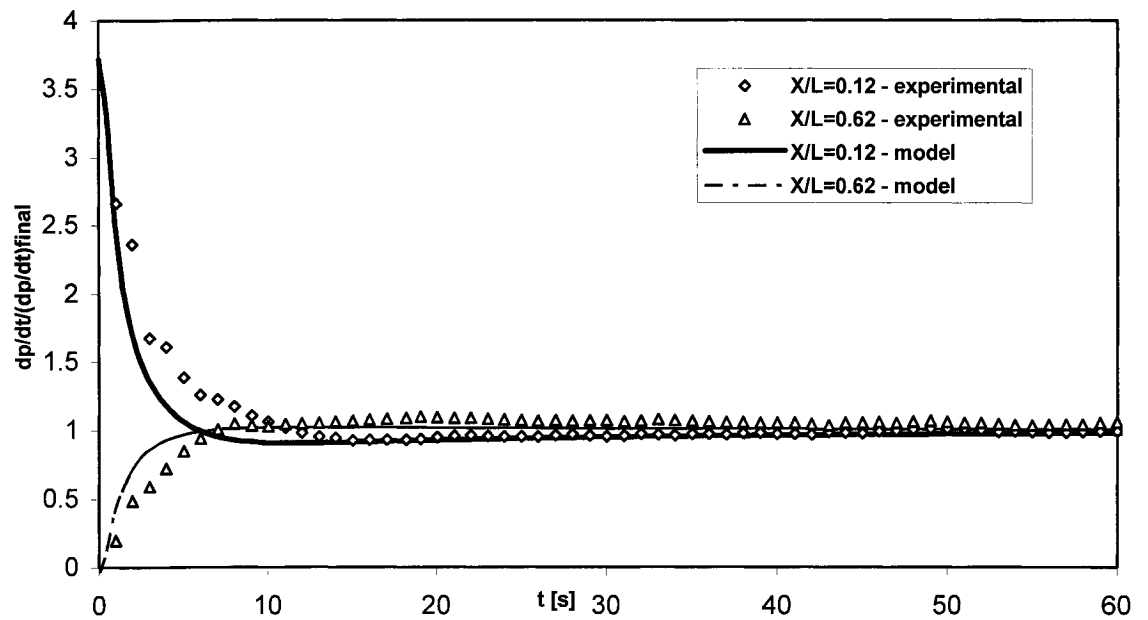

Figure AB-2-b The effect of initial pressure, dimensionless pressure responses to actual flow of 0.024 cm3 (STP)/min in 1/4" tube with length of 3.6 m at two different location x1=0.44 m and X2=0.222 m and initial pressure of 5.57 Pa.

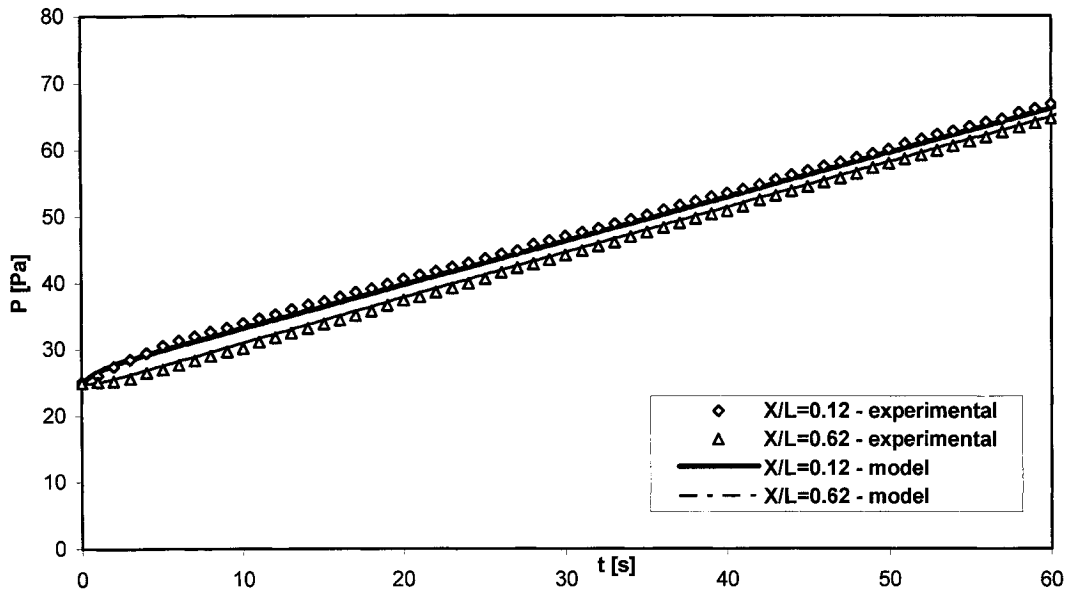

Figure AB-3-a Effect of initial pressure, pressure responses to actual flow of 0.024 cm3 (STP)/min in 1/4" tube with length of 3.6 m at two different location x1=0.44 m and X2=0.222 m and initial pressure of 25.01 Pa.

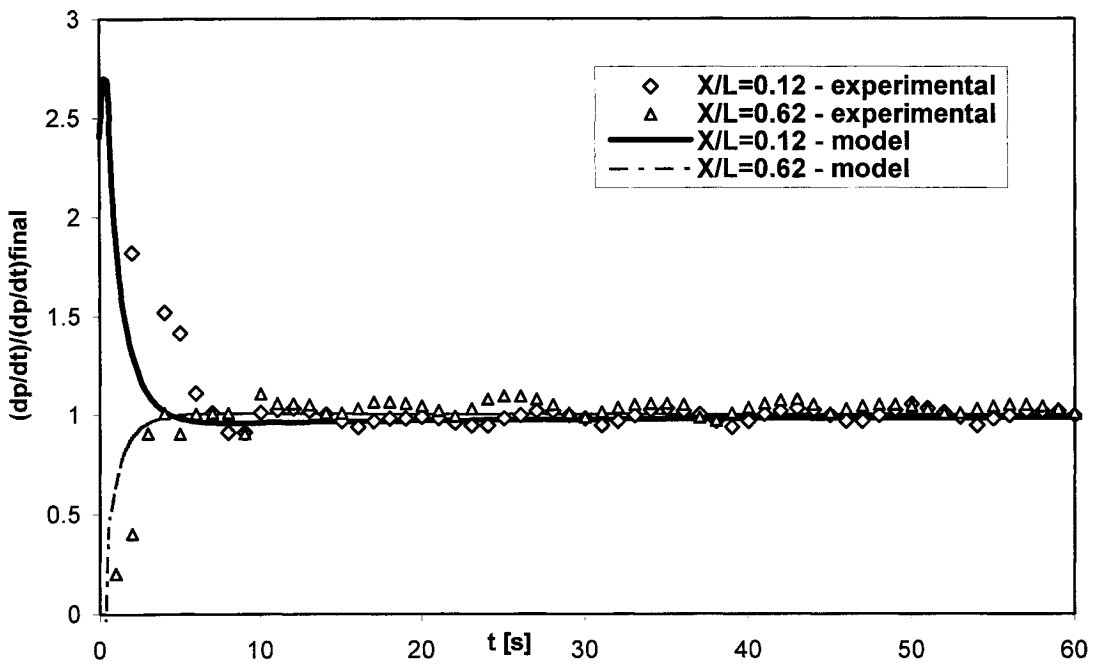

Figure AB-3-b Effect of initial pressure, dimensionless pressure responses to actual flow of 0.024 cm3 (STP)/min in 1/4" tube with length of 3.6 m at two different location x1=0.44 m and X2=0.222 m and initial pressure of
25.01 Pa.

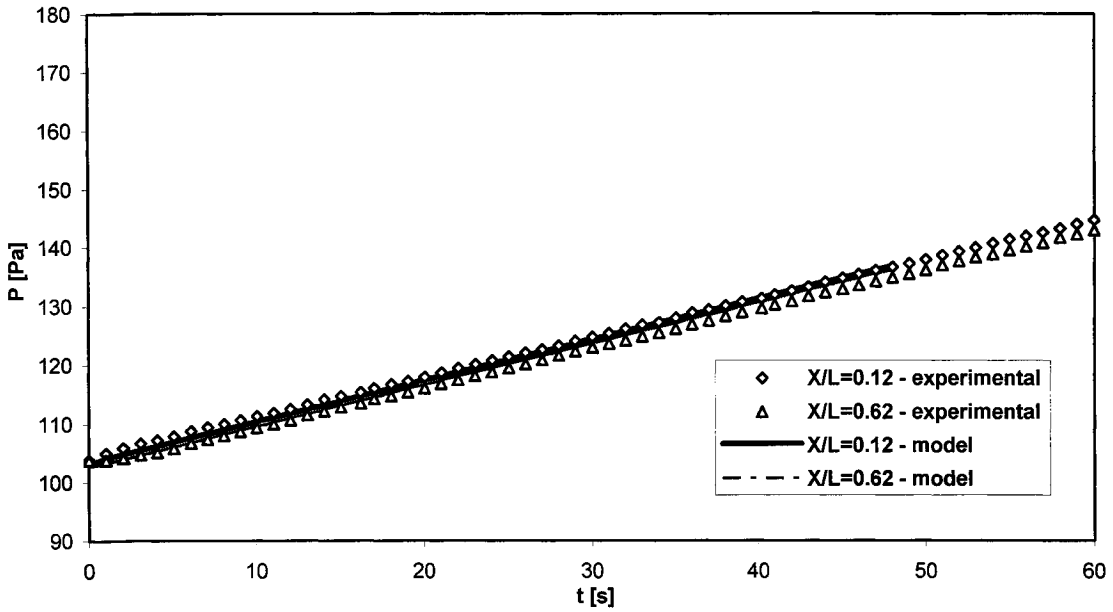

Figure AB-4-a Effect of initial pressure, pressure responses to actual flow of 0.024 cm3(STP)/min in 1/4" tube with lenght of 3.60 m and initial pressure of 103.86 Pa at two different location X1=0.44 m and X2=0.222 m. The model expectations also are available.

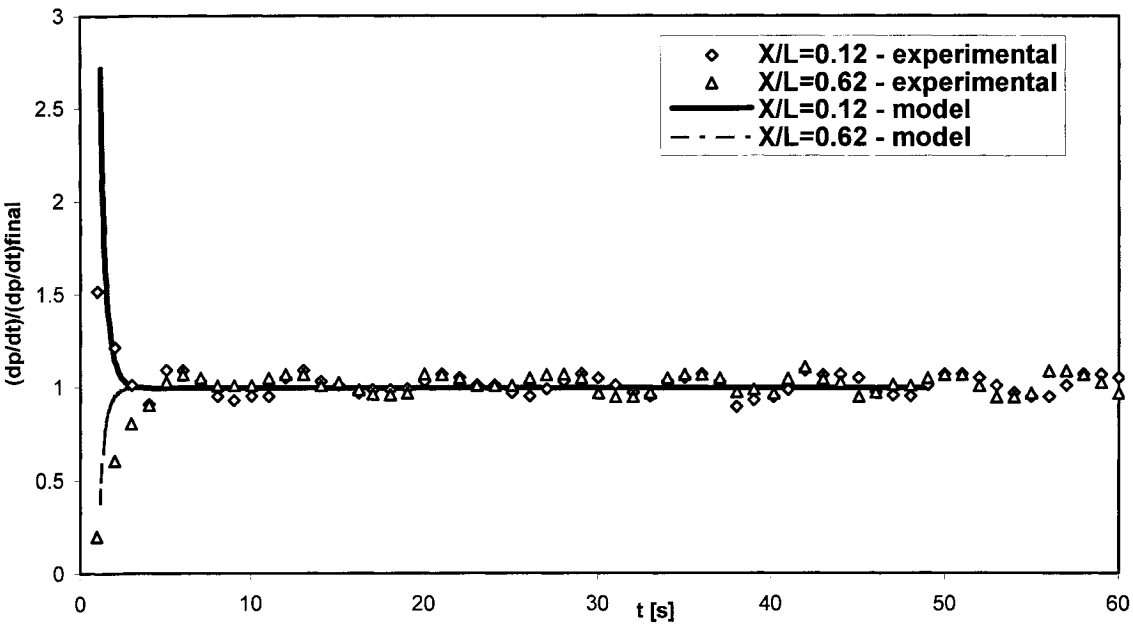

Figure AB-4-b The effect of initial pressure, dimensionless pressure responses to actual flow of 0.024 cm3 (STP)/min in 1/4" tube with length of 3.6 m at two different location x1=0.44 m and X2=0.222 m and initial pressure of 103.86Pa.

APPENDIX B

This appendix provides all experiments with mass flow controller and short tube, which contains two parts:

BA- Effect of flow

BB- Effect of initial pressure

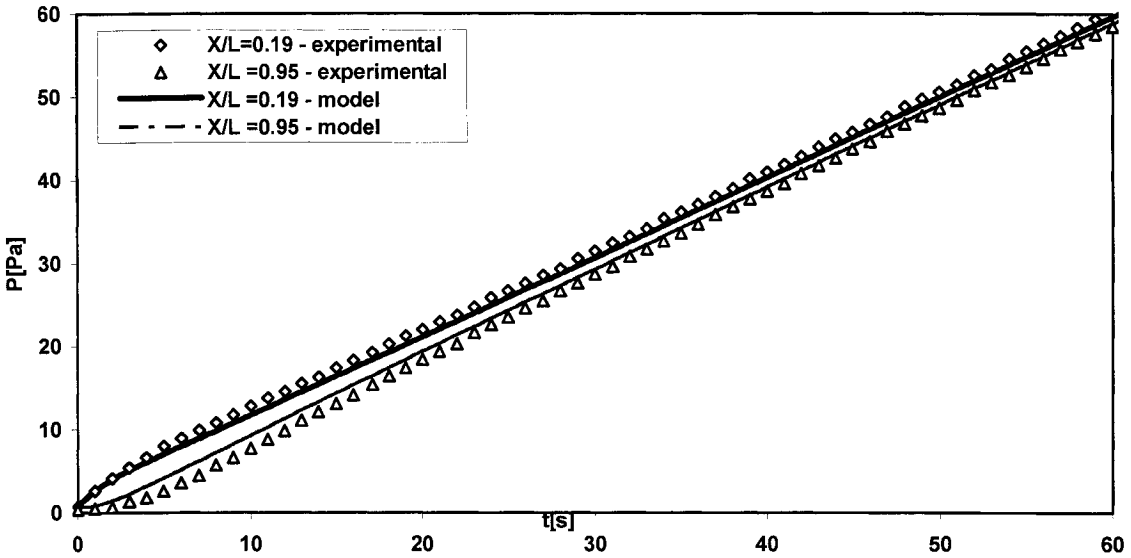

Figure BA-1- a Pressure responses to the constant set flow of N2 of 0.005 cm3 (STP)/min at two positions x=0.44 m and x=2.22 m in a 2.34 m short tube with internal diameter of 0.00386 m. The initial pressure is equal to 0.76 Pa comparing with pressure responses from non-constant D model at the same positions.

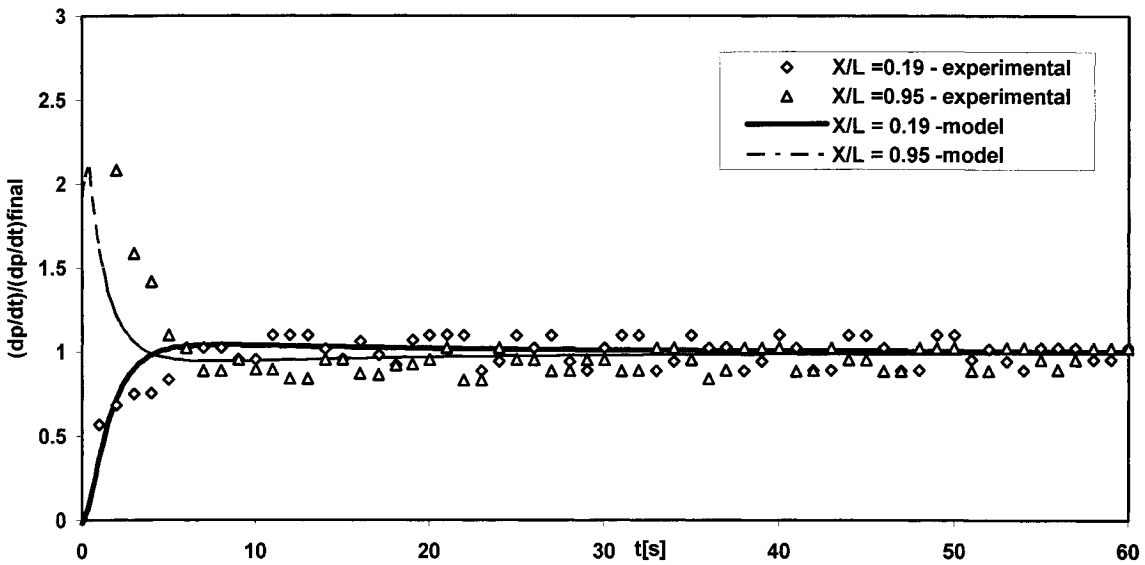

Figure BA-1-b Dimensionless Pressure response which indicates the error to the constant set flow of N2 of 0.005 cm3 (STP)/min at two positions x=0.44 m and x=2.22 m in a 2.34 m short tube with internal diameter of 0.00386 m. The initial pressure is equal to 0.76 Pa comparing with dimensionless pressure responses from non-constant D model at the same positions.

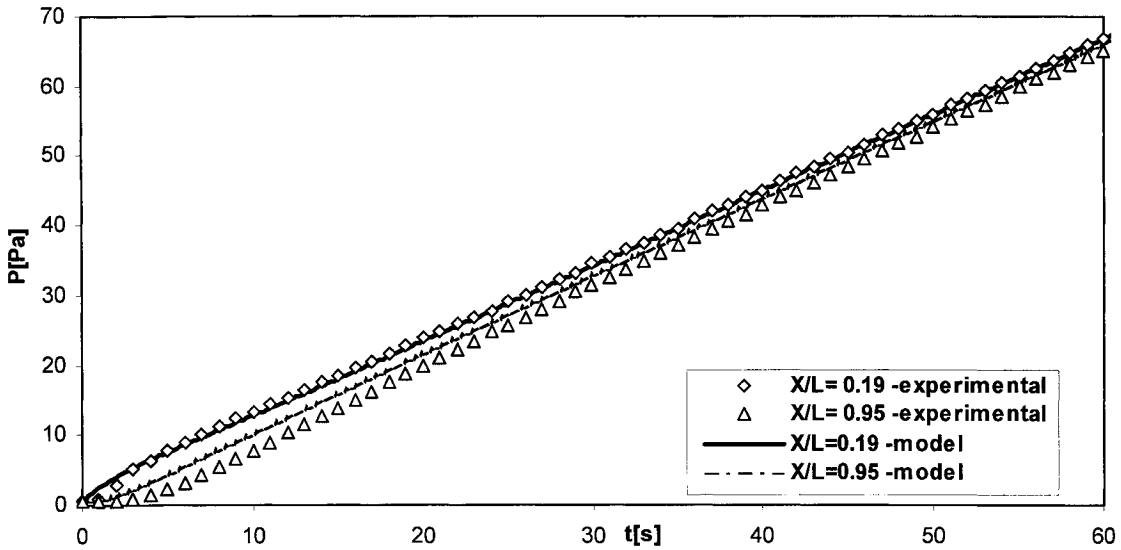

Figure BA-2- a Pressure responses to the constant actual flow of N2 of 0.032 cm3 (STP)/min at two positions x=0.44 m and x=2.22 m in a 2.34 m short tube with internal diameter of 0.00386 m. The initial pressure is equal to 0.54 Pa. comparing with pressure responses from non-constant D model at the same positions.

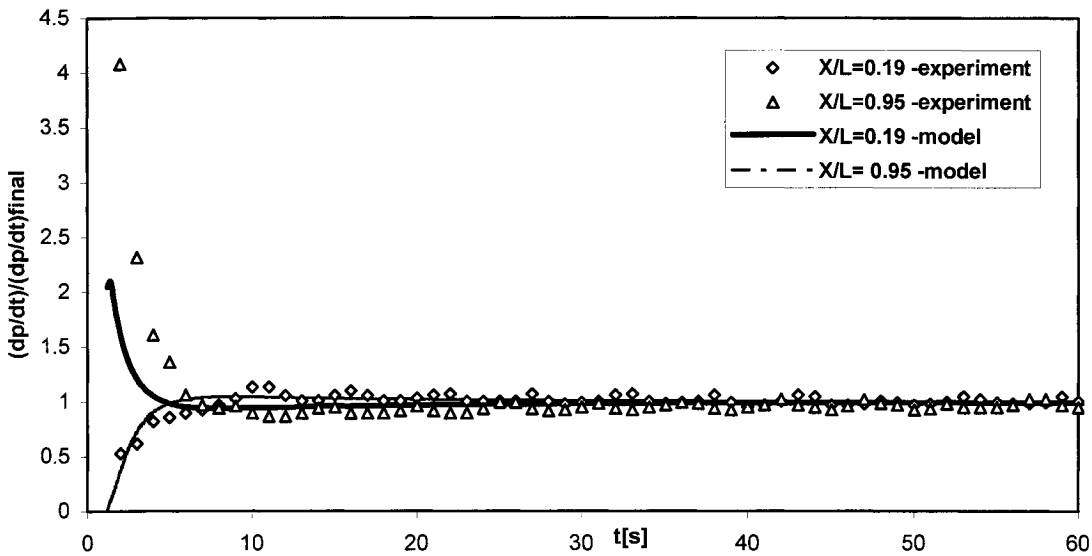

Figure BA-2-b Dimensionless Pressure response which indicates the error to the constant actual flow of N2 of 0.032 cm3 (STP)/min at two positions x=0.44 m and x=2.22 m in a 2.34 m short tube with internal diameter of 0.00386 m. The initial pressure is equal to 0.54 Pa comparing with dimensionless pressure responses from non-constant D model at the same positions.

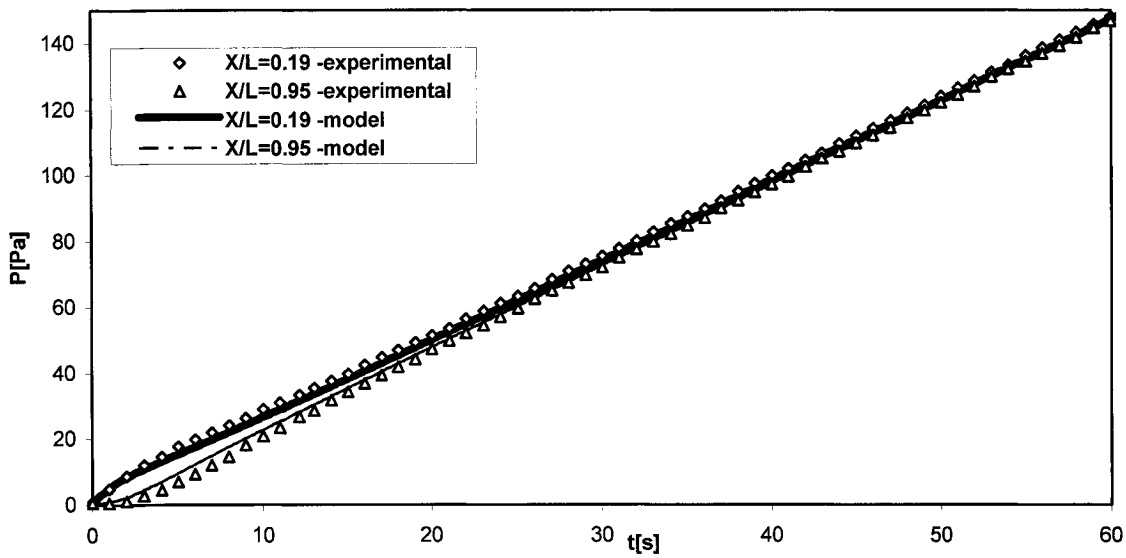

Figure BA-3- a Pressure responses to the constant actual flow of N2 of 0.073 cm3 (STP)/min at two positions x=0.44 m and x=2.22 m in a 2.34 m short tube with internal diameter of 0.00386 m. The initial pressure is equal to 0.54 Pa. comparing with pressure responses from non-constant D model at the same positions.

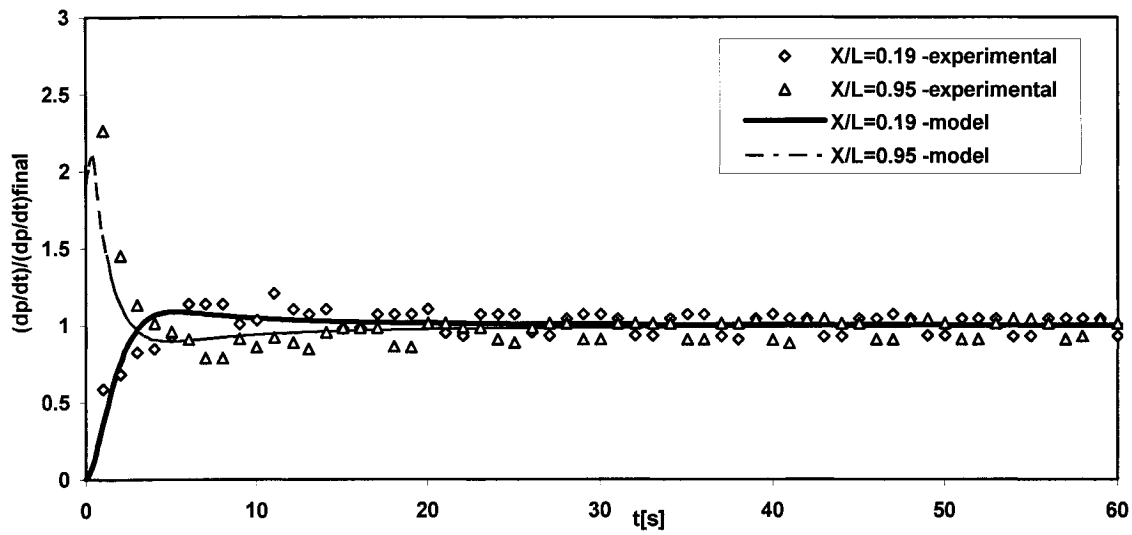

Figure BA-3-b Dimensionless Pressure response which indicates the error to the constant actual flow of N2 of 0.073 cm3 (STP)/min at two positions x=0.44 m and x=2.22 m in a 2.34 m short tube with internal diameter of 0.00386 m. The initial pressure is equal to 0.54 Pa. comparing with dimensionless pressure responses from non-constant D model at the same positions.

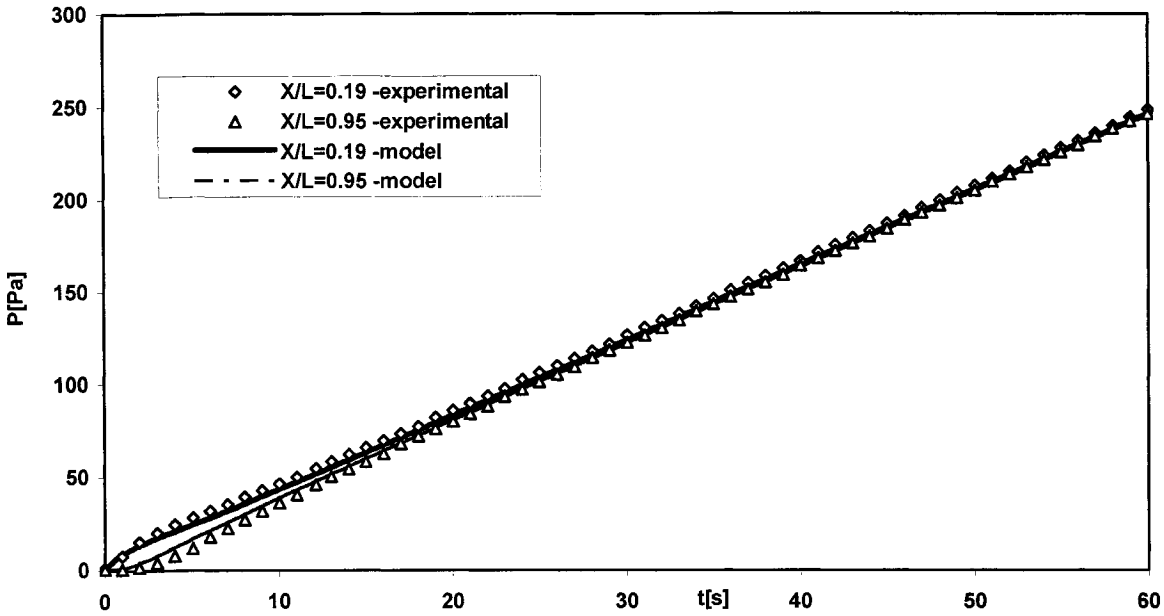

Figure BA-4- a Pressure responses to the constant actual flow of N2 of 0.12 cm3 (STP)/min at two positions x=0.44 m and x=2.22 m in a 2.34 m short tube with internal diameter of 0.00386 m. The initial pressure is equal to 0.73 Pa. comparing with pressure responses from non-constant D model at the same positions.

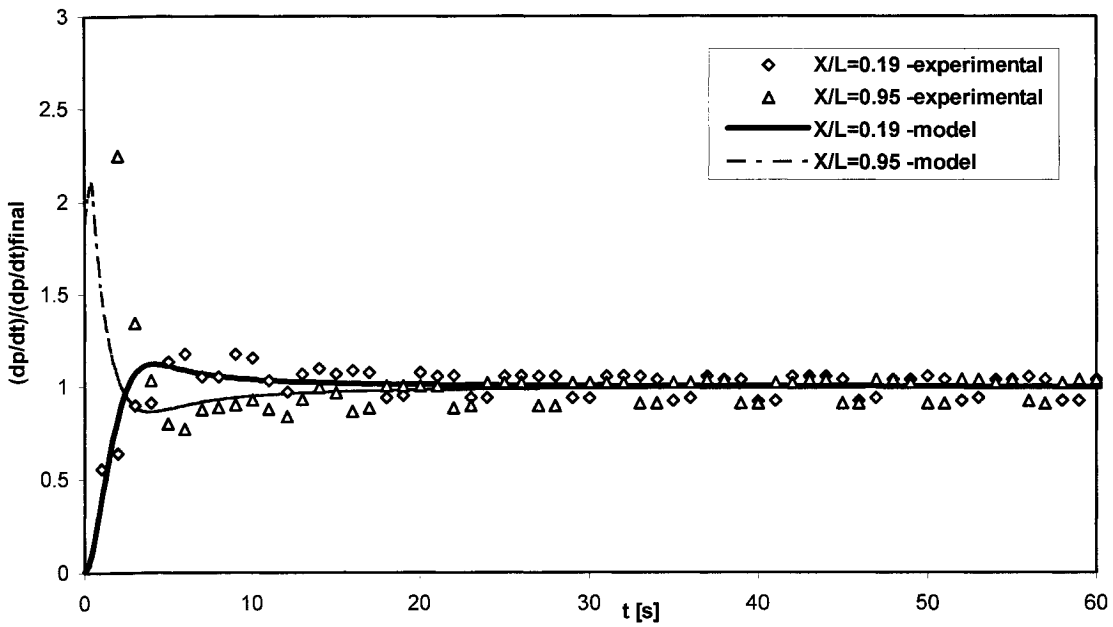

Figure BA-4-b Dimensionless Pressure responses which indicate the error to the constant actual flow of N2 of 0.12 cm3 (STP)/min at two positions x=0.44 m and x=2.22 m in a 2.34 m short tube with internal diameter of 0.00386 m. The initial pressure is equal to 0.73 Pa. comparing with dimensionless pressure responses from non-constant D model at the same positions.

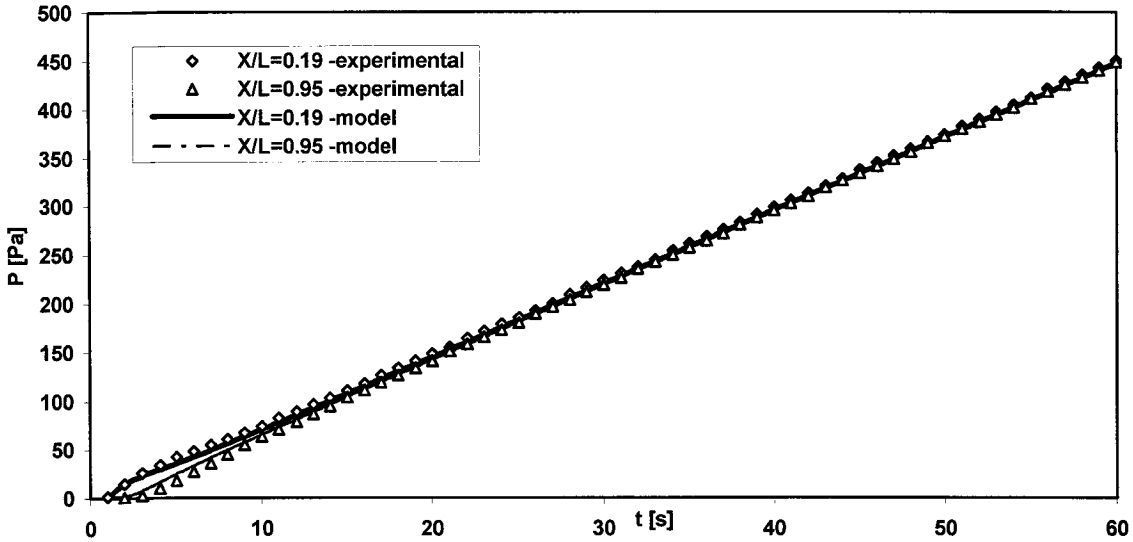

Figure BA-5- a Pressure responses to the constant actual flow of N2 of 0.22 cm3 (STP)/min at two positions x=0.44 m and x=2.22 m in a 2.34 m short tube with internal diameter of 0.00386 m. The initial pressure is equal to 1.27 Pa. comparing with pressure responses from non-constant D model at the same positions.

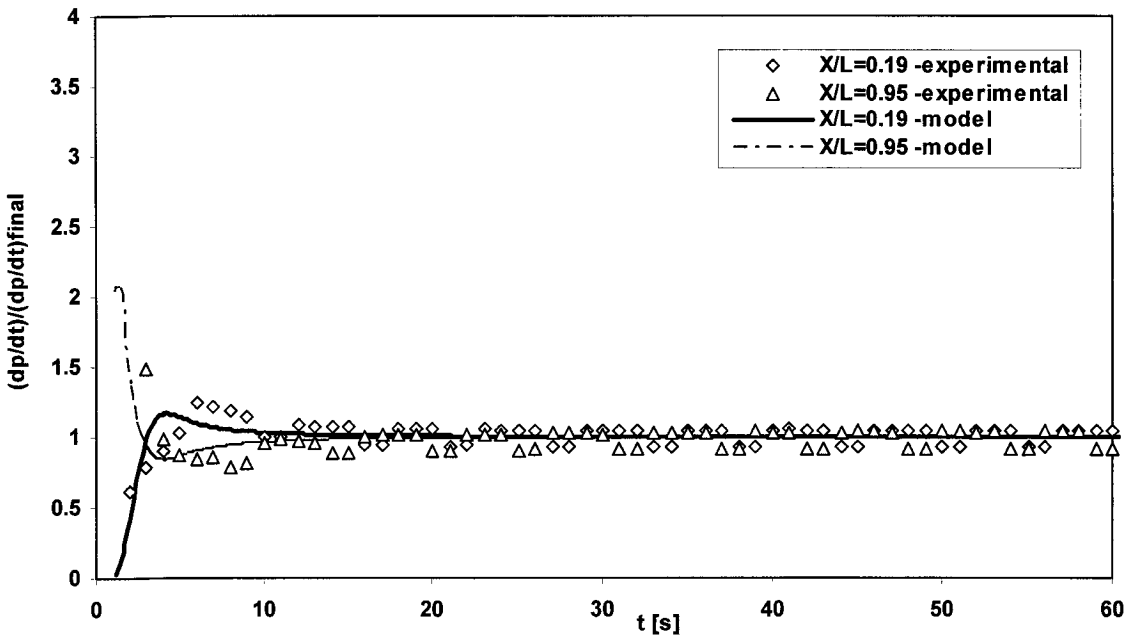

Figure BA-5-b Dimensionless Pressure response which indicates the error to the constant actual flow of N2 of 0.22 cm3 (STP)/min at two positions x=0.44 m and x=2.22 m in a 2.34 m short tube with internal diameter of 0.00386 m. The initial pressure is equal to 1.27 Pa. comparing with dimensionless pressure responses from non-constant D model at the same positions.

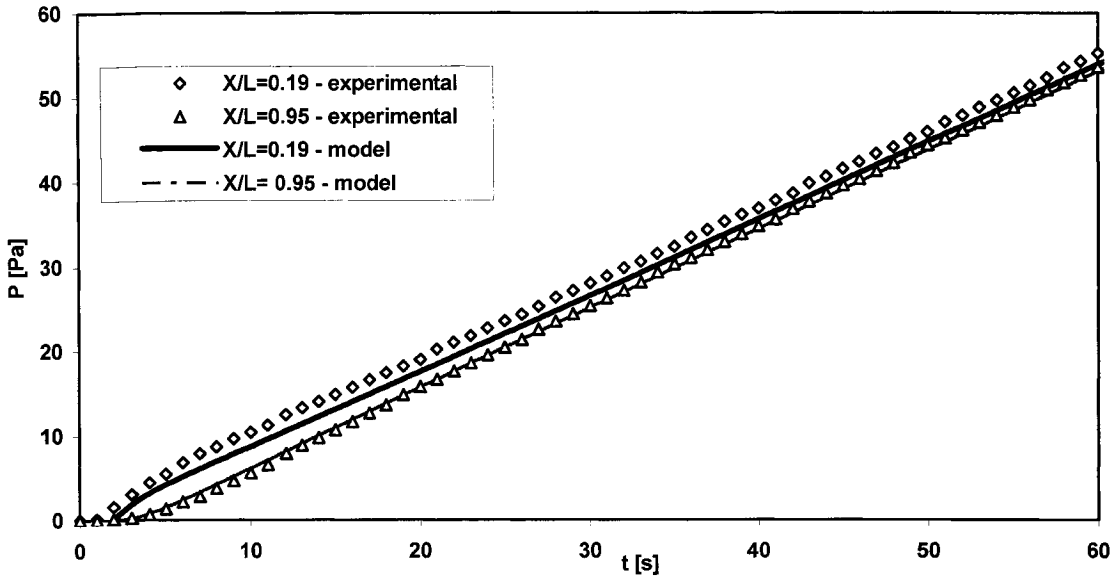

Figure BB-1-a Effect of initial pressure, pressure responses to actual flow of 0.024 cm3 (STP)/min in 1/4" tube with length of 2.34 m at two different lpositions X1=0.44 m and X2=0.222 m and initial pressure of 0.12 Pa. Comparison between the model with non-constant D and the experimental data at the same conditions.

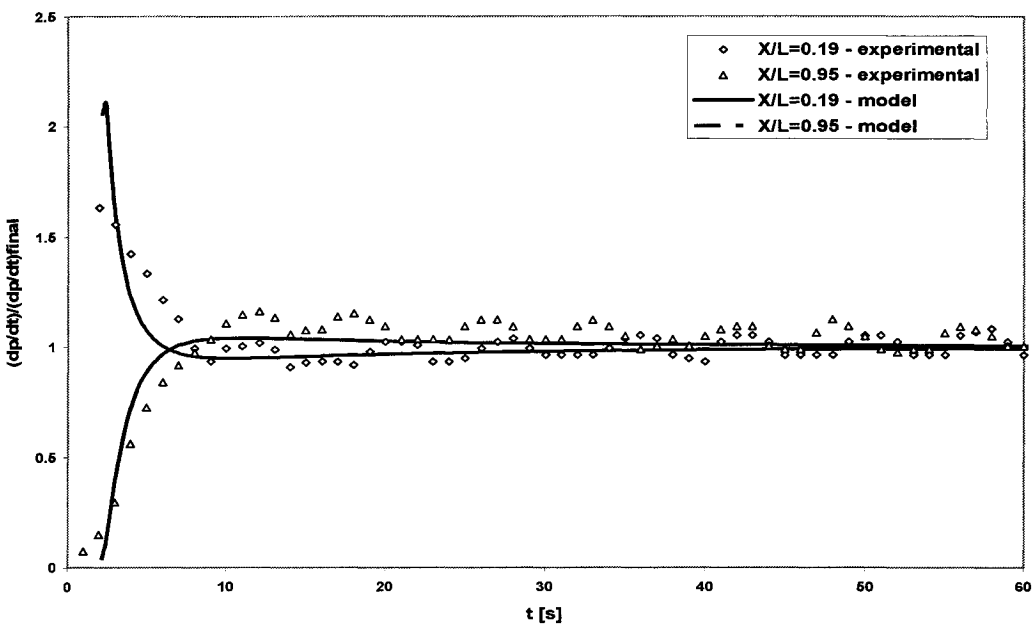

Figure BB-1-b The effect of initial pressure, dimensionless pressure responses to actual flow of 0.024 cm3 (STP)/min in 1/4" tube with length of 2.34 m at two different location X1=0.44 m and X2=0.222 m and initial pressure of 0.13 Pa. Comparison between the model with non-constant D and the experimental data.

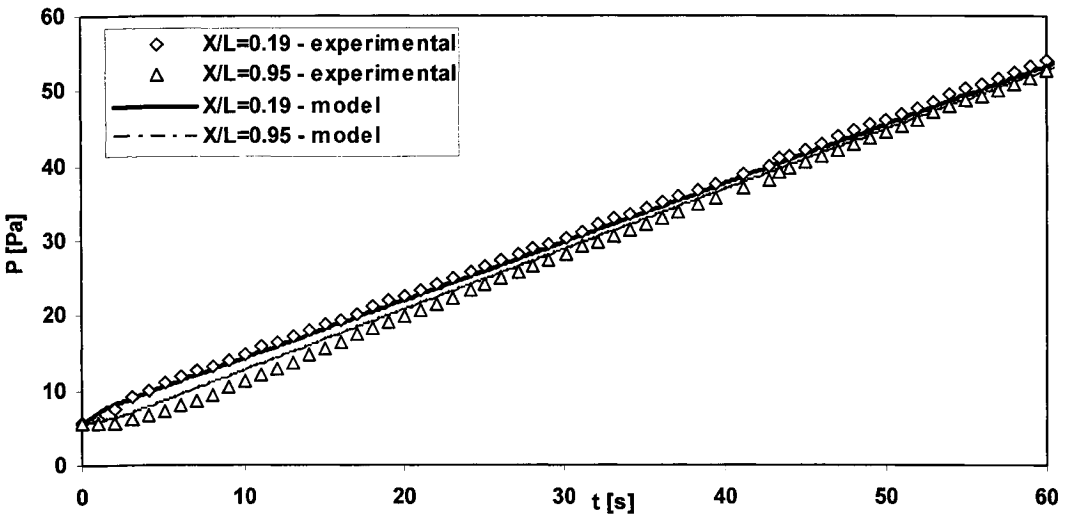

Figure BB-2-a Effect of initial pressure, pressure responses to actual flow of 0.024 cm3 (STP)/min in 1/4" tube with length of 2.34 m at two different location X1=0.44 m and X2=0.222 m and initial pressure of 5.62 Pa. Comparison between the model with non-constant D and the experimental data at the same conditions.

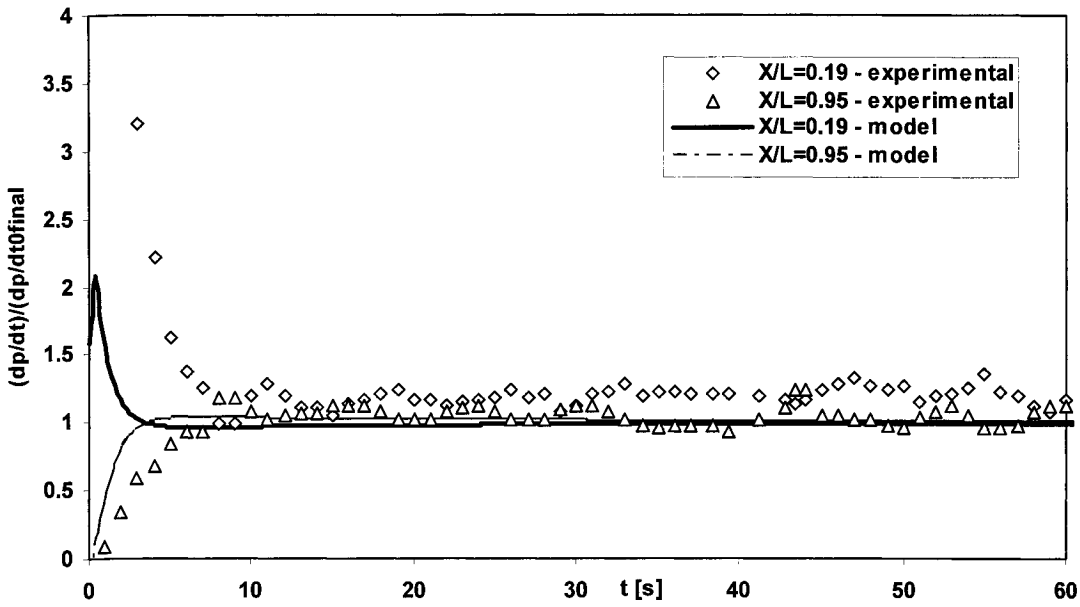

Figure BB 2-b Effect of initial pressure, dimensionless pressure responses to actual flow of 0.024 cm3 (STP)/min in 1/4" tube with length of 2.34 m at two different location x1=0.44 m and X2=0.222 m and initial pressure of 5.62 Pa. Comparison between the model with non-constant D and the experimental

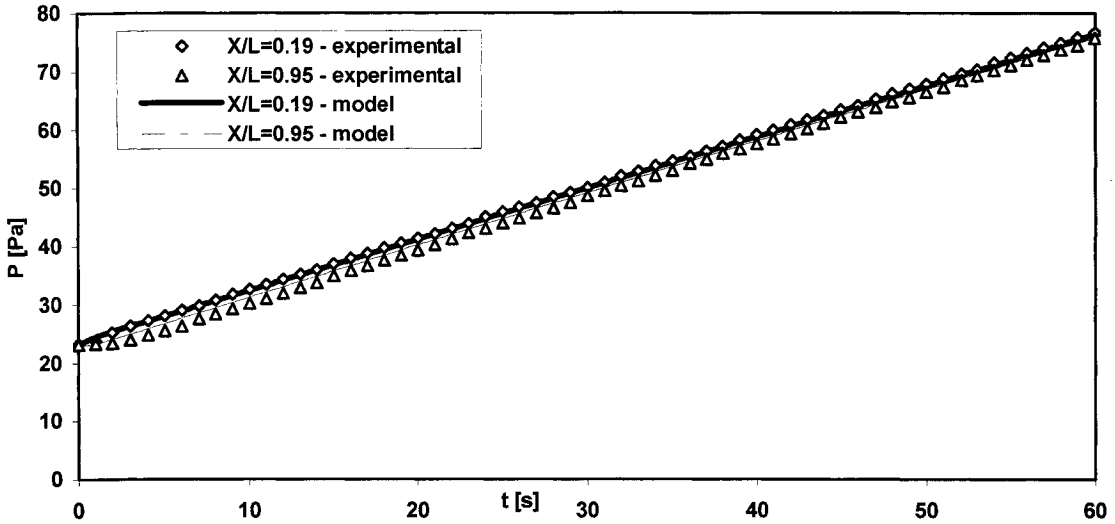

Figure BB-3-a Effect of initial pressure, pressure responses to actual flow of 0.024 cm3 (STP)/min in 1/4" tube with length of 2.34 m at two different location x1=0.44 m and X2=0.222 m and initial pressure of 23.28 Pa. Comparison between the model with non-constant D and the experimental data at the same conditions.

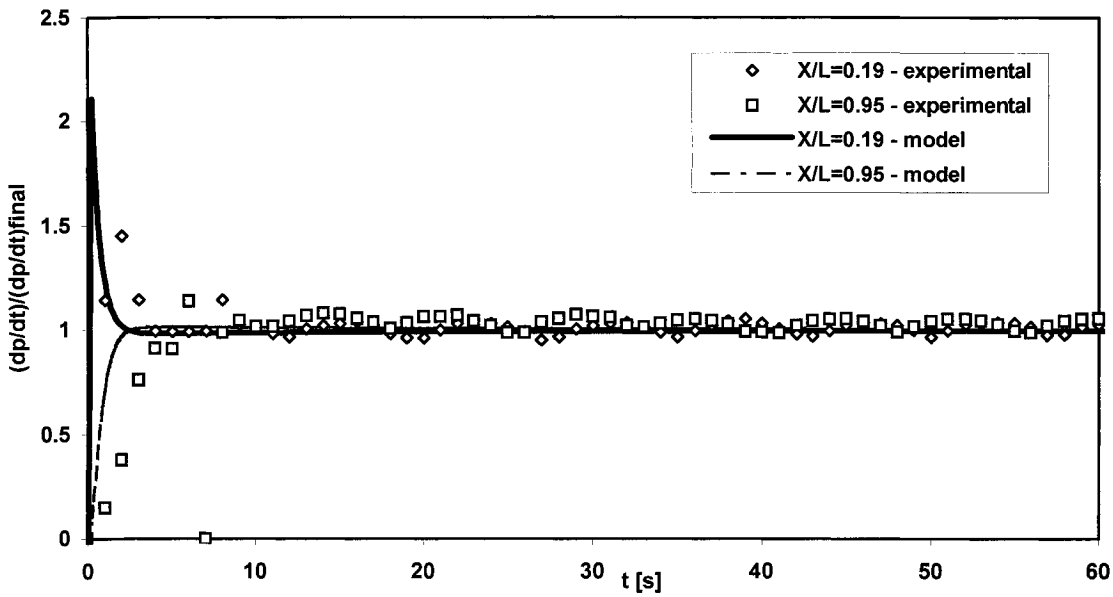

Figure BB-3-b Effect of initial pressure, dimensionless pressure responses to actual flow of 0.024 cm3 (STP)/min in 1/4" tube with length of 2.34 m at two different location X1=0.44 m and X2=0.222 m and initial pressure of 23.28 Pa. Comparing with pressure responses from the non-constant D model at the same positions.

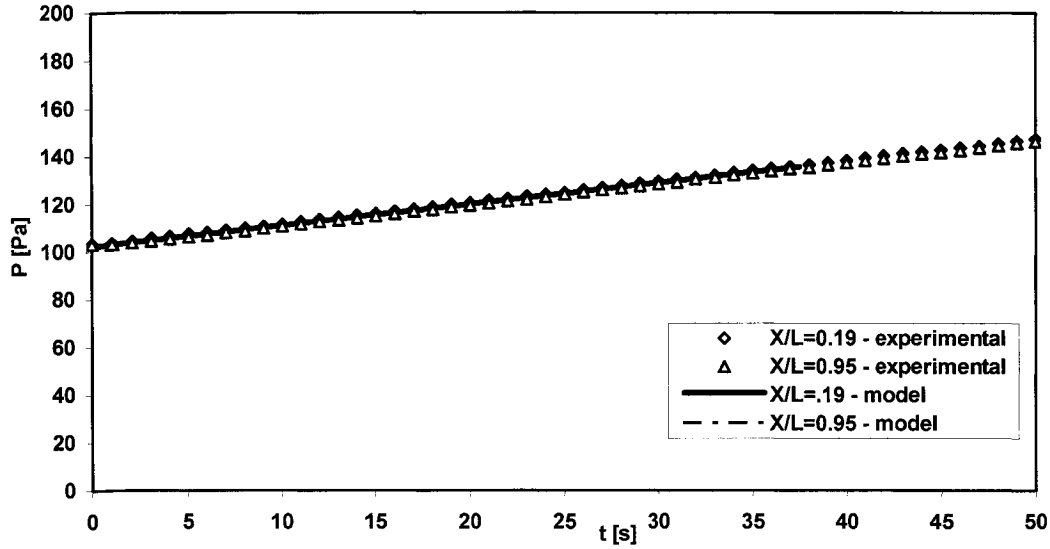

Figure 4-a Effect of initial pressure, pressure responses to actual flow of 0.024 cm3 (STP)/min in 1/4" tube with length of 2.34 m at two different location x1=0.44 m and X2=0.222 m and initial pressure of 103.03 Pa. Comparison between the model with non-constant D and the experimental data at the same conditions.

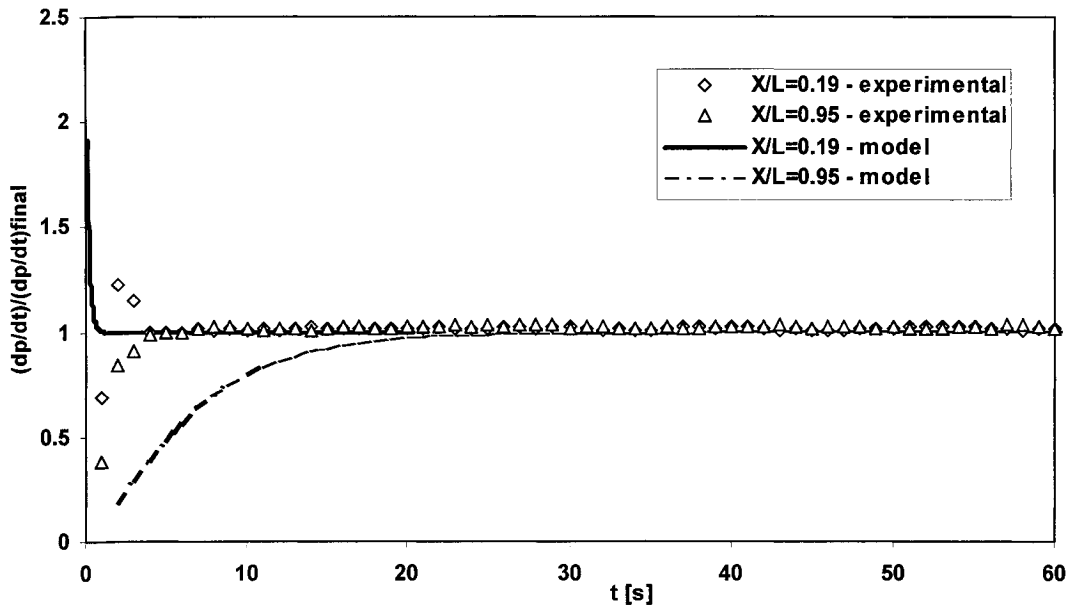

Figure BB-4-b Effect of initial pressure, dimensionless pressure responses to actual flow of 0.024 cm3 (STP)/min in 1/4" tube with length of 2.34 m at two different location X1=0.44 m and X2=0.222 m and initial pressure of 103.03 Pa. Comparing with pressure responses from the non-constant D model at the same positions.

APPENDIX C

This appendix provides all experiments with PPO membrane, which contains four parts:

CA- Experiment with PPO membrane and long tube

CB- Experiment with PPO membrane and short tube

CC- Experiment with PPO membrane and ½ "tube

CD- Experiment with PPO membrane and accumulation tank

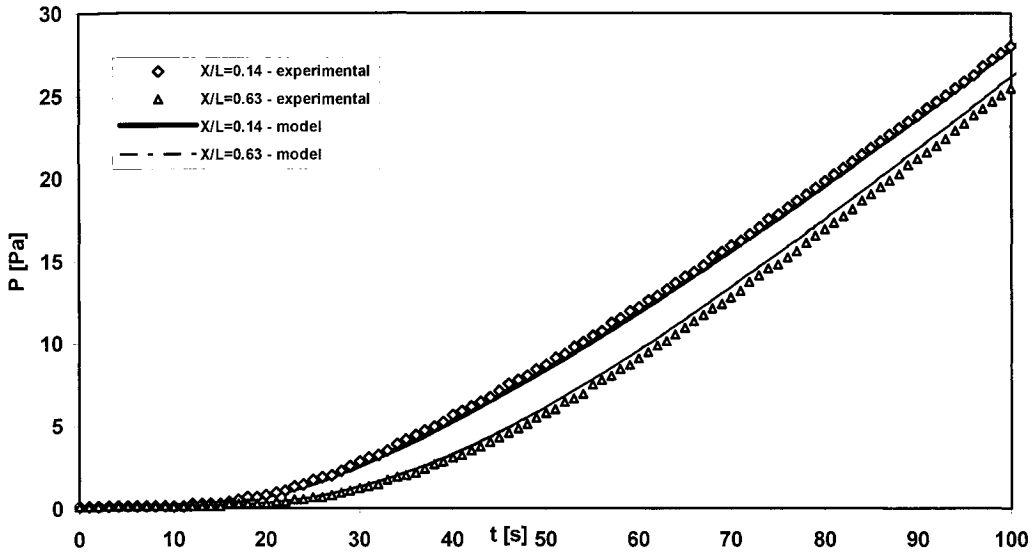

Figure CA-1- Pressure responses at two positions in ¼" tube with a length of 3.65 m and initial pressure of 0.133Pa to determine transport properties of N2 in PPO membrane. The feed pressure is 206800 Pa and temperature is 23°C.

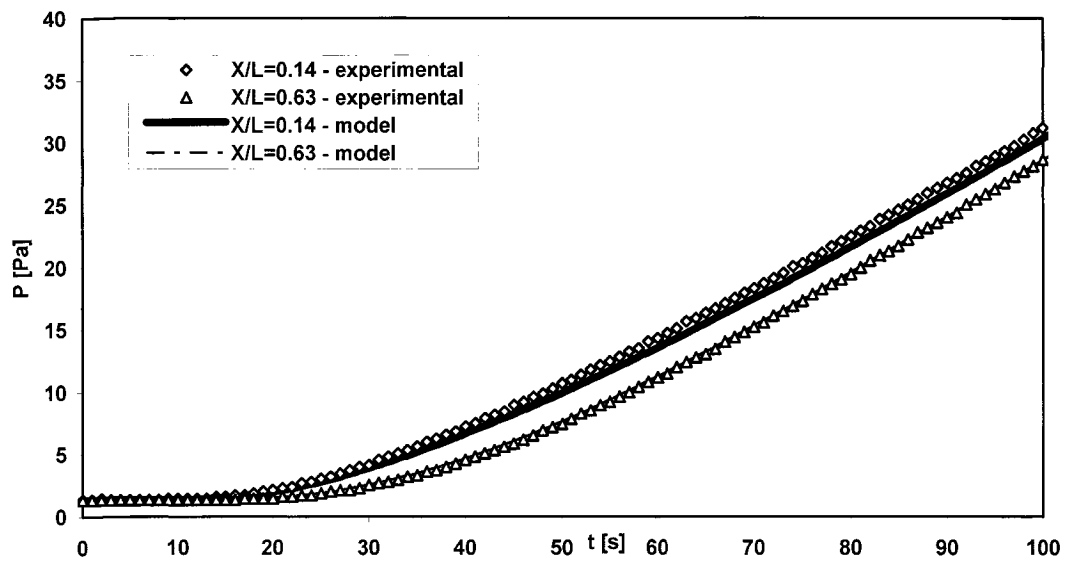

Figure CA-2- Pressure responses at two positions in ¼" tube with a length of 3.65 m and initial pressure of 1.33 Pa to determine transport properties of N2 in PPO membrane. The feed pressure is 206800 Pa and temperature is 23°C.

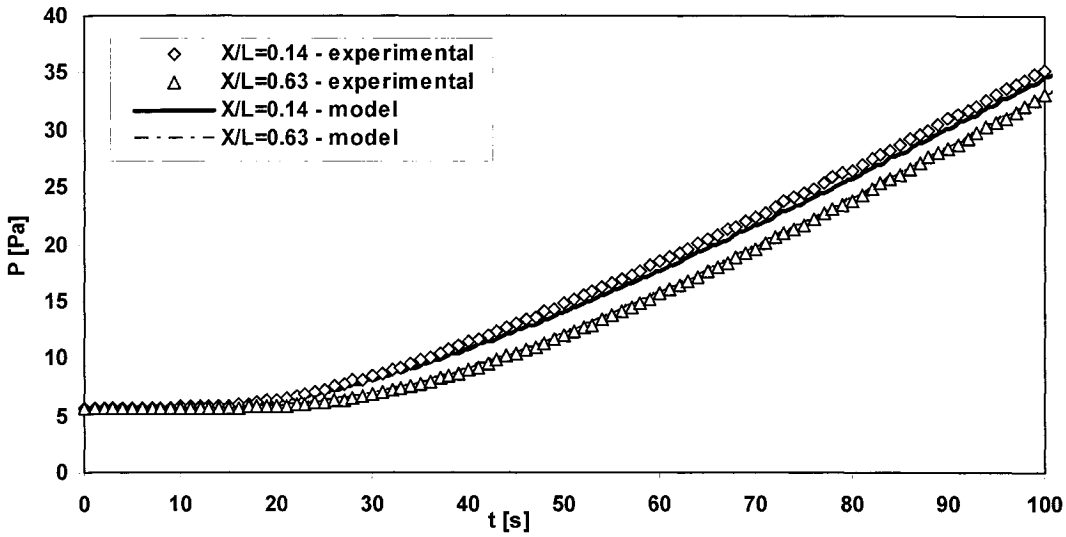

Figure CA-3- Pressure responses at two positions in ¼" tube with a length of 3.65 m and initial pressure of 5.6 Pa to determine transport properties of N2 in PPO membrane. The feed pressure is 206800 Pa and temperature is 23^{o} C.

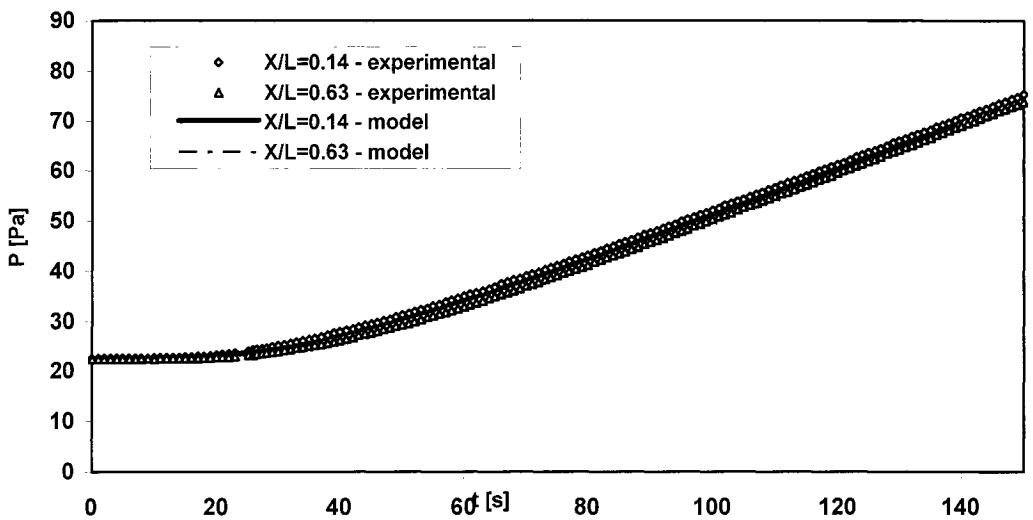

Figure CA-4- Pressure responses at two positions in ¼" tube with a length of 3.65 m and initial pressure of 22.63 Pa to determine transport properties of N2 in PPO membrane. The feed pressure is 206800 Pa and temperature is 23^{o}C.

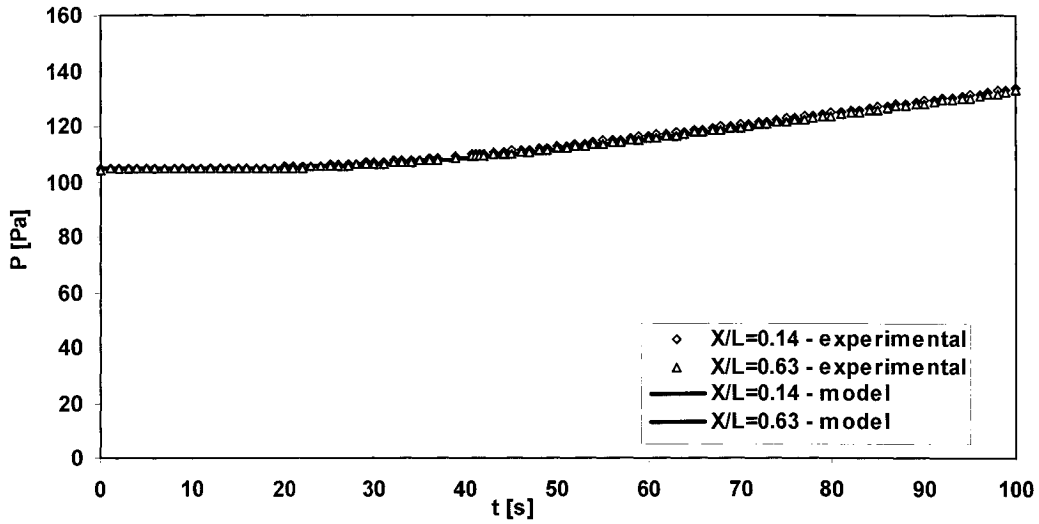

Figure CA-5- Pressure responses at two positions in ¼" tube with a length of 3.65 m and initial pressure of 104 Pa to determine transport properties of N2 in PPO membrane. The feed pressure is 206800 Pa and temperature is 23 °C.

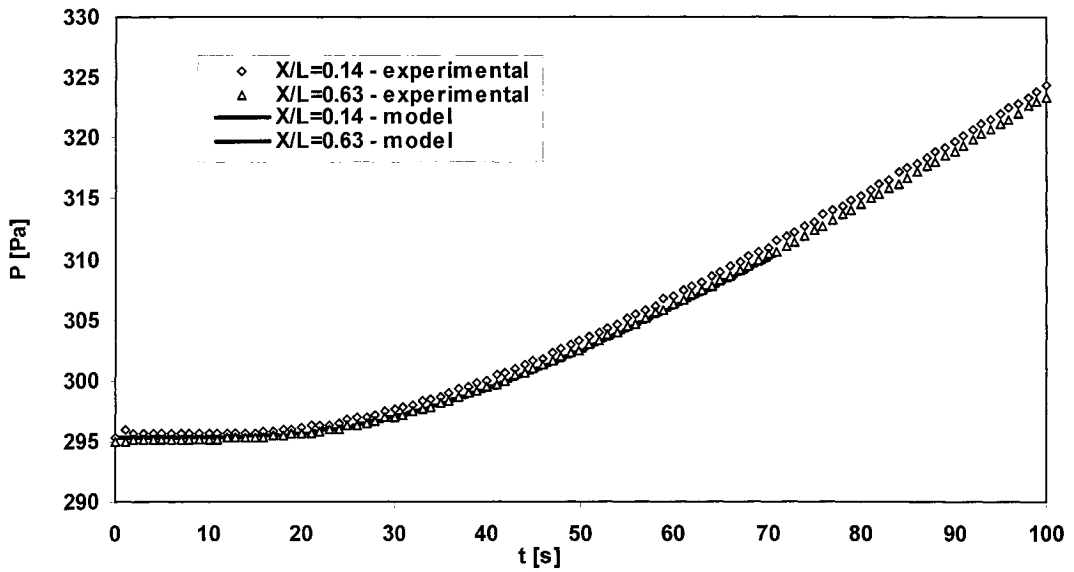

Figure CA-6- Pressure responses at two positions in ¼" tube with a length of 3.65 m and initial pressure of 293.84 Pa to determine transport properties of N2 in PPO membrane. The feed pressure is 206800 Pa and temperature is 23 °C.

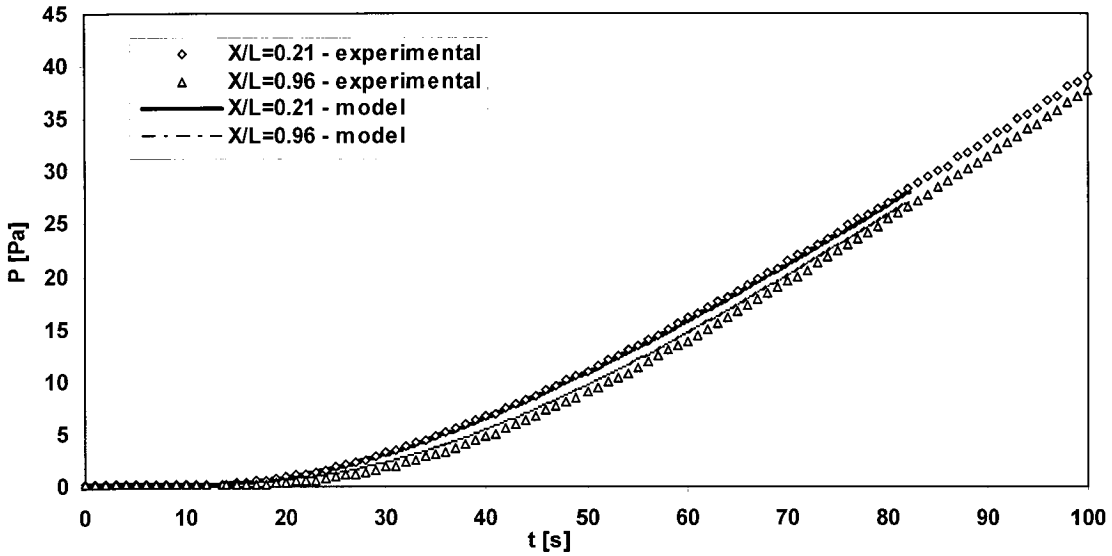

Figure CB-1- Pressure responses at two positions in ¼" tube with a length of 2.36 m and initial pressure of 0.133 Pa to determine transport properties of N2 in PPO membrane. The feed pressure is 206800 Pa and temperature is 23 °C.

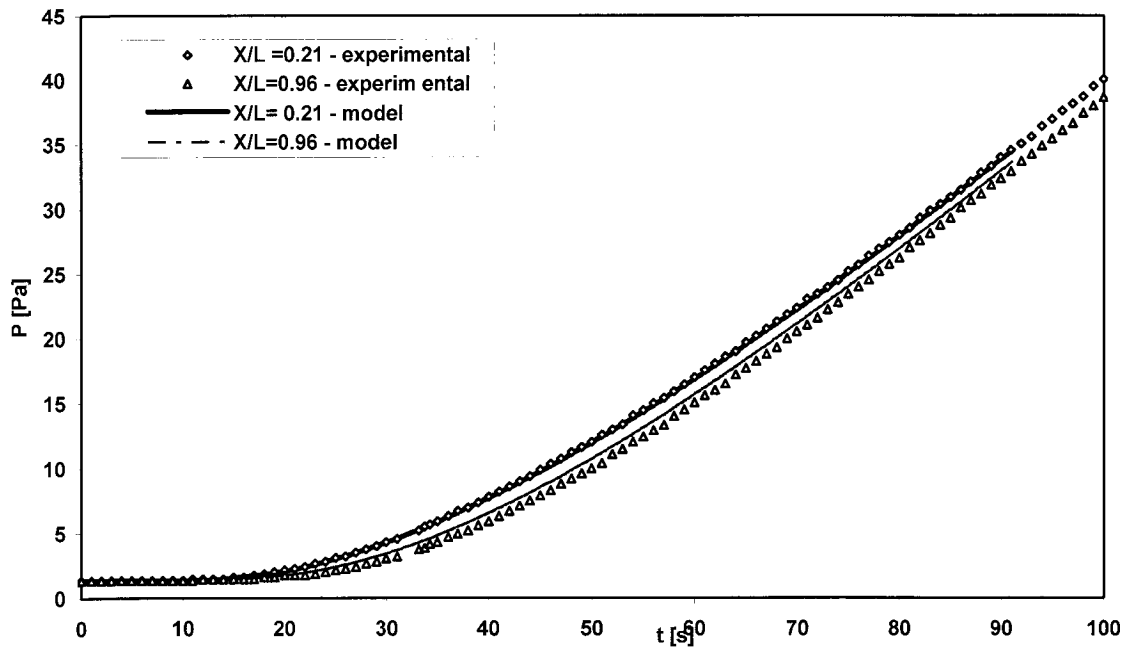

Figure CB-2- Pressure responses at two positions in ¼" tube with a length of 2.36 m and initial pressure of 1.33 Pa to determine transport properties of N2 in PPO membrane. The feed pressure is 206800 Pa and temperature is 23 °C.

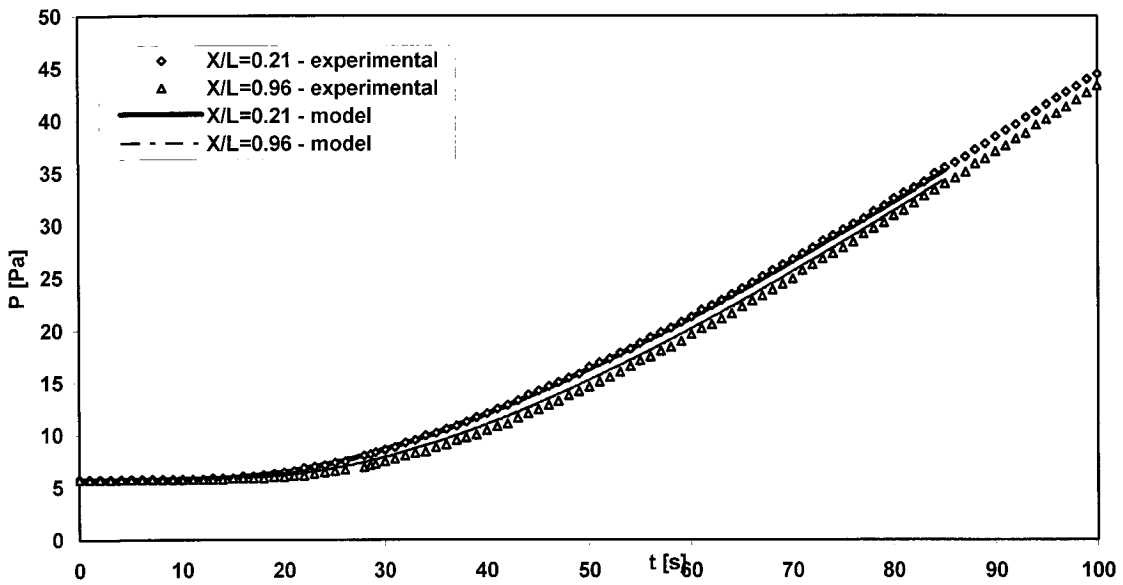

Figure CB-3- Pressure responses at two positions in ¼" tube with a length of 2.36 m and initial pressure of 5.75 Pa to determine transport properties of N2 in PPO membrane. The feed pressure is 206800 Pa and temperature is 23°C .

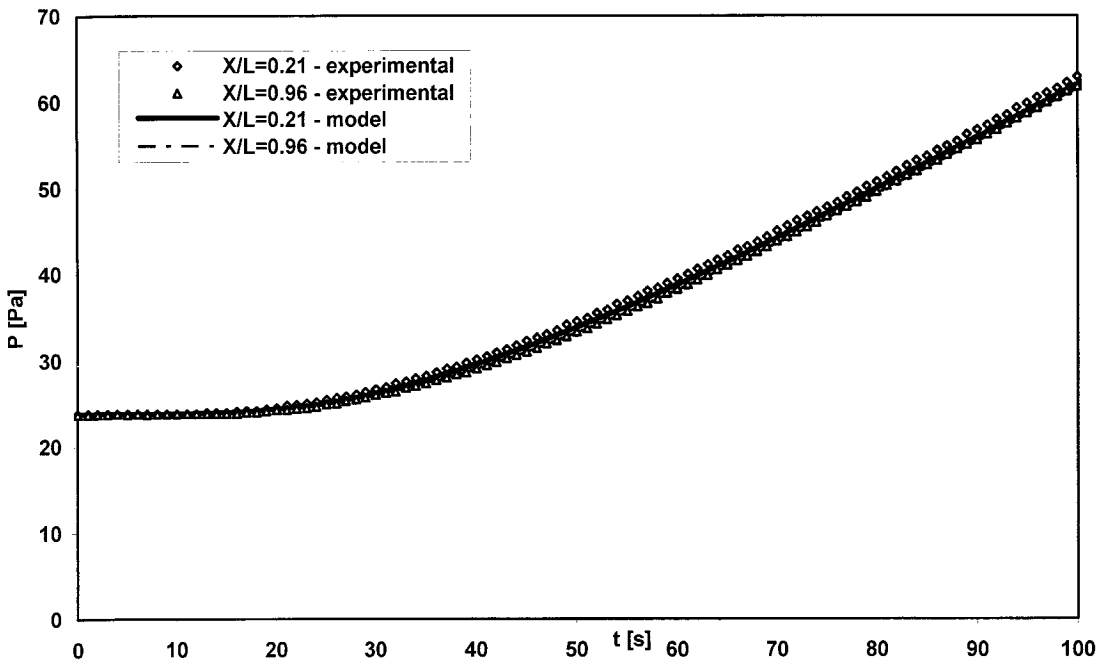

Figure CB-4- Pressure responses at two positions in ¼" tube with a length of 2.36 m and initial pressure of 23.84 Pa to determine transport properties of N2 in PPO membrane. The feed pressure is 206800 Pa and temperature is 23°C .

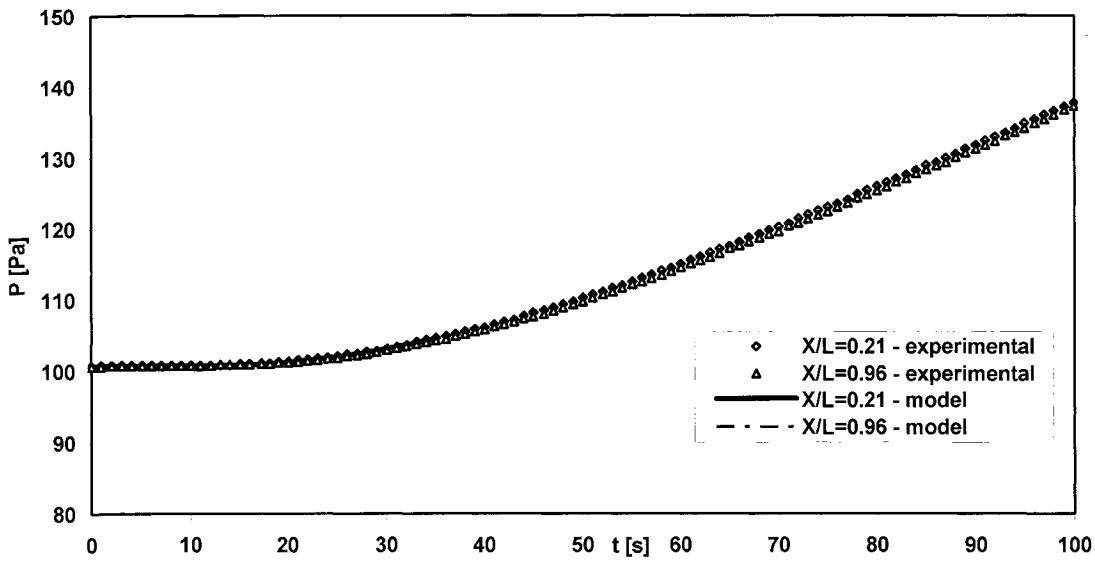

Figure CB-5- Pressure responses at two positions in ¼" tube with a length of 2.36 m and initial pressure of 100.75 Pa to determine transport properties of N2 in PPO membrane. The feed pressure is 206800 Pa and temperature is 23 °C .

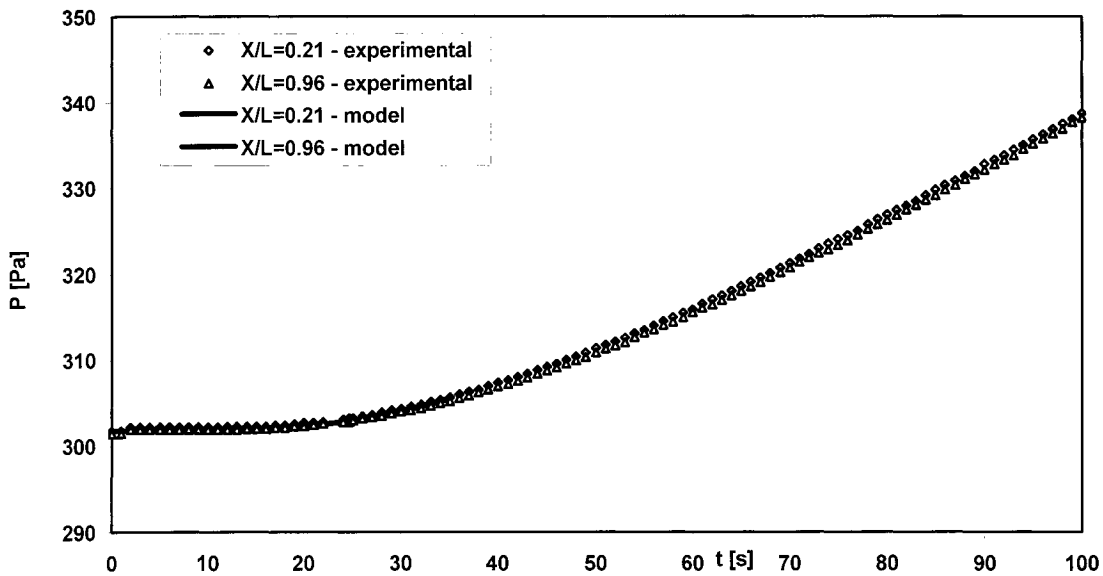

Figure CB-6- Pressure responses at two positions in ¼" tube with a length of 2.36 m and initial pressure of 301.73 Pa to determine transport properties of N2 in PPO membrane. The feed pressure is 206800 Pa and temperature is 23° C.

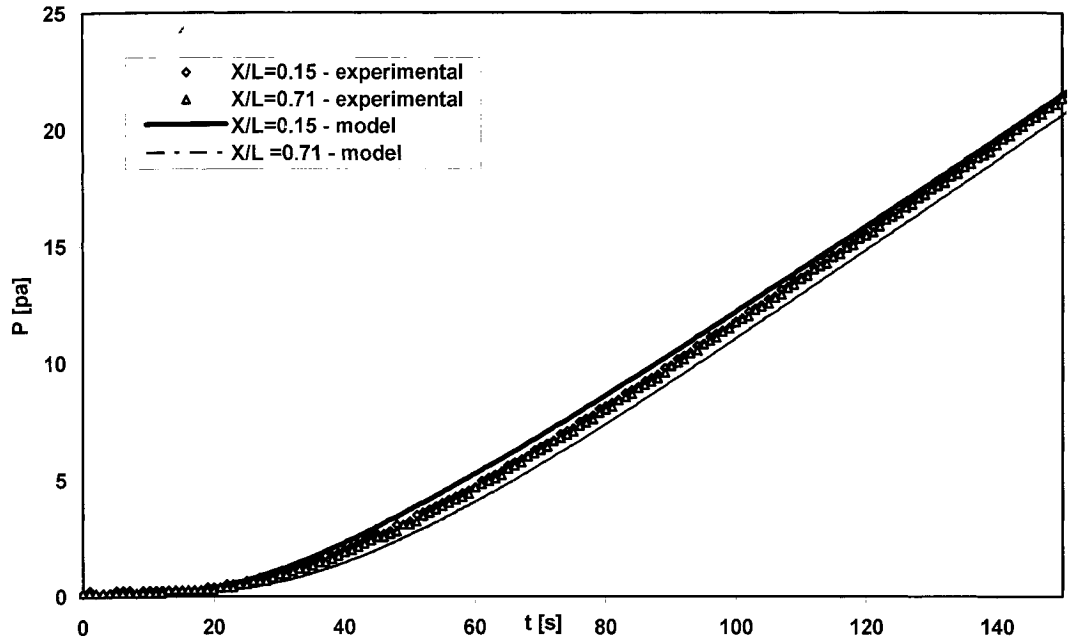

Figures CC-1- Pressure responses at two positions in ½" tube with a length of 3.65 m and initial pressure of 0.13 Pa to determine transport properties of N2 in PPO membrane. The feed pressure is 206800 Pa and temperature is 23 ^{O}C.

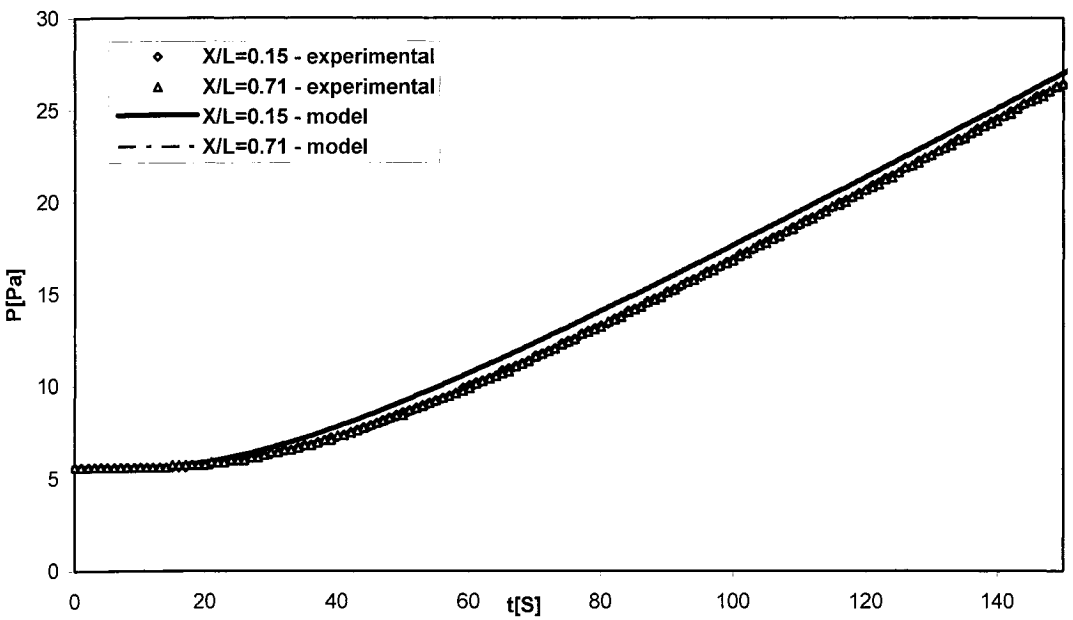

Figures CC-2- Pressure responses at two positions in ½" tube with a length of 3.65 m and initial pressure of 5.61 Pa to determine transport properties of N2 in PPO membrane. The feed pressure is 206800 Pa and temperature is 23 ^{O}C.

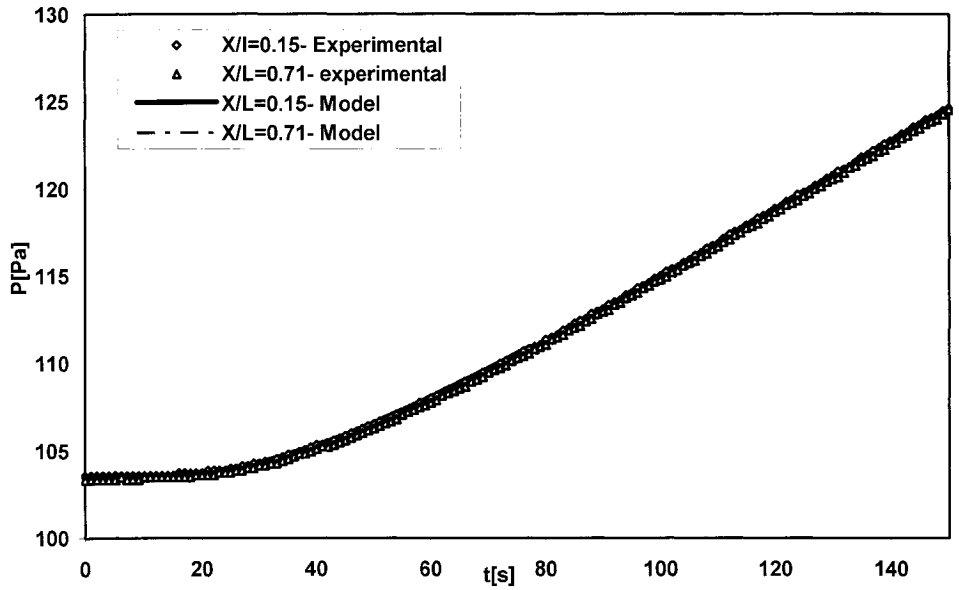

Figures CC-3- Pressure responses at two positions in ½" tube with a length of 3.65 m and initial pressure of 104.3 Pa to determine transport properties of N2 in PPO membrane. The feed pressure is 206800 Pa and temperature is 23 ^{O}C.

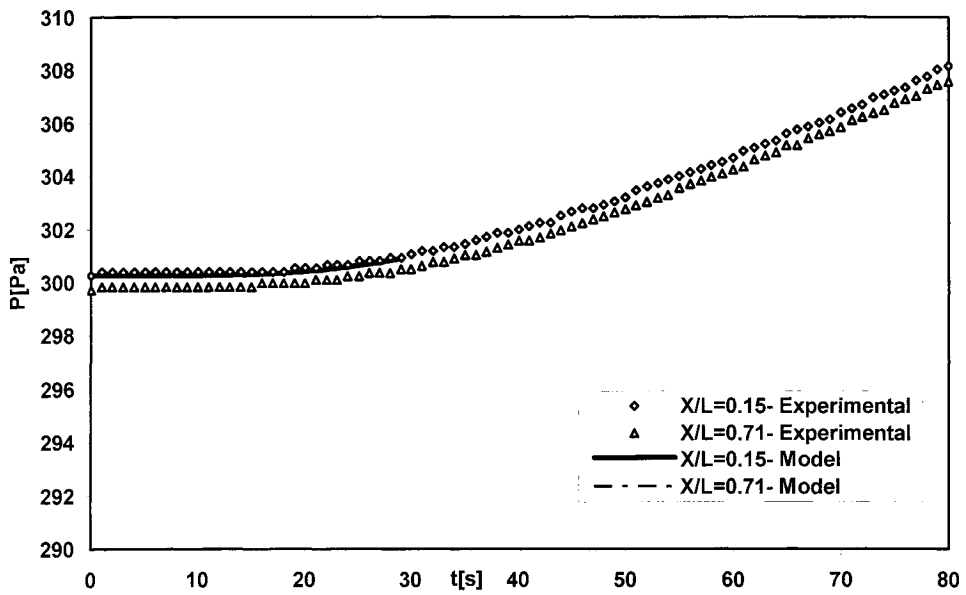

Figures CC-4- Pressure responses at two positions in ½" tube with a length of 3.65 m and initial pressure of 300.26 Pa to determine transport properties of N2 in PPO membrane. The feed pressure is 206800 Pa and temperature is 23 ^{O}C.

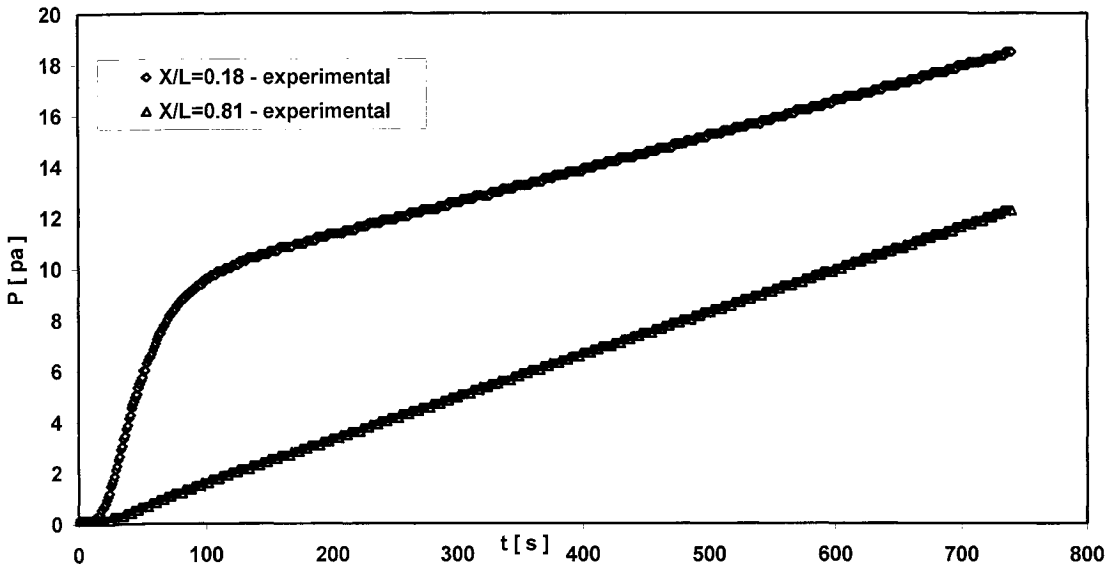

Figure CD-1- Experiment with accumulation tank and PPO membrane. The effect of feed pressure on pressure responses at two positions x1=0.18, x2=0.81 in ¼" stainless steel tube with a length of 2.36 m and initial pressure of 0.13 Pa and feed pressure of 30 PSI. The volume of tank is V=2250 cm3 attached at the end of the tube, T=23^{o}C.

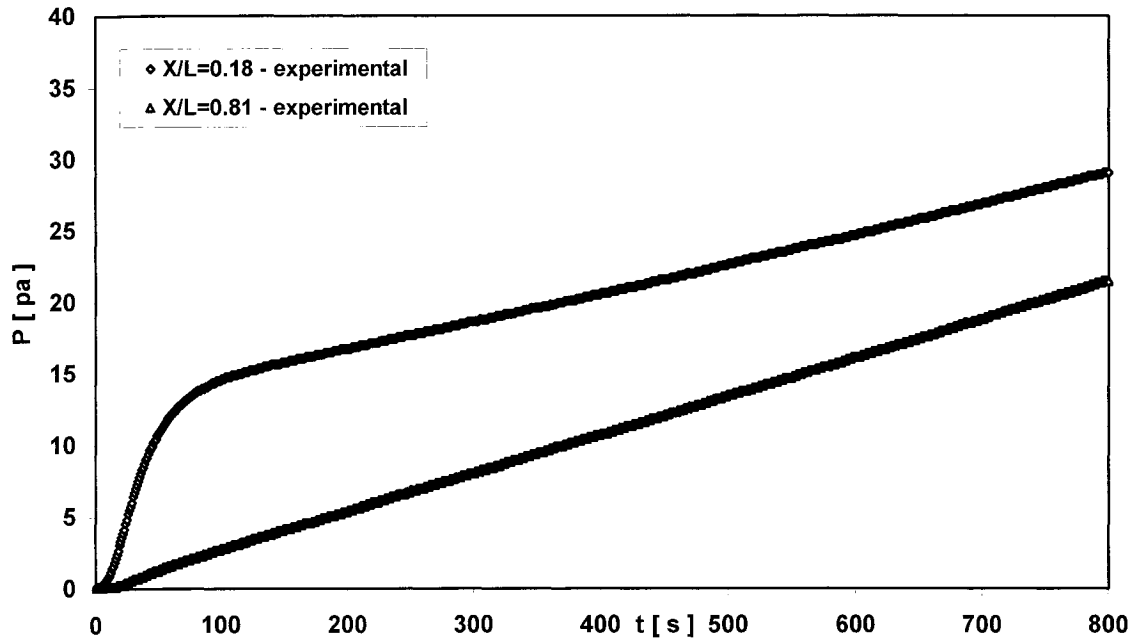

Figures CD-2- experiment with accumulation tank and PPO membrane. The effect of feed pressure on pressure responses at two positions x1=0.18, x2=0.81 in ¼" stainless steal tube with a length of 2.36 m and initial pressure of 0.13 pa and feed pressure of 50 PSI. The volume of tank is V=2250 cm^3 attached at the end of tube, T= 23 ^{O}C.

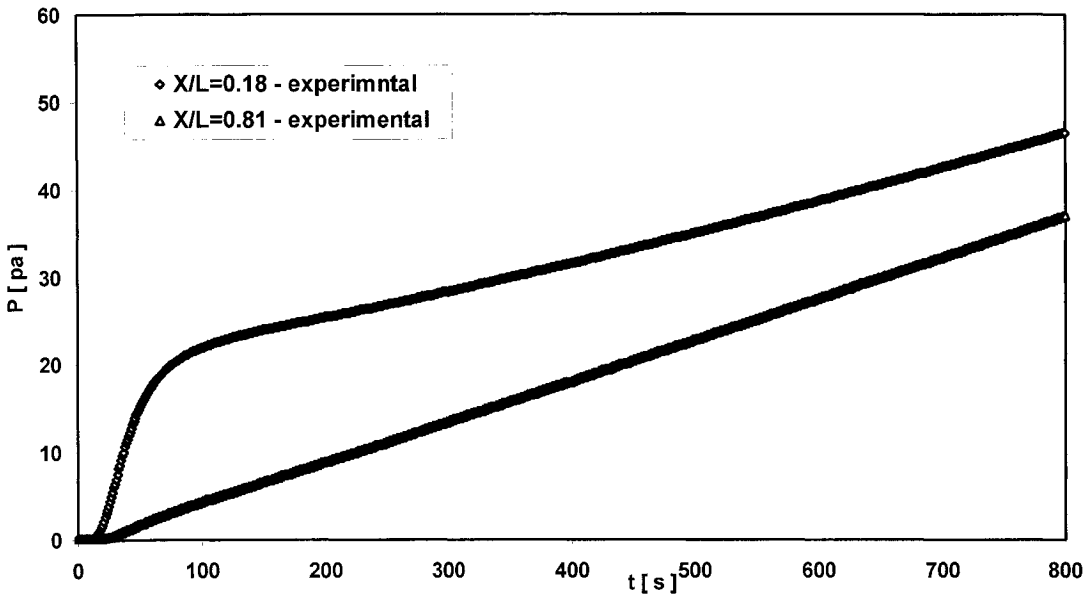

Figures CD-3- experiment with accumulation tank and PPO membrane. The effect of feed pressure on pressure responses at two positions x1=0.18, x2=0.81 in ¼" stainless steal tube with a length of 2.36 m and initial pressure of 0.13 pa and feed pressure of 90 PSI. The volume of tank is V=2250 cm^3 attached at the end of tube, T= 23 ^{O}C.

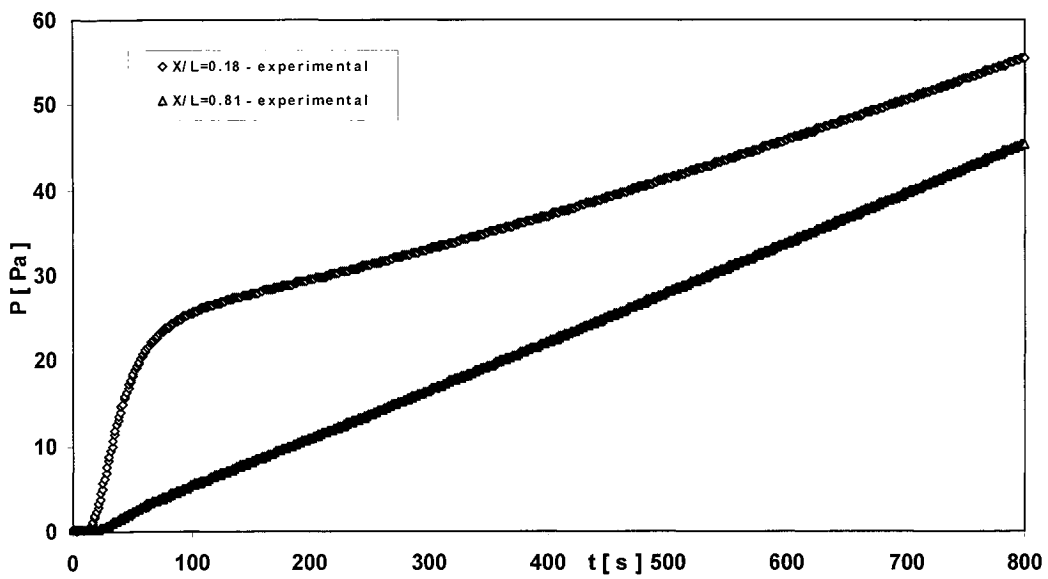

Figures CD-4- experiment with accumulation tank and PPO membrane. The effect of feed pressure on pressure responses at two positions x1=0.18, x2=0.81 in ¼" stainless steal tube with a length of 2.36 m and initial pressure of 0.13 pa and feed pressure of 110 PSI. The volume of tank is V=2250 cm^3 attached at the end of tube, T= 23 ^{O}C.

Appendix D

Membrane preparation

To prepare the membrane, polyphenylene oxide (P.P.O) was utilized as the medium. The polymer was dried in air at room temperature for at least 24 hours. 1-gram polymer was dissolved in 50 ^{cc} trichloroethylene in a glass bottle. To assure of complete dissolution of the polymer, the content of the bottle was stirred with a magnetic stirrer for 24 hours. The solution was filtered through 3 μm Teflon filters. Then 4 ^{cc} of a dilute P.P.O solution (2%wt) was poured onto a glass plate, which was surrounded by a 5 cm diameter metal ring, and the solvent was removed by evaporation mechanism for 2 days in room temperature. To remove the membrane, the glass plate was immersed into a distilled water bath for 5 minutes. The dried membrane had an average thickness of l = 39.5 μm, determined by a micrometer.

Appendix E1

Numerical solution procedure for the C.V. system with constant flow rate entering into the system

Fick's 2nd law of diffusion:

$$\frac{\partial c}{\partial t} = \frac{\partial}{\partial x}\left(D(x,t)\frac{\partial c}{\partial x} \right) \qquad \textbf{(E1-1)}$$

Initial condition:

$$C(x, t=0) = C_0 \qquad \textbf{(E1-2)}$$

Boundary conditions:

B.C.1 $$\left(-D\frac{\partial c}{\partial x} \right)_{x=0} = N = cons\tan t \qquad \textbf{(E1-3)}$$

B.C.2 $$\left(\frac{\partial c}{\partial x} \right)_{x=L} = 0 \qquad \textbf{(E1-4)}$$

Dimensionless units:

$$\theta = \frac{C - C_0}{NL/D_0}, \quad \phi = \frac{D}{D_0}, \quad Z = \frac{x}{L}, \quad \tau = \frac{D_0}{L^2}t \qquad \textbf{(E1-5)}$$

$$\Rightarrow \qquad \frac{\partial \theta}{\partial \tau} = \frac{\partial}{\partial Z}\left(\phi\frac{\partial \theta}{\partial Z} \right) \qquad \textbf{(E1-6)}$$

To solve equation (E1-6) numerically using implicit method and taking step size=1/2

Give the following result:

$$\frac{\partial \theta}{\partial \tau} = \frac{\theta_i^{\,j} - \theta_i^{\,j-1}}{\Delta \tau} \qquad \textbf{(E1-7)}$$

$$\frac{\partial}{\partial Z}\left(\phi\frac{\partial\theta}{\partial Z}\right)=\frac{\phi_{i-1/2}\theta_{i-1}{}^{j}-(\phi_{i+1/2}+\phi_{i-1/2})\theta_{i}{}^{j}+\phi_{i+1/2}\theta_{i+1}{}^{j}}{(\Delta Z)^2} \qquad \textbf{(E1-8)}$$

$$\Rightarrow A\theta^{j}=\theta^{j-1} \qquad \textbf{(E1-9)}$$

$$B.C.1\quad \left(\frac{\partial\theta}{\partial Z}\right)_{z=0}=-1/\phi\Rightarrow\frac{\theta_2-\theta_1}{\Delta Z}=-1/\phi\Rightarrow-\theta_1+\theta_2=-\Delta Z/\phi \qquad \textbf{(E1-10)}$$

$$B.C.2\quad \left(\frac{\partial\theta}{\partial Z}\right)_{z=1}=0\quad\Rightarrow\theta_{N+1}-\theta_N=0\Rightarrow\theta_{N+1}=\theta_N \qquad \textbf{(E1-11)}$$

The first boundary condition has been used as the first row of descritization matrix.

Appendix E2

Numerical solution for system contains membrane (time dependant flow leaving the membrane and entering into the tube)

The governing equations for the one-dimensional gas transfer through porous media are Fick's 1[nd] and 2[nd] law of diffusion:

$$J = -D\nabla C \qquad \textbf{(E2-1)}$$

$$\frac{\partial c}{\partial t} = \frac{\partial}{\partial x}\left(D(x,t)\frac{\partial c}{\partial x}\right) \qquad \textbf{(E2-2)}$$

Initial condition:

$$C(x, t=0) = C_f \qquad \textbf{(E2-3)}$$

Boundary conditions:

$$\text{B.C.1} \quad J\,|_{x=0} = \frac{P_f * P_m * A_m}{l * A} + \frac{2P_f * P_m * A_m}{A * l}\sum_{n=0}^{\infty}(-1)^n \exp\left(\frac{-n^2 * \pi^2 * D_m * t}{l^2}\right) \qquad \textbf{(E2-4)}$$

$$\text{B.C.2} \quad \left(\frac{\partial c}{\partial x}\right)_{x=L} = 0 \qquad \textbf{(E2-5)}$$

Dimensionless units:

$$\theta = \frac{C - C_f}{C_f}, \quad \phi = \frac{D}{D_0}, Z = \frac{x}{L}, \tau = \frac{D_0}{L^2}t, \; f = \frac{J}{J_0}, \; J_0 = \frac{P_f * P_m * A_m}{l * A} \qquad \textbf{(E2-6)}$$

f = Dimensionless flux

Boundary conditions in terms of dimensionless units are:

B.C. 1 $$\left(\frac{\partial\theta}{\partial Z}\right)_{z=0} = \beta \quad , \qquad \beta = \frac{-L * j_0 * f}{C_0 * D_0 * \phi} \qquad \textbf{(E2-7)}$$

B.C. 2 $$\left(\frac{\partial\theta}{\partial Z}\right)_{z=1} = 0 \qquad \textbf{(E2-8)}$$

$$\Rightarrow \qquad \frac{\partial\theta}{\partial\tau} = \frac{\partial}{\partial Z}\left(\phi\frac{\partial\theta}{\partial Z}\right) \qquad \textbf{(E2-9)}$$

To solve equation (1) numerically using implicit method and taking step size=1/2
Will result:

$$\frac{\partial\theta}{\partial\tau} = \frac{\theta_i^{\,j} - \theta_i^{\,j-1}}{\Delta\tau} \qquad \textbf{(E2-10)}$$

$$A\theta^j = \theta^{j-1} \qquad \textbf{(E2-11)}$$

ENDENDend of tube, T= 23 ^{O}C.

APPENDIX F

MATLAB CODE FOR MASS FLOW CONTROLLER AND CV SYSTEM

```
%APPENDIX F
clear
clc

format long

D0 = 1;
C0 = 0;

Conc0 = 1.403/8.31451e3/(273.16+23)*1e-6;
Press0= (Conc0*1e6)*8.314e3*296.16;
D0 = (0.0278*Press0+0.6057*((1+0.342*Press0)/(1+0.581*Press0)))*1e4;
V= 80.4; %cm3
L = 360.5;    %cm
Area = (0.386/2)^2*pi;    %cm2
N = 0.073/V*L/60;     %cm/s

time =600;  %For dp/dt t=1400
n = 20;
dt = 0.02;       %for dp/dt dt=0.001
dx = 1/n;
Delta = dt/dx^2;
Beta = -1;
for j=1:time

    timec(j) = (j-1)*dt;
end

X(1) = 0;
Press(1,1) = Press0;

for i= 2:n+1
    X(i) = (i-1)*dx;
    Press(i,1) = Press0;
end

D(1,1) = 1;
C(1,1) = 0;

P00 = Press0;
for i = 2:n+1
    D(i,1) = 1;
    C(i,1) = 0;
end

for j = 2:time
j
        for i = 1:n+1
            D(i,j) = D(i,j-1);

        end
    ErrorD = 1;
   while(ErrorD > 1e-16)

        A(1) = 0;
        B(1) = -1;
```

```
        E(1) = 1;
        for i=2:n
            A(i) = - Delta/2*(D(i-1,j)+D(i,j));
            B(i) = 1+Delta/2*(D(i+1,j)+D(i-1,j)+2*D(i,j));
            E(i) = - Delta/2*(D(i+1,j)+D(i,j));
        end
        A(n+1) = 1;
        B(n+1) = -1;

        Beta = -1/D(1,j);
        K(1) = Beta * dx;
        for i=2:n
            K(i) = C(i,j-1);
        end
        K(n+1) = 0;

        for i=1:n
           E(i) = E(i)/B(i);
           K(i) = K(i)/B(i);
           B(i+1) = -A(i+1)*E(i)+B(i+1);
           K(i+1) = -A(i+1)*K(i)+K(i+1);
        end
        C(n+1,j) = K(n+1)/B(n+1);
        for i = n:-1:1
          C(i,j) = K(i)-E(i)*C(i+1,j);
        end

        ErrorD = 0;
        for i=1:n+1
           Di = D(i,j);
           Conc = C(i,j)*N*L/D0/22400e3 + Conc0;
           Press(i,j)= (Conc*1e6)*8.314e3*293.16;

              Diff = (0.0278*Press(i,j)+0.6057*((1+0.342*Press(i,j))/(1+0.581*Press(i,↙
j))))*1e4;

           D(i,j) = Diff / D0;
           ErrorD = ErrorD + (Di - D(i,j))^2;
        end

    end
end

NoofX = 20;
i2 = 1;
i3 = i2;
dxtime = 1/NoofX;
for i= 1:NoofX+1
    XPL1(i) =  (i-1)*dxtime;
        ERRX = (XPL1(i)-X(i2))^2;
    for i1 = i2+1:n+1
        if (ERRX > ((XPL1(i)-X(i1))^2))
            i3 = i1;
            ERRX = ((XPL1(i)-X(i1))^2);
        else
            break;
```

```
        end
    end
    i2 = i3;
    XPL2(i) =  i3;
end

for i = 1:NoofX+1
    for j = 1:time
         PRESSURE(i,j) = Press(XPL2(i),j);
         Diffusivity(i,j) = D(XPL2(i),j);
    end
end

%plot(X,Press);
%plot(X,PRESSURE);
%for j = 1:time-1
    %for i=2:NoofX+1
      %   dPpdtt(i,j) = (Press(i+1,j)-Press(i,j))/dx;
   % end
%end
%j = time;
%for i=2:NoofX+1
   % dPpdtt(i,j) = (Press(i+1,j)-Press(i,j))/dx;
%end

dPpdtfinal=(PRESSURE(n/2,time)-PRESSURE(n/2,time-2))/dt/2;

dPpdtfinal2=dPpdtfinal/((L^2)/D0);
dPpdtfinal2
for j = 2:time-1
    for i=1:NoofX+1
         dPpdtx(i,j) = (PRESSURE(i,j+1)-PRESSURE(i,j-1))/dt/2/dPpdtfinal;
    end
end
j = 1;
for i=1:NoofX+1
    dPpdtx(i,j) = (PRESSURE(i,j+1)-PRESSURE(i,j))/dt/dPpdtfinal;
end
j=time;
for i=1:NoofX+1
    dPpdtx(i,j)=(PRESSURE(i,j)-PRESSURE(i,j-1))/dt/dPpdtfinal;
end

%i= n/2;
for j=1:time;
    for i1 = 2:NoofX
        i = XPL2(i1);

        dpdx(i1,j)= (-Press(i-1,j)+Press(i+1,j))/(2*dx);
    end
       i1 = 1;
       i = XPL2(i1);

       dpdx(i1,j)= (-Press(i,j)+Press(i+1,j))/(dx);
       i1 = NoofX+1;
       i = XPL2(i1);
```

```
       dpdx(i1,j)= (-Press(i-1,j)+Press(i,j))/(dx);

end
for j=1:time;
    for i1=2:NoofX
        i=XPL2(i1);
        flux(i1,j)= D(i,j)*(-Press(i-1,j)+Press(i+1,j))/ (2*dx);
    end
    i1=1;
    i= XPL2(i1);
    flux(i1,j)= D(i,j)*(-Press(i,j)+Press(i+1,j))/(dx);
    i1=NoofX+1;
    i=XPL2(i1);
    flux(i1,j)= D(i,j)*(-Press(i-1,j)+Press(i,j))/(dx);
end

%plot(timec,dpdx);
%plot(X, D);
%plot(timec,D);
%plot(timec,PRESSURE);
%plot(timec,Press);
 %surf(timec,X,D);
%plot(timec,dPpdtx);
```

APPENDIX G

MATLAB CODE FOR TIME DEPENDANT FLOW WITH MEMBRANE AND CV SYSTEM

```
%APPENDIX G
clear
clc

format long

D0 = 1;
C0 = 0;
Press0=0.121;
Conc0 =(Press0)/8.314/(273.16+23);

D0 = 0.0278*Press0+0.6057*((1+0.342*Press0)/(1+0.581*Press0));
R=8.314;
T=296.16;
Pm1=7.16e-17;
Dm=6.14e-12;
l=3.95e-5;
Pt=217000;
Pm= Pm1/22.4e-3;
V=83.40e-6;
L = 3.73;
Area =9.08e-4;

time=800;
n = 100;
dt = 0.02 ;
dx = 1/n;
Delta = dt/dx^2;

for j=1:time

    timec(j) = (j-1)*dt;
end

X(1) = 0;
Press(1,1) = Press0;

for i= 2:n+1
    X(i) = (i-1)*dx;
    Press(i,1) = Press0;
end

D(1,1) = 1;
C(1,1) = 0;

P00 = Press0;
for i = 2:n+1
    D(i,1) = 1;
    C(i,1) = 0;
end

for j = 2:time
j;
f(j)=1;
m=100;
for i=1:m
```

```
    f(j)=f(j)+2*(-1)^i*exp(-timec(j)*Dm/D0*(pi*i*L/l)^2);
end
if(timec(j) == 0)
    f(j) = 0;
end

        for i = 1:n+1
            D(i,j) = D(i,j-1);
        end
    ErrorD = 1;
  while(ErrorD > 1e-16)

        A(1) = 0;
        B(1) = -1;
        E(1) = 1;
        for i=2:n
            A(i) = - Delta/2*(D(i-1,j)+D(i,j));
            B(i) = 1+Delta/2*(D(i+1,j)+D(i-1,j)+2*D(i,j));
            E(i) = - Delta/2*(D(i+1,j)+D(i,j));
        end
        A(n+1) = 1;
        B(n+1) = -1;
        f0=Pt*Pm*Area*L/l/V;
        Beta = -f0*L/D0/Conc0*f(j)/D(1,j);
        Betaj(j) = Beta;
        K(1) = Beta * dx;
        for i=2:n
            K(i) = C(i,j-1);
        end
        K(n+1) = 0;

        for i=1:n
           E(i) = E(i)/B(i);
           K(i) = K(i)/B(i);
           B(i+1) = -A(i+1)*E(i)+B(i+1);
           K(i+1) = -A(i+1)*K(i)+K(i+1);
        end
        C(n+1,j) = K(n+1)/B(n+1);
        for i = n:-1:1
          C(i,j) = K(i)-E(i)*C(i+1,j);
        end

        ErrorD = 0;
        for i=1:n+1
           Di = D(i,j);
           Conc = (C(i,j)+1)* Conc0;
           Press(i,j)= Conc*R*T;

              Diff = 0.0278*Press(i,j)+0.6057*((1+0.342*Press(i,j))/(1+0.581*Press(i,↙
j)));

           D(i,j) = Diff / D0;
           ErrorD = ErrorD + (Di - D(i,j))^2;
        end

    end
```

```
end

NoofX =100;
i2 = 1;
i3 = i2;
dxtime = 1/NoofX;
for i= 1:NoofX+1
    XPL1(i) =(i-1)*dxtime;
        ERRX = (XPL1(i)-X(i2))^2;
    for i1 = i2+1:n+1
        if (ERRX > ((XPL1(i)-X(i1))^2))
            i3 = i1;
            ERRX = ((XPL1(i)-X(i1))^2);
        else
            break;
        end
    end
    i2 = i3;
    XPL2(i) =  i3;
end

for i = 1:NoofX+1
    for j = 1:time
         PRESSURE(i,j) = Press(XPL2(i),j);
         Diffusivity(i,j) = D(XPL2(i),j);
    end
end

%plot(X,Press);
%plot(X,PRESSURE);
%for j = 1:time-1
    %for i=2:NoofX+1
      %   dPpdtt(i,j) = (Press(i+1,j)-Press(i,j))/dx;
   % end
%end
%j = time;
%for i=2:NoofX+1
   % dPpdtt(i,j) = (Press(i+1,j)-Press(i,j))/dx;
%end

dPpdtfinal=(PRESSURE(n/2,time)-PRESSURE(n/2,time-2))/dt/2;

for j = 2:time-1
    for i=1:NoofX+1
         dPpdtx(i,j) = (PRESSURE(i,j+1)-PRESSURE(i,j-1))/dt/2/dPpdtfinal;
    end
end
j = 1;
for i=1:NoofX+1
    dPpdtx(i,j) = (PRESSURE(i,j+1)-PRESSURE(i,j))/dt/dPpdtfinal;
end
j=time;
for i=1:NoofX+1
    dPpdtx(i,j)=(PRESSURE(i,j)-PRESSURE(i,j-1))/dt/dPpdtfinal;
end
```

```
for j=1:time;
    for i1 = 2:NoofX
        i = XPL2(i1);

        dpdx(i1,j)= (-Press(i-1,j)+Press(i+1,j))/(2*dx);
    end
       i1 = 1;
       i = XPL2(i1);

       dpdx(i1,j)= (-Press(i,j)+Press(i+1,j))/(dx);
       i1 = NoofX+1;
       i = XPL2(i1);


       dpdx(i1,j)= (-Press(i-1,j)+Press(i,j))/(dx);

end
for j=1:time;
    for i1=2:NoofX
        i=XPL2(i1);
        flux(i1,j)= D(i,j)*(-Press(i-1,j)+Press(i+1,j))/ (2*dx);
    end
    i1=1;
    i= XPL2(i1);
    flux(i1,j)= D(i,j)*(-Press(i,j)+Press(i+1,j))/(dx);
    i1=NoofX+1;
    i=XPL2(i1);
    flux(i1,j)= D(i,j)*(-Press(i-1,j)+Press(i,j))/(dx);
end

%plot(timec,dpdx);
%plot(X, D);
%plot(timec,D);
%plot(timec,PRESSURE);
%plot(timec,Press);
 %surf(timec,X,D);
%plot(timec,dPpdtx);
%plot(timec,PRESSURE);

%March 27'2004
%p=1.13;
%format short
%j = time;
%for i = 1:NoofX+1
 %   timelag(i) = timec(j)+(p-PRESSURE(i,j))/((PRESSURE(i,j)-PRESSURE(i,j-1))/dt);
  %  Y(i,1)=XPL1(i);
   % Y(i,2) = timelag(i);
   %end
%format short
%Y;
%PRESSURE
%w=timec*l^2/Dm;
%plot(w,PRESSURE);

%format short
```

```
%Y;
%PRESSURE
for j = 1:time
    h(j)=timec(j)*L^2/D0;
end
%plot(h,dPpdtx);
%plot(h,PRESSURE);
%plot(h,Betaj);
```